Relicensing Study 3.3.19

Ultrasound Array Control and Cabot Station Shad Mortality Study

2019 Study Report

Northfield Mountain Pumped Storage Project (No. 2485) and Turners Falls Hydroelectric Project (No. 1889)

Prepared for:

FirstLight

Prepared by:

Kleinschmidt

Gomez and Sullivan Engineers

MARCH 2020

TABLE OF CONTENTS

LIST OF TABLES

LIST OF FIGURES

LIST OF APPENDICES

LIST OF ABBREVIATIONS

AIC	Akaikes Information Criteria
ANOVA	Analysis of Variance
cfs	cubic feet per second
kcfs	thousand cubic feet per second
CJS	Cormack Jolly Seber
CRC	Connecticut River Conservancy
COXPH	Cox Proportional Hazards Regression
CRWC	Connecticut River Watershed Council
dB	Decibel
DIDSON	Dual Frequency Identification Sonar
FERC	Federal Energy Regulatory Commission
FirstLight	Northfield Mountain LLC (owner of Northfield Mountain Pumped Storage Project) and FirstLight MA Hydro LLC (owner of Turners Falls Hydroelectric Project)
GLM	Generalized Linear Model
GOF	Goodness of fit
HR	Hazard ratio
ILP	Integrated Licensing Process
LRDR	Live Recapture Dead Recovery
MHz	megahertz
NHFGD	New Hampshire Fish and Game Department
NMFS	National Marine Fisheries Service
PIT	Passive Integrated Transponder
QAQC	Quality Assurance and Quality Control
RM	River Miles
SPLs	sound pressure levels
TFD	Turners Falls Dam
TFI	Turners Falls Impoundment
USFWS	United States Fish and Wildlife Service
USGS	United States Geological Survey

EXECUTIVE SUMMARY

Northfield Mountain LLC is the current licensee of the Northfield Mountain Pumped Storage Project (Northfield Mountain Project, FERC No. 2485). FirstLight MA Hydro LLC is the current licensee of the Turners Falls Hydroelectric Project (Turners Falls Project, FERC No.1889). Northfield Mountain LLC and FirstLight MA Hydro, LLC is collectively referred to as FirstLight in this report. FirstLight has initiated with the Federal Energy Regulatory Commission (FERC, the commission) the process of relicensing the Northfield Mountain and Turners Falls Projects using the FERC's Integrated Licensing Process (ILP). The current licenses for the Northfield Mountain and Turners Falls Projects were issued on May 14, 1968 and May 5, 1980, respectively. This report documents the 2019 *American Shad Ultrasound Array Control and Cabot Station Mortality Study.*

The purpose of this study was to build on knowledge gained from the 2016 and 2018 ultrasound investigation and to further investigate whether the use of ultrasound technology is an effective method to minimize shad attraction to the Cabot Station fish ladder while allowing shad to continue migrating up the bypass reach toward the Turners Falls Dam (TFD). The configuration of the 2016 ultrasound array because of its proximity to the Cabot Station discharge was affected by significant air entrainment, which likely increased the attenuation and scattering of sound propagating through the water, causing reduced effectiveness of the sound barriers unless American Shad were within the immediate vicinity of the Array. In 2018, a new configuration of ultrasound transducers was designed to optimize signal strength, minimize air entrainment, and produce a continuous sound field spanning across Cabot Station tailrace. The results of the 2018 study indicated that the Ultrasound Array was effective in keeping a proportion of migrating shad out of the Cabot tailrace and facilitating movement into the Bypass reach. However, two elements (additional flow in the bypass reach and the ultrasound array) were both added as part of the 2016 and 2018 studies, and it was not possible to ascertain which contributed to the increased number of fish that moved upstream and entered the bypass reach. As a result, this 2019 study was conducted to test varying flows in the Bypass reach without an ultrasound array present. In addition, the 2018 study revealed that fish encountered a velocity barrier when moving upstream through the Rawson island complex. Additional receivers were added around Rawson Island in 2019 to distinguish route of passage through this area.

The second part of the 2019 study included an investigation of the rates of immediate and latent survival for emigrating post-spawn adult shad that pass through the Cabot Station turbines as they move back downstream.

In 2019, 241 adult American Shad were tagged and released at the Holyoke Dam fish lift. From there, 137 fish reached the Project area, and 74 of those fish made it to the Cabot Station tailrace. Out of the 74 fish that reached the tailrace, 49 (66%) moved up into the Bypass reach. In the 2018 study, when the ultrasound array was in place and operational, 112 tagged shad were detected in the Cabot tailrace and 85 (76%) made it up the Bypass reach. Cox Proportional Hazard models were constructed to determine which environmental or operational variables most influenced movement from the tailrace to the Bypass reach, for all years (2015, 2016, 2018, and 2019). Out of 27 models constructed, the best model (lowest AIC value) included the ultrasound array being in place and operational, and it was highly significant ($p<0.001$). This suggests that when the ultrasound array was operational, fish were much more likely (HR = 3.9) to move from the Cabot Station tailrace to the entrance of the Bypass reach. In addition, the fish making this transition did so much quicker when the array was in place and on as compared to when it was not in place.

In 2015, 2016, and 2018, the majority of fish that moved upstream within the bypass reach did so when bypass flows ranged from 3,000 to 6,000 cfs. In 2019, bypass flows were much higher when tagged shad moved within the bypass reach. This year the majority of fish moved when bypass flows were between 5,000 and 22,000 cfs. As a result of the high flows in the Bypass reach during peak movement times (May 15 to May 30, 2019), there was no way to safely access the telemetry receivers around the Rawson Island

complex for regular maintenance. Thus, the receivers experienced a power outage and it was impossible to distinguish routes of upstream passage through the Rawson Island complex in 2019.

An evaluation of Station No.1 to Bypass flow ratio was conducted to determine if adult shad migrate by the Station No.1 tailrace under a flow split of 50% spill from the TFD and 50% from Station No.1. In 2019, due to the high river flow, all tagged shad moved from the entrance of the Bypass reach to the TFD spillway when Bypass flow was at least double that of Station No.1 discharge. A Cox Proportional Hazard model constructed that looked at the Station No.1 to Bypass Flow ratio for all years, but was not significant.

FirstLight assessed the survival of adult shad as they pass with a combination of Live Recapture Dead Recovery (LRDR) mark recapture modeling and a dead drift study to compare the rates of travel of fish known to be dead with their live counterparts. The LRDR method is an improvement over traditional Cormack Jolly Seber (CJS) mark recapture modeling because information from mortalities found during mobile tracking (dead recoveries) are included in the estimates. Traditional CJS modeling only includes information from live recoveries, therefore we do not know if a fish has survived and simply wasn't recaptured, permanently emigrated from the study, or died somewhere in between. After removing both live recapture and dead recovery data after the 48-hour mortality window (1 week for mobile tracking), 65% of the fish known to pass via the Cabot powerhouse were expected to survive 48 hours while 89% of the fish that passed via the Cabot log sluice survived after 48 hours. FirstLight calculated the median transit time of fish that passed downstream into the tailrace and traveled to Montague (37 minutes) and from Montague to Fourth Island (18 minutes). Compared with fish known to have died, these fish traveled much farther and much faster than the median dead drift fish which only traveled 1090 feet after 5 weeks of mobile tracking.

1 INTRODUCTION

Unlike most other fish species, it has been demonstrated that American Shad (*Alosa sapidissima*) are able to detect sound up to 180 kilohertz (kHz) (Higgs et al., 2004). Previously, it was proposed that ultrasound detection in shad involves swim bladder extensions; however, more recent work indicates that the utricle, an organ found in the inner ear of some Clupeids, allows detection of ultrasonic stimulation (Higgs et al., 2004). The researchers speculated that Clupeids can detect the ultrasonic clicks of one of their major predators, echolocating cetaceans. There are examples of high frequency sound being used successfully to deter fish in the family Clupeidae including Alewife, Blueback Herring and American Shad (shad). High frequency sound used at the James A. Fitzpatrick nuclear power plant on Lake Ontario was found to reduce impingement of Alewife by more than 80%, and its use was approved by the regulatory agencies. Adult American Shad and Blueback Herring avoided the ultrasound field in the Holyoke Canal system (Kynard and Taylor, 1984). Acoustic barriers have been used for migrating Blueback Herring on the Savannah River (Richard B. Russell Dam) and Santee River (St. Stephen fish lift) in South Carolina and emigrating juvenile Blueback Herring on the Mohawk River in New York (Crescent Project, FERC No. 4678; Vischer Ferry, FERC No. 4679). Evidence from previous studies that attempted to produce behavioral avoidance by adult shad suggests that ultrasound is an effective stimulus (Carlson and Popper, 1997).

Since 2006, Hydro-Québec has successfully used an ultrasound device in front of the water intakes of the Rivière-des-Prairies Hydroelectric Facility to guide downrunning spent adult shad away from the intakes (Guindon and Desrocher, 2016a). Based on the success of the ultrasound guidance system, Hydro-Québec is currently studying efforts using ultrasound to prevent adult shad from entering Rivière des Prairies and guide them to other outlets (Guindon and Desrocher, 2016b).

An evaluation of the use of an ultrasound array to deter adult shad from the Cabot Station tailrace and facilitate their upstream movement through the bypass reach to Turners Falls Dam (TFD) was a study request by U.S. Fish and Wildlife Service (USFWS), New Hampshire Fish & Game Department (NHFGD) and Connecticut River Conservancy (CRC). A potential alternative to the current configuration of fish ladders at the Turners Falls Project would be to minimize[1] attraction to the Cabot Station ladder and operate a single fish passage facility further upstream near the TFD. In the spring of 2016, a study was conducted to evaluate the use of an ultrasound system for deterring adult shad from entering the Cabot Station tailrace and facilitating upstream movement into the bypass reach. Fish behavior was evaluated with a combination of radio telemetry and Passive Integrated Transponders (PIT) technologies, as well as a Dual-Frequency Identification Sonar (DIDSON) camera installed at the entrance to Cabot Station ladder, within the vicinity of the ultrasound array. Count data from the DIDSON camera revealed that there was no significant difference between median daily fish counts on days that the array was on and when it was off. However, when the count data from the DIDSON were further analyzed on an hourly scale, within the first two hours of activating the ultrasound system ("on"), there was a significant interaction effect between the system status (on or off) and shad counts at the Cabot ladder. This suggested that the ultrasound array affected adult shad, but they may have been able to acclimate to the sound when the array was on for relatively long periods of time.

The 2018 Ultrasound Array Study conducted at Cabot Station helped build upon knowledge gained in 2016 and further investigated whether the use of ultrasound technology is an effective method to minimize shad attraction to the Cabot ladder, while moving shad up the bypass reach. In 2016, air entrainment from the Cabot Station turbine discharge and fish ladder flow significantly increased the attenuation and scattering of the sound field, effectively reducing sound pressure levels below thresholds that would elicit strong and prolonged avoidance reactions from adult shad unless fish were within the immediate vicinity of the transducers including at the fish ladder entrance. This is most likely why we observed a reaction near the

[1] What is considered effective at minimizing the attraction to the Cabot tailrace is discussed later in this document.

fish ladder entrance for the two hours subsequent to reactivating the system in 2016. In the 2016 study, there were three transducers with different horizontal orientations mounted to a pole located on the fish ladder wall near the entrance and two transducers, with different horizontal orientations, mounted on a pole installed approximately at the midpoint on the back of the powerhouse (discharge location). Using data from sound measurements collected on November 15, 2017 and from the results of sound modeling, transducer locations, numbers, and orientations for the 2018 study were selected to minimize interference from air entrainment and optimize signal strength in an attempt to produce a continuous sound field spanning across the edge of the tailrace and with sound pressure levels (SPLs) greater than the 160 decibels (dB).

Results of the 2018 study indicated that of the 112 adult American Shad that arrived at the Cabot Station tailrace, 85 fish (76%) moved upstream into the bypass reach entrance. Since two elements (additional flow in the bypass reach and the ultrasound array) were added as part of the previous studies, it is not possible to ascertain which contributed to the increased number of fish moving upstream past Cabot Station and into the bypass reach. To determine if increased bypass flow or the ultrasound array or a combination of the two contributed to 76% of the tagged fish moving upstream to the bypass reach, it was proposed to conduct a movement study in 2019 with varying levels of increased flow in the bypass reach, but without an ultrasound array in place and the Cabot Station fish ladder operating as normal.

In addition, the 2018 study revealed that Rock Dam and the side channels around Rawson Island create physical and velocity barriers, respectively, which obstructed shad migration to the fishway at TFD. The 2019 study was designed to collect additional information in these two areas of the bypass reach by including additional receivers in the areas around Rock Dam and Rawson Island.

1.1 Background

Every spring, mature adult American Shad enter the Connecticut River to search for spawning and rearing habitat necessary for their anadromous life history. Shad migrate inland from marine waters and spawn in areas of suitable habitat as they move upstream. During the upstream migration, prior to entering Project waters, shad first encounter the Holyoke Dam in Holyoke, MA. The Holyoke Dam provides upstream passage via two fish lifts and allows access to approximately 35 river miles of mainstem habitat in the Connecticut River between Holyoke Dam and TFD. All fish used in this study were captured at the Holyoke Dam fish lift at the existing fish trapping facility.

The next manmade barrier encountered by upstream migrating fish is the TFD, located at approximately river mile (RM) 122 on the Connecticut River mainstem. Upstream migrating fish may pass the TFD via two potential routes. Downstream of TFD, fish may use the Cabot Station fish ladder, located at approximately RM 120, to enter the power canal. The Gatehouse fishway is located at the upstream end of the 2.1-mile-long power canal and provides access to Turners Falls Impoundment (TFI). Fish that bypass the Cabot Station ladder may continue to move upstream via the bypass reach toward to the base of the TFD where they can find passage via the Spillway fish ladder into the upper power canal, just below the Gatehouse. Here, they rejoin fish that have passed via the Cabot Station ladder and are able to access the TFI via passage at the Gatehouse ladder.

The purpose of this study was to evaluate if the use of an ultrasound array to deflect shad away from the Cabot Station tailrace or the addition of water into the bypass reach facilitated upstream movement toward the Spillway ladder. A potential alternative to the current configuration of fishways at the Turners Falls Project would be to minimize attraction to the Cabot Station ladder and operate a single fishway facility further upstream, closer to the TFD.

1.2 Objectives

In 2016 and 2018, FirstLight evaluated the use of an ultrasound array to deter shad from the Cabot Station tailrace and facilitate upstream movement of American Shad toward the TFD. The goal was to determine if an ultrasound barrier could be used to repel adult shad from the Cabot Station tailrace and guide them into the bypass reach.

The objective of the 2019 study was to determine if the magnitude of the bypass reach flow or the ultrasound array was primarily responsible for adult American Shad moving upstream to the bypass reach. Specific study objectives included:

- To determine if a similar proportion of tagged migrating adult shad will migrate upstream of Cabot Station and into the bypass reach without the ultrasound array in place;
- To investigate adult shad migration in the area of Rawson Island and Rock Dam (both features are located in the bypass reach); and
- To determine if adult shad migrate by the Station No.1 tailrace under a flow split of 50% spill from the TFD and 50% from Station No.1 for two different total bypass flow scenarios (4,400 and 6,500 cubic feet per second [cfs]).

In addition to the objectives associated with the upstream migrants, FirstLight also investigated the rates of immediate and latent survival for emigrating post-spawn adult shad that pass through the Cabot Station turbines as they move back downstream.

2 STUDY AREA

The study area generally consisted of the Connecticut River extending from the Holyoke Dam in Holyoke, MA to the TFD, in Turners Falls, MA (Figure 2-1). Fish were considered to enter the study area when they arrived at the Montague Wastewater Treatment Facility, which is located just downstream of the Deerfield River confluence. Between the Montague Wastewater Treatment Facility and the Spillway at the TFD, fish encounter the following:

Cabot Station

Fish moving into and/or through the Cabot Station tailrace encounter flows from Cabot generation, the log sluice, and the Cabot Ladder/attraction flow. Depending on inflow, flows from Cabot Station generation can range from no flow up to its capacity of approximately 13,728 cfs. Continuous flows of approximately 200 cfs and 368 cfs are released from the log sluice and Cabot Ladder/attraction flow, respectively, during typical operations within the shad passage season.

The Cabot Ladder is a modified "ice harbor" design consisting of 66 pools. Each pool is situated approximately one foot higher than the previous pool. The entrance to the fishway is located adjacent to the Cabot Station tailrace and the exit deposits fish into the power canal. Approximately 2.1 miles upstream at the head of the canal, the Gatehouse Ladder permits access to the TFI.

Bypass Reach

Fish moving into the bypass reach encounter Smead Island across from Cabot Station (see Figure 2-2). Adult shad moving by Smead Island and beyond the adjacent Conte Lab encounter Rawson Island, which divides the river into two channels (see Figure 2-2). On river-left (looking downstream), fish would encounter Rock Dam, a natural rock falls having a steep vertical drop. On river-right (looking downstream), fish would have to negotiate through the river-right channel or a second smaller channel to continue upstream.

Fish moving beyond Rawson Island encounter the Station No. 1 discharge (if operating). As discussed later in this report, different flow splits – the percentage of flow passed via the TFD and the percentage of flow passed via Station No. 1- were evaluated in the 2019 study.

Spillway Ladder

Fish moving beyond the Station No. 1 discharge arrive at the TFD where they can find passage via the Spillway Ladder (modified ice harbor design with 42 pools). Flow from the fish ladder includes attraction flow and fishway totaling 368 cfs. The ladder allows fish to move into the Gatehouse's vertical slot fishway, where they rejoin fish that have used the fish ladder at Cabot Station to pass upstream through the power canal.

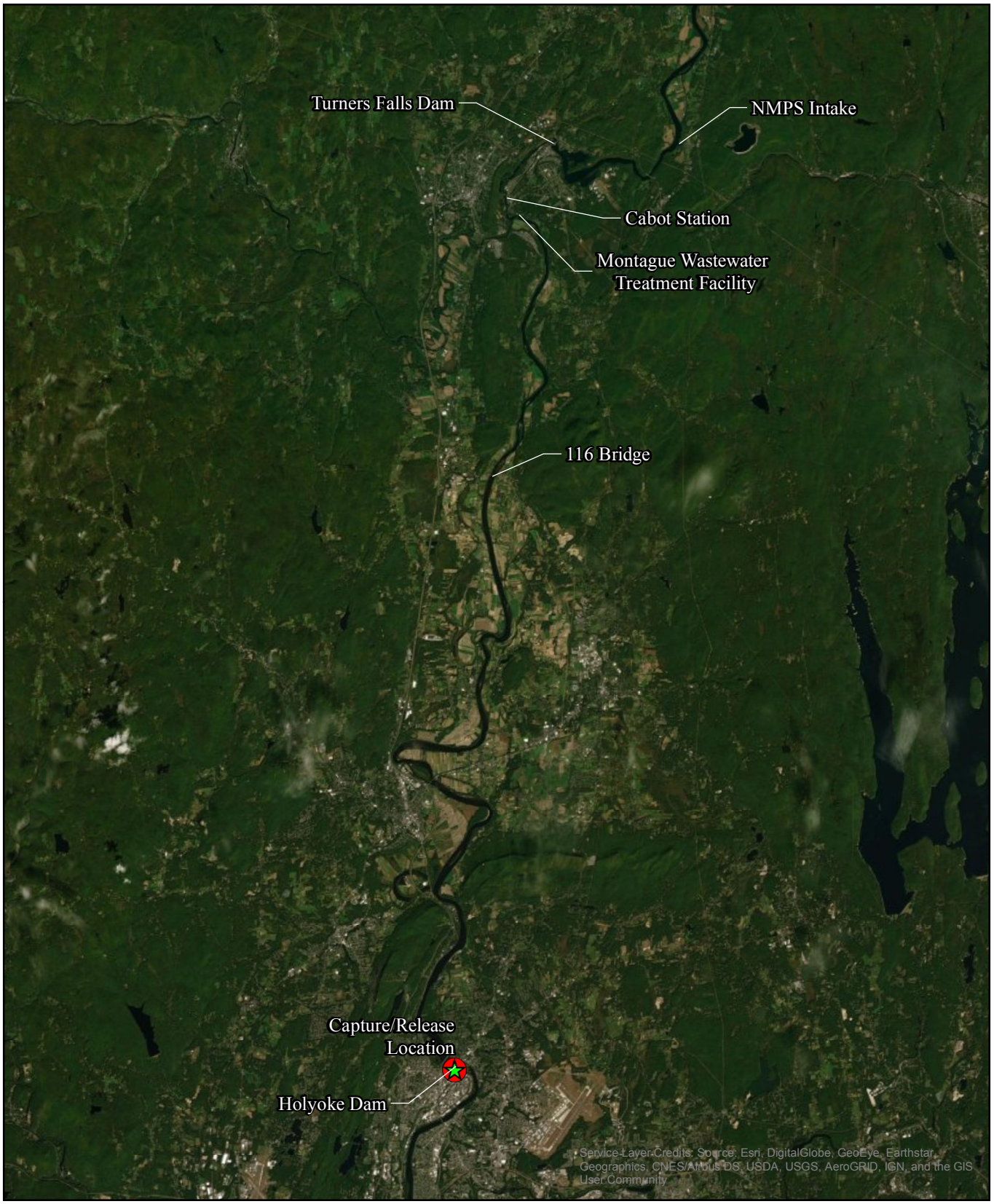

FirstLight

N

Northfield Mountain Pumped Storage Project (No. 2485) and Turners Falls Hydroelectric Project (No. 1889)

Relicensing Study 3.3.19

0 2 4 8 Miles

Figure 2-1: Overview of the study area extending from the Turners Falls Impoundment to Holyoke, MA

Path: W:\gis\studies\3_3_19\maps\2019 Figures\figure_2-1.mxd

Northfield Mountain Pumped Storage Project (No. 2485)
and Turners Falls Hydroelectric Project (No. 1889)

Relicensing Study 3.3.19

N

0 0.125 0.25 0.5 Miles

Figure 2-2:
Lower Bypass Reach Features

Path: W:\gis\studies\3_3_19\maps\ReportFigure2018\figure_2-2_bypass_features.mxd

3 METHODS

3.1 Study Design

Beginning in the first week of May 2019, FirstLight installed a series of active radio telemetry monitoring equipment within the study area. Fixed monitoring stations were installed from the area just upstream of the Holyoke Dam (Rt. 202 Bridge) to the Spillway ladder entrance just below the TFD (see Figures 3.1-1, 3.1-2 and 3.1-3 for the locations). In previous ultrasound telemetry studies, the downstream-most site was located at the Montague Wastewater Treatment facility. In 2019, three additional fixed monitoring stations were installed further downstream: at the Rt. 202 Bridge in Holyoke, at the Hatfield Wastewater Treatment facility, and Nourse Farm, which is located just downstream of Fourth Island. Fixed monitoring locations were sited to evaluate some of the specific study objectives listed in Section 2 above.

The same fixed radio telemetry stations were used to monitor shad tagged and released at Holyoke Fish Lift for the upstream movement assessment portion of this study, as well as shad tagged at the Cabot Fish ladder and released into the power canal for the downstream movement and survival assessment of the study. Fish that were tagged and released into the canal and return days or weeks later will likely have spawned further upstream and have begun emigrating downstream.

In addition, two groups of 12 (24 total) euthanized shad were tagged in mid-June and injected directly into Unit No. 2 turbine at Cabot Station via a custom pipe during low flow and high flow scenarios. The low flow scenario consisted of one unit running (Unit No. 2) and the high flow scenario consisted of five units running at Cabot Station.

3.2 Telemetry Network

FirstLight deployed 25 radio telemetry monitoring stations within the study area (Table 3.2-1, Figures 3.1-1, 3.1-2 and 3.1-3). Radio telemetry monitoring was achieved through the use of Orion receivers manufactured by Sigma Eight, and SRX 800 receivers manufactured by Lotek. Orion and Lotek receivers were deployed to maximize the effectiveness of monitoring stations. The Orion receiver is a broadband receiver capable of monitoring multiple frequencies simultaneously within a 1-megahertz (MHz) band. These receivers are particularly well-suited for monitoring tagged fish in areas where movement through a monitoring zone can occur quickly, such as intakes or bypasses. Lotek receivers are narrowband receivers that have longer detection ranges than Orion receivers. However, narrowband receivers can only monitor a single frequency at once and require frequency switching, which can result in less detection reliability in areas where fish move quickly. The telemetry receivers were powered by 12-volt deep-cycle batteries, which were maintained via alternating current or solar powered chargers.

The radio telemetry monitoring network was designed to monitor tagged shad as they migrated within the study area. Prior to initiating the study, all monitoring locations were tested for calibration to ensure that the desired detection zones were achieved. The results of the calibration efforts are detailed in Appendix A.

In addition to monitoring all tagged shad with fixed telemetry receivers, mobile tracking was employed to monitor the location of tagged euthanized shad from Cabot Station down to the Hatfield Wastewater Treatment Facility. Mobile tracking began after the 24 dead shad were tagged and released on June 12 and 13. Mobile tracking was performed weekly and extended to July 11, 2019.

Table 3.2-1: Shad monitoring locations and equipment used in the 2019 ultrasound evaluation.

Station Location	Telemetry Receiver	Station ID	RM	Receiver Station Equipment
Route 202 Bridge just upstream of Holyoke Dam	T23	S24	86.5	A Lotek SRX receiver with two 6-Element Yagis
Hatfield Wastewater	T22	S23	106.0	A Lotek SRX receiver with two 3-Element Yagis
Nourse Farm	T21	S22	117.5	A Lotek SRX receiver with 6-Element Yagi
Montague Wastewater	T01	S01	118.3	A Lotek SRX receiver with two 3-Element Yagis
Entrance to Deerfield River	T02	S02	118.8	An Orion receiver with 3-Element Yagi
Smead Island West	T03e	S03	119.0	An Orion receiver with 3-Element Yagi
Smead Island East	T03w	S04	119.0	A Lotek SRX receiver with 3-Element Yagi
Downstream Cabot Tailrace	T04	S05	119.3	An Orion receiver with 3-Element Yagi
Upstream Cabot Tailrace	T05	S06	119.3	An Orion receiver with 3-Element Yagi
Cabot Ladder Entrance	T06	S07	119.3	An Orion receiver with dipole antenna
Cabot Farfield	T07	S08	119.3	A Lotek receiver with 3-Element Yagi
Conte Discharge	T08	S09	119.7	An Orion receiver with 3-Element Yagi
Rock Dam Pool	T09	S10	120.2	An Orion receiver with 3-Element Yagi
Upstream Rock Dam	T24	S25	120.3	A Lotek receiver with 3-Element Yagi
Lower West Channel Rawson Island	T10	S11	120.2	An Orion receiver with 3-Element Yagi
Middle Channel Rawson Island	T11	S12	120.3	An Orion receiver with 3-Element Yagi
West Channel Rawson Island	T12	S13	120.4	An Orion receiver with 3-Element Yagi
Bypass Reach upstream Rawson Island	T13	S14	120.4	A Lotek SRX receiver with 6-Element Yagi
Downstream of Station No.1	T14	S15	121.1	A Lotek SRX receiver with 6-Element Yagi
Upstream of Station No.1	T15	S16	121.2	A Lotek SRX receiver with 6-Element Yagi
Spillway Ladder Entrance	T16	S17	122.2	An Orion receiver with dipole antenna
Spillway Ladder Vicinity	T17	S18	122.2	A Lotek SRX receiver with 6-Element Yagi
Cabot Forebay	T18	S19	119.3	An Orion receiver with 3-Element Yagi
Cabot Log Sluice	T19	S20	119.3	An Orion receiver with dipole antenna
Canal at Copley Tunnel	T20	S21		A Lotek SRX receiver with 3-Element Yagi

FirstLight

Northfield Mountain Pumped Storage Project (No. 2485) and Turners Falls Hydroelectric Project (No. 1889)

Relicensing Study 3.3.19

N

0 1 2 4 Miles

Figure 3.1-1: Radio Telemetry Sites for Ultrasound Array Study-Lower Connecticut River

Path: W:\gis\studies\3_3_19\maps\2019 Figures\figure_3_1-1.mxd

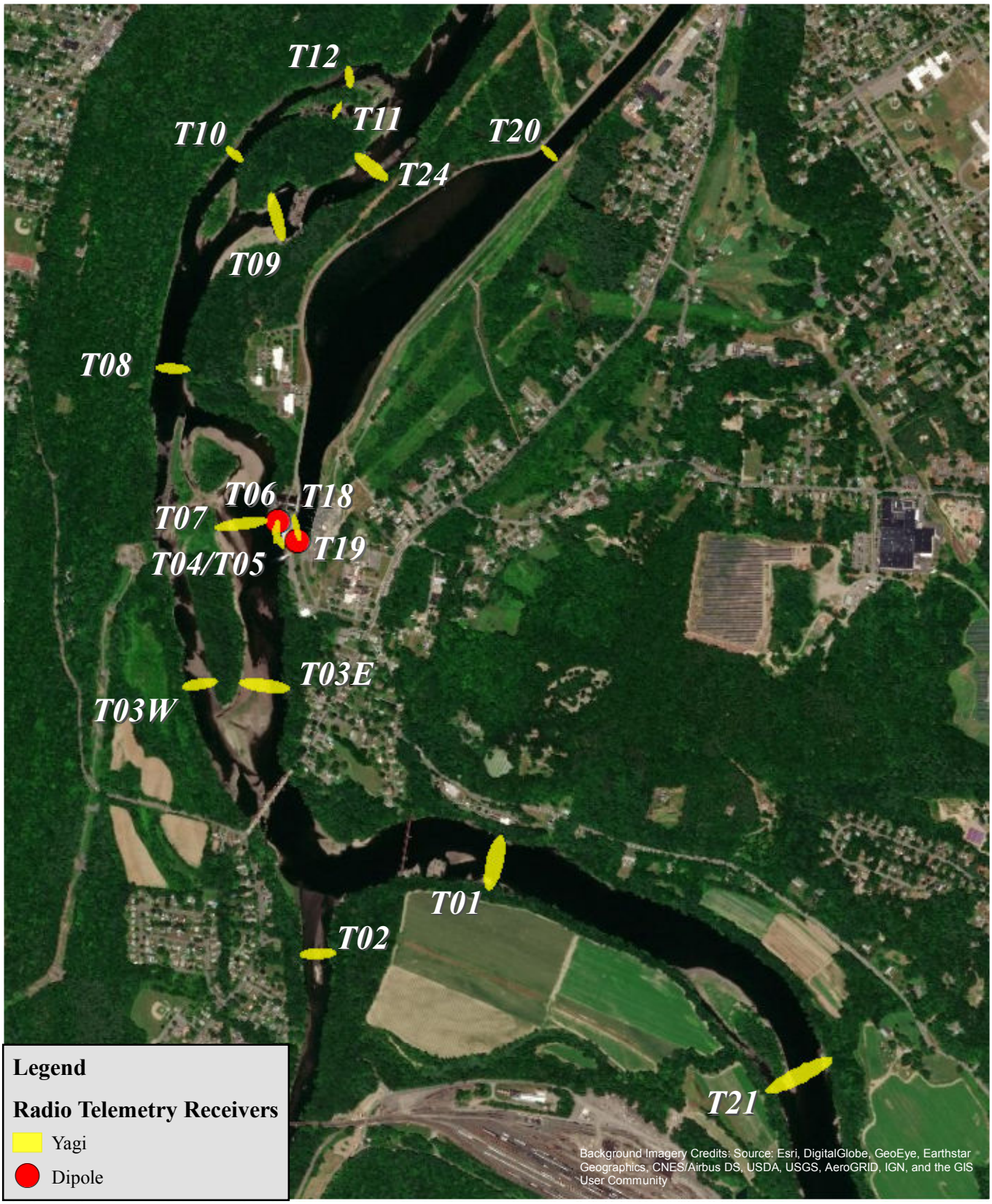

FirstLight

Northfield Mountain Pumped Storage Project (No. 2485) and Turners Falls Hydroelectric Project (No. 1889)

Relicensing Study 3.3.19

N

0 0.125 0.25 0.5 Miles

Figure 3.1-2: Radio Telemetry Sites for Ultrasound Array Study- Lower Bypass

Path: W:\gis\studies\3_3_19\maps\2019 Figures\figure_3_1-2.mxd

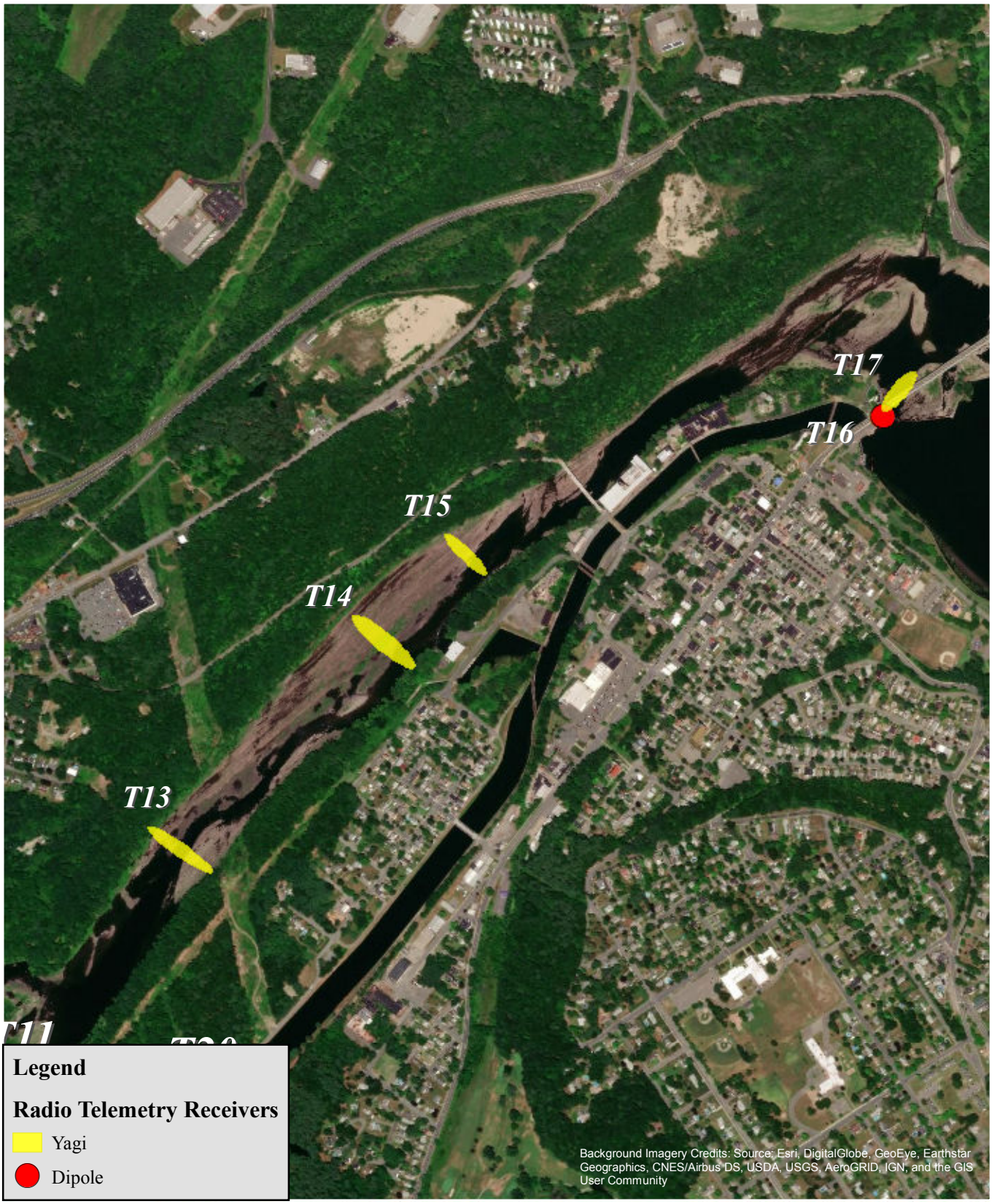

FirstLight

Northfield Mountain Pumped Storage Project (No. 2485)
and Turners Falls Hydroelectric Project (No. 1889)

Relicensing Study 3.3.19

N

0 500 1,000 2,000 Feet

Figure 3.1-3: Radio Telemetry Sites for Ultrasound Array Study- Upper Bypass

Path: W:\gis\studies\3_3_19\maps\2019 Figures\figure_3_1-3.mxd

3.3 Adult Shad Collection and Tagging

Test fish were collected and tagged at the fish trapping facilities at the Holyoke Dam and at Cabot Station. At Holyoke Dam, three cohorts were tagged and immediately released upstream of the dam via the fish lift exit flume. Tagging priority was given to the first groups of shad arriving at Holyoke based on previous telemetry study results indicating that shad arriving first are more motivated and more biologically fit to successfully make the upstream journey from Holyoke to Turners Falls, MA as compared to the fish arriving later in the migratory season. A full description of results and comparisons of tagging early and late in the season are discussed in the 2018 Ultrasound Study report. The first groups of shad captured and tagged at the Holyoke fish trapping facility were used for the upstream migrating portion of the telemetry study (n = 241). Two additional cohorts were captured and tagged at the Cabot Station fish trapping facility and released into the power canal in mid-June (n = 198). These fish represented the downstream emigrating portion of the telemetry study. An additional 24 dead shad were tagged and released directly into Cabot Station Unit #2 for the Cabot mortality portion of this study.

Tagging consisted of esophageal implantation of radio tags. Data were recorded on field data sheets and only included tag identification number for each tagged shad. No sexing or length measurements were attempted to minimize the amount of handling time associated with the tagging process. In previous telemetry studies, no fish less than 400 mm in total length was radio tagged. In 2019, although length was not measured during tagging, experienced tagging technicians visually inspected the fish to ensure tagging of an equal distribution of larger and smaller shad as representative of the male and female adult population. Previous shad telemetry studies conducted in 2015, 2016 and 2018 by FirstLight have shown that increased handling time during tagging decreases the performance of upstream migrating fish. Shad were selected at random, but only those that exhibited vigor and minimal scale loss (less than 10%, evaluated subjectively in the field) were tagged. Shad were tagged with TX-PSC-I-80-M Pisces transmitters manufactured by Sigma Eight. The tags measured 10 mm by 28 mm and operated on three frequencies, 148.340, 148.380 and 148.480 MHz. They were programed with a three-second burst and a mortality function, which defaulted to an eleven-second burst upon activation. Activation of mortality was based on relative motionlessness for a period of 15 minutes. The expected tag life was approximately 90 days.

3.4 Project Operations

A series of test flows was proposed for release into the bypass reach during the 2019 study. Bypass reach flows were split between spill at TFD and generation from Station No.1 as shown in Table 3.4-1. Note that a 50-50 flow split was not possible at a total bypass flow of 6,500 cfs because the Station No. 1 hydraulic capacity is 2,210 cfs.

Table 3.4-1: Split of Bypass Flow between TFD and Station No. 1 Generation

TFD Discharge	Station No. 1 Generation Flow	Total Bypass Flow
3,000 cfs (68%)	1,400 cfs (32%)	4,400 cfs
2,190 cfs (50%)	2,210 cfs (50%)	4,400 cfs
4,290 cfs (66%)	2,210 cfs (34%)	6,500 cfs

Flows were dependent on ambient river flow conditions. The target release flow schedule for the various bypass flow splits included in Table 3.4-1 are shown in Figure 3.4-1. The period of manipulated bypass reach flows spanned May 17 to June 28, 2019.

The bypass reach was separated into three smaller reaches (Figure 3.4-2) as defined in Study 3.3.1 *Instream Flow Habitat Assessments in the Bypass Reach and below Cabot Station* and described below:

- Reach 1: TFD to just upstream of the Station No.1 tailrace

- Reach 2: Just upstream of the Station No.1 tailrace to the upstream end of Rawson Island / Rock Dam
- Reach 3: The upstream end of Rawson Island / Rock Dam to the Montague United States Geological Survey (USGS) gage, which includes Cabot Station discharges and flow from the Deerfield River.

Flow data at 15-minute intervals in Reach 1 are shown in Figure 3.4-3. Flow sources included:

- Bascule Gate releases,
- Tainter Gate releases,
- Spillway ladder fishway (18 cfs) and attraction flow (300 cfs) releases; the combined flow was assumed to be a constant 318 cfs, and
- Estimated inflow from the Fall River[2].

Flow data at 15-minute intervals in Reach 2 are shown in Figure 3.4-4. Flow sources included:

- Inflow from Reach 1, and
- Station No. 1 generation and leakage flow; leakage was assumed to be a constant 98 cfs.

Flow data at 15-minute intervals in Reach 3 are shown in Figure 3.4-5. Flow sources included:

- Inflow from Reach 2,
- Cabot ladder fishway (33 cfs) and attraction flow (335 cfs); the combined flow was assumed to be a constant 368 cfs,
- Downstream log sluice fish passage flow (assumed to be a constant 200 cfs),
- Cabot generation flow (0 to 13,728 cfs), and
- Deerfield River flow[3] (varied between about 250 to 2,790 cfs).

Note that the total bypass flow in this study references the flow in Reach 2. Figure 3.4-6 shows the 15-minute flows at the Montague USGS gage during the study period.

In addition to regular operations listed above, Turners Falls Hydro (Eagle Creek) is authorized by the 1988 water use agreement to operate when Turners Falls canal inflows are greater than 15,000 cfs. The nominal discharge at Turners Falls Hydro is 289 cfs and in 2019 operated as follows during the fish passage season:

- 5/1/2019 00:00 to 6/4/2019 08:25, continuous operation
- 6/4/2019 08:25 to 6/6/2019, offline
- 6/6/2019 22:42 to 6/11/2019, continuous operation
- 6/11/2019 14:32 to 6/30/2019 23:59 offline

As part of Relicensing Study 3.3.1, in Reach 1 and the upper part of Reach 2, water levels and habitat suitability were modeled at different flows. A two-dimensional (2-D) hydraulic model was developed for

[2] As described in detail in the report for Study No. 3.3.1 (IFIM) on page 3-2, 15-minute flows for the Fall River were estimated by prorating, by a ratio of drainage areas, the flow recorded at the USGS Gage No. 01170100 Green River near Colrain, MA.
[3] Inflow from the Deerfield which enters the downstream portion of Reach 3 was estimated by prorating the total drainage area of the Deerfield River (665 mi^2) divided by the drainage area at USGS Gage No. 01170000 Deerfield River near West Deerfield, MA (557 mi^2).

the upstream end of the Rawson Island complex downstream to just below the Deerfield River confluence. This includes the lower part of Reach 2 and all of Reach 3. A 2-D approach best represents hydraulics in this area due to the relatively wide and shallow river channel with complex multiple-channel characteristics and hydraulics. The 2-D hydraulic modeling was performed using River2D modeling software, which is described in Steffler and Blackburn (2002). River2D is a depth-averaged two-dimensional (lateral-longitudinal), finite-element hydraulic and habitat model. Output from the River2D provides depths and velocities on a fine scale throughout the 2D modeled area, including near Rawson Island.

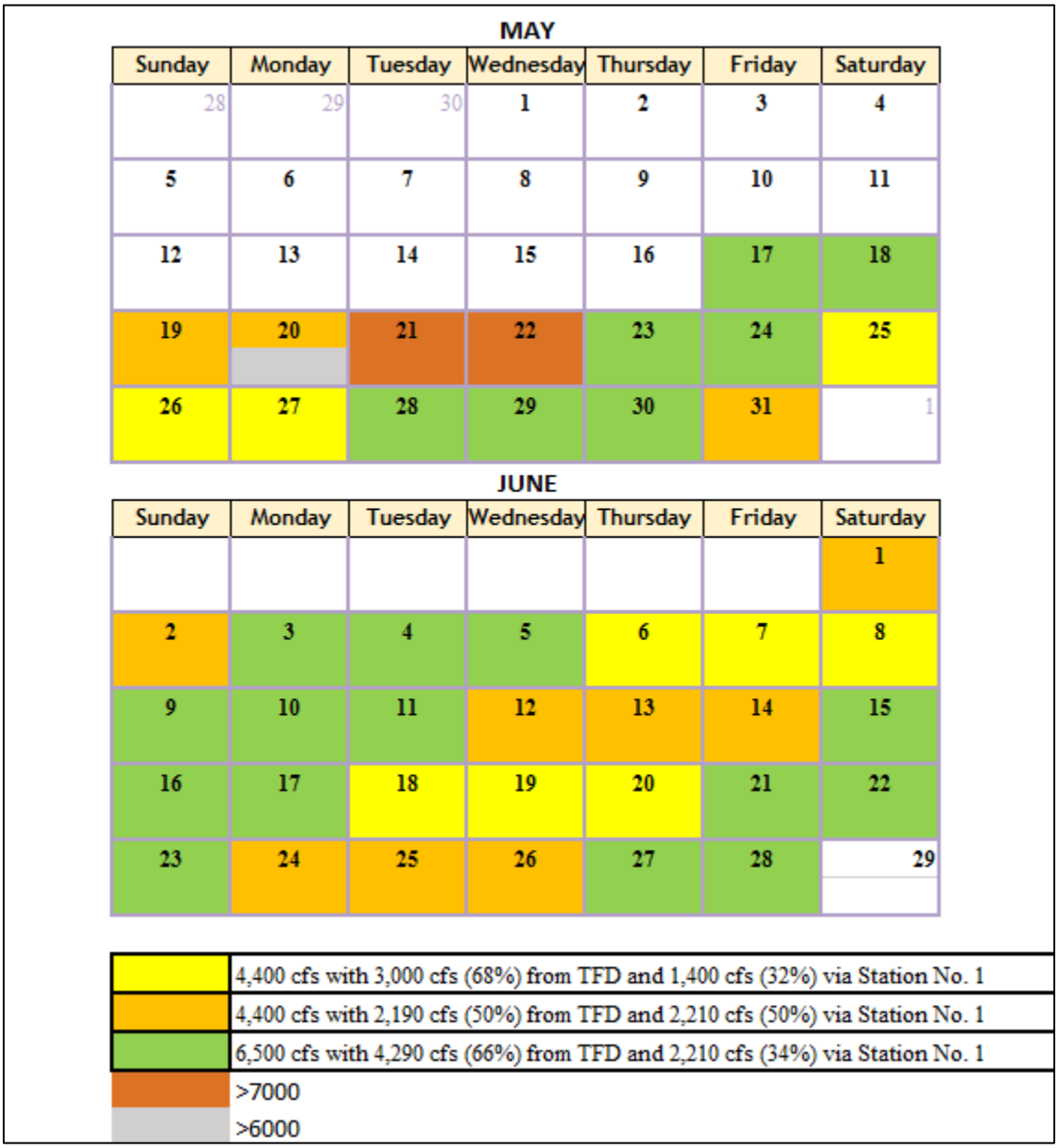

Figure 3.4-1: 2019 Ultrasound Array Flow Calendar

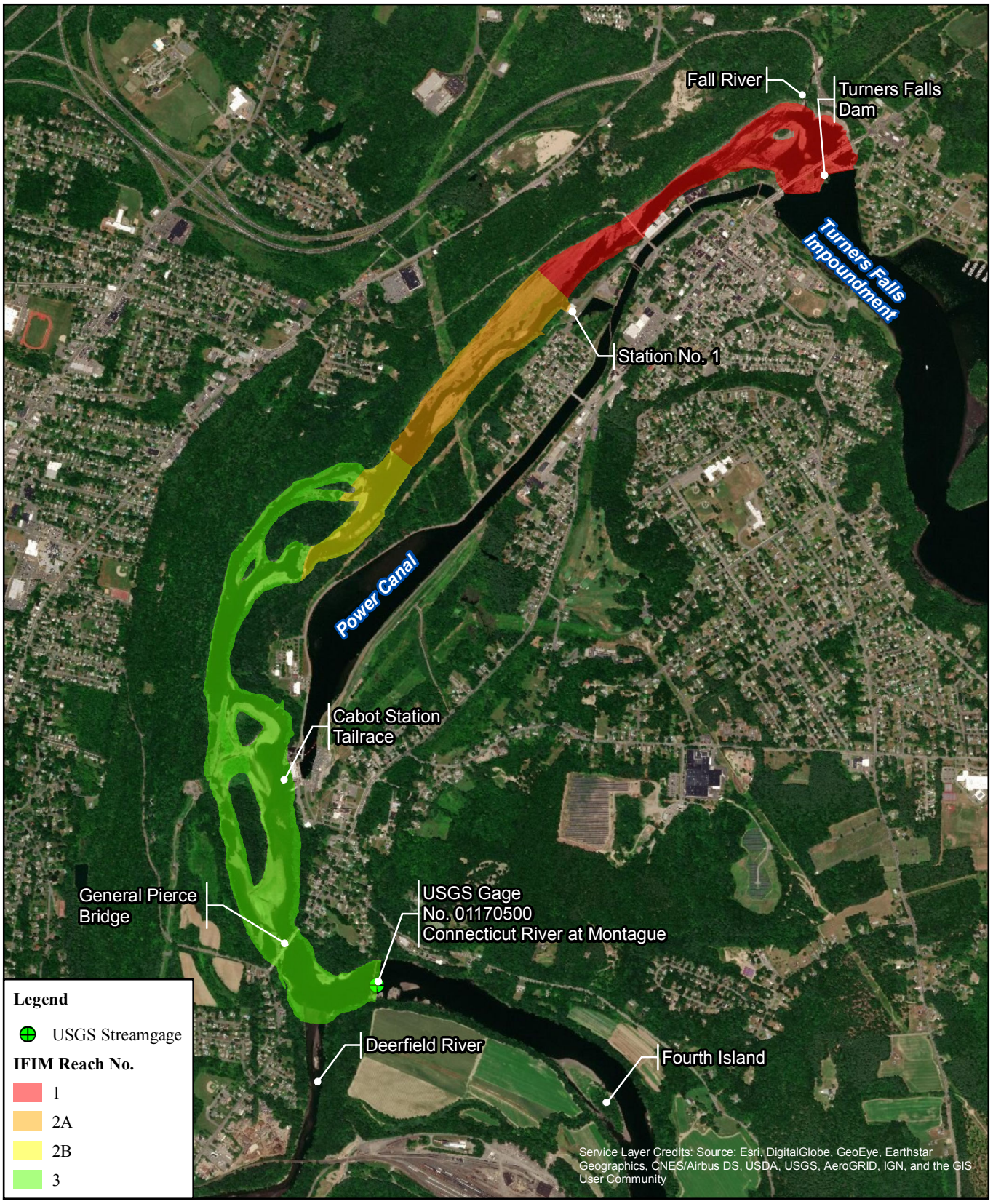

Northfield Mountain Pumped Storage Project (No. 2485) and Turners Falls Hydroelectric Project (No. 1889)

Relicensing Study 3.3.19

N

0 1,000 2,000 4,000 Feet

Figure 3.4-2:
Instream Flow Study Reach 1, 2 and 3 in the Turners Falls Bypass

Path: W:\gis\studies\3_3_19\maps\2019 Figures\figure_3_4-2.mxd

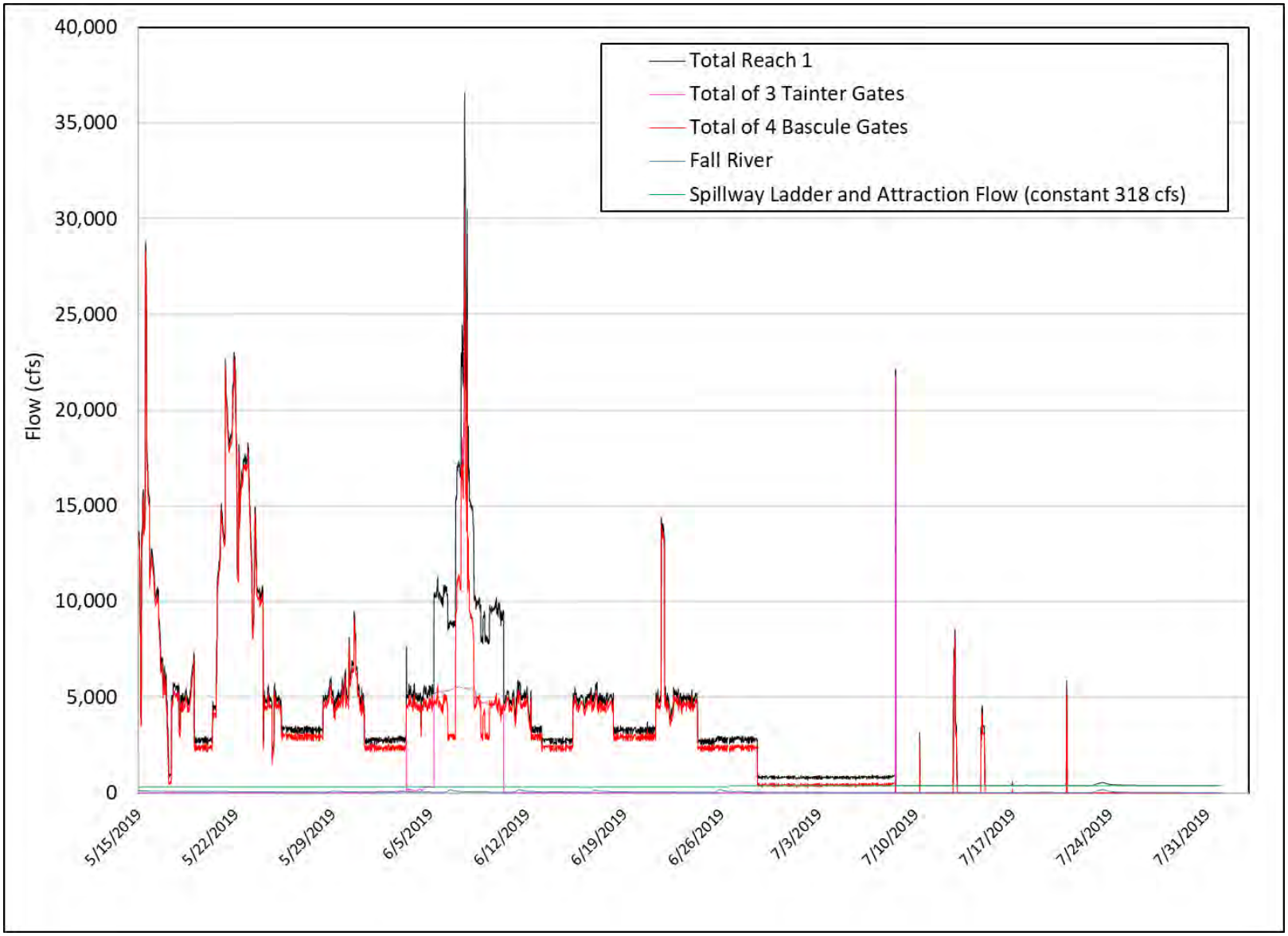

Figure 3.4-3: 2019 15-Minute Flow in Reach 1 (Turners Falls Dam to Station No.1) during Telemetry Study

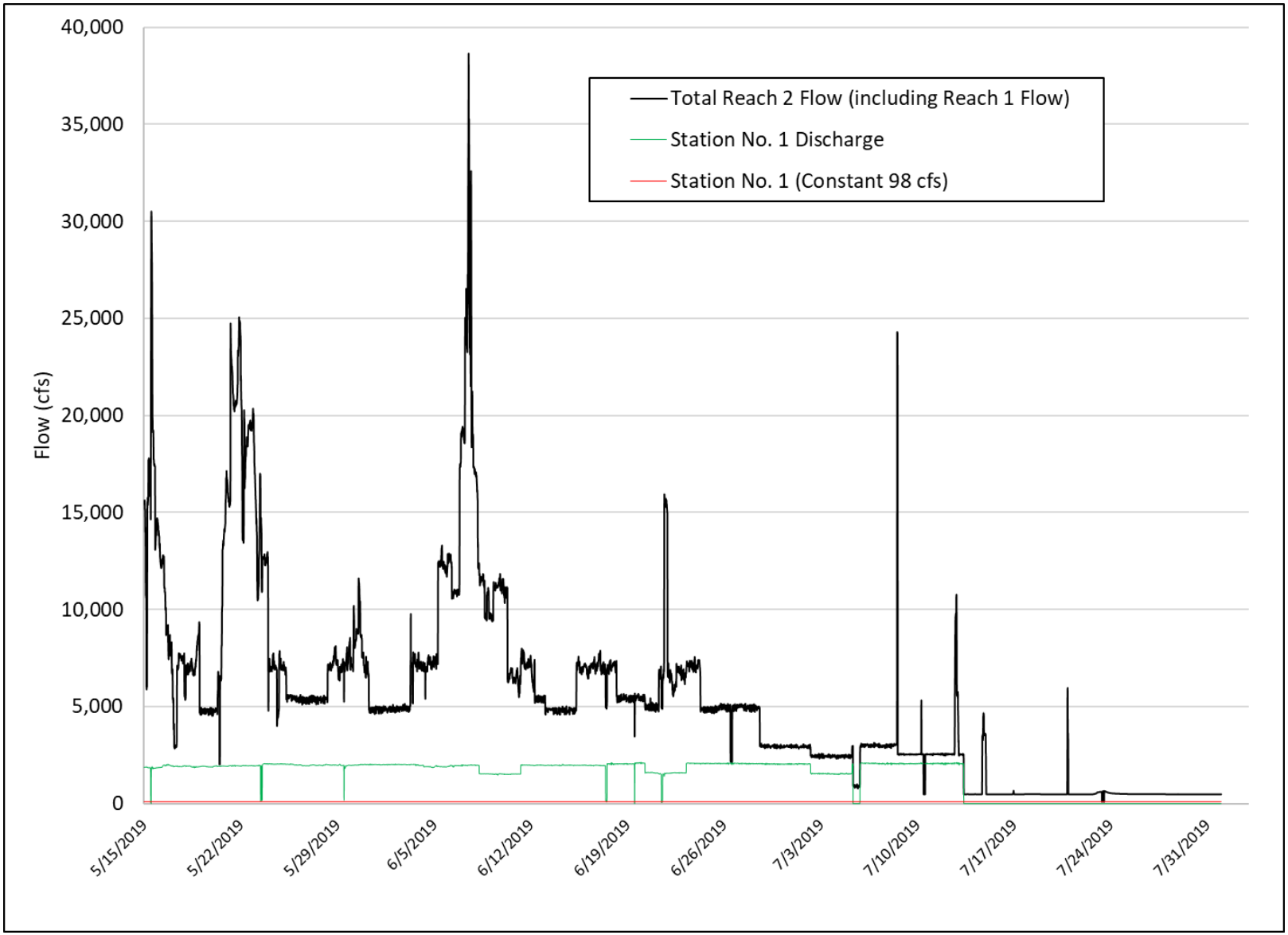

Figure 3.4-4: 2019 15-Minute Flow in Reach 2 (Station No. 1 to upstream of Rawson/Rock Dam) during Telemetry Study

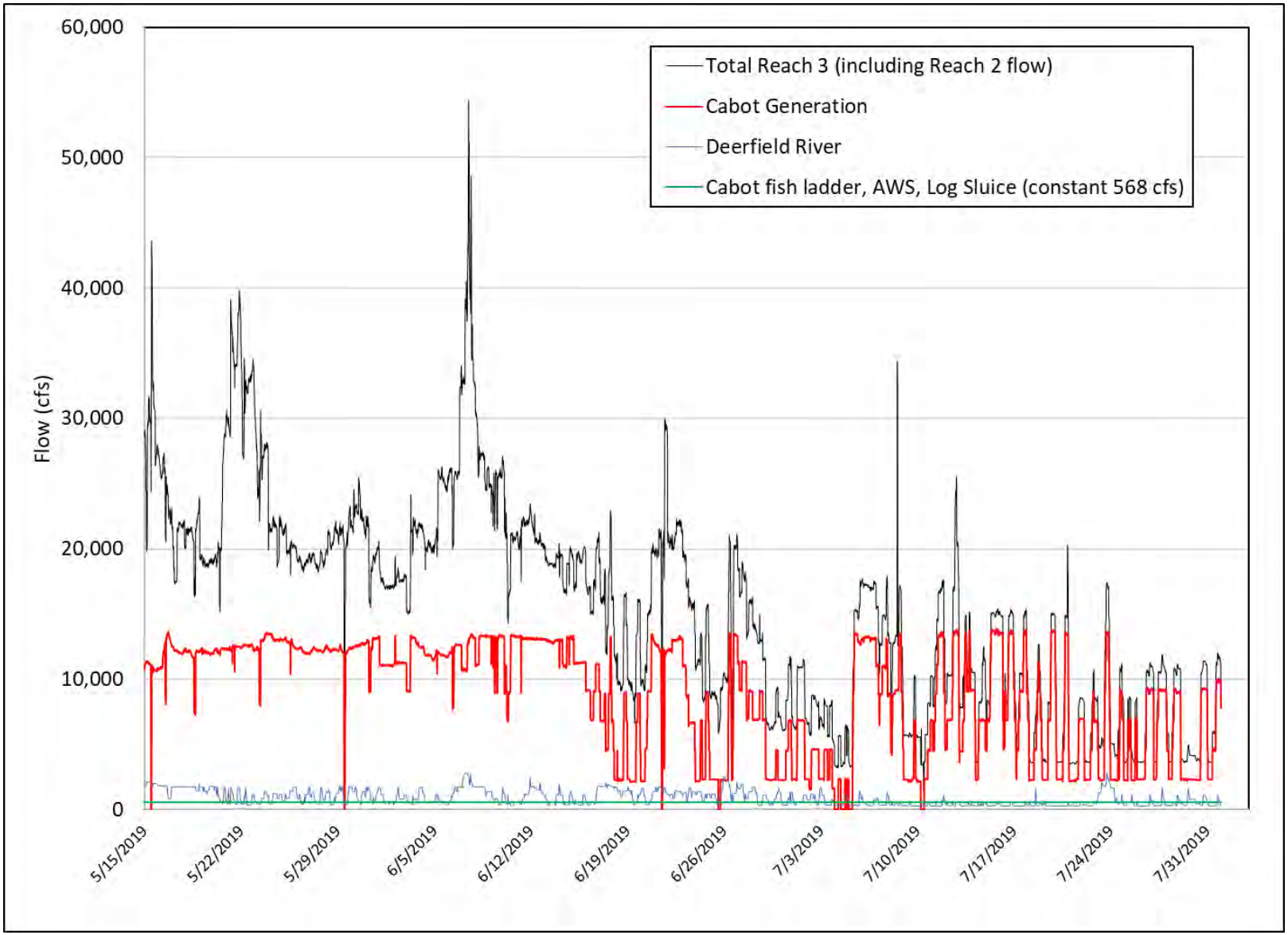

Figure 3.4-5: 2019 15-Minute Flow in Reach 3 (Rawson/Rock Dam to Montague) during Telemetry Study

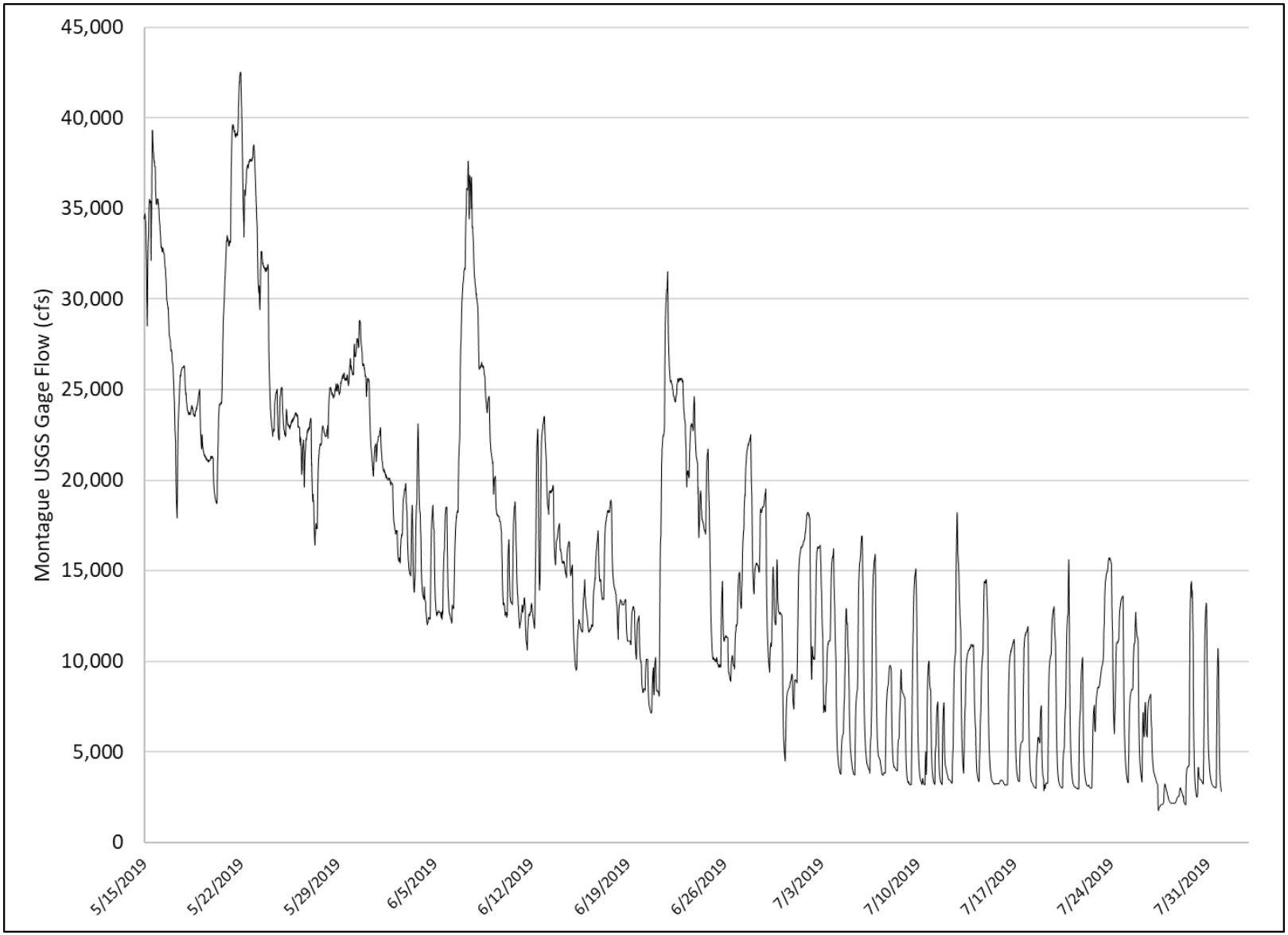

Figure 3.4-6: 2019 15-Minute Flow data at Montague USGS Gage (cfs) during Telemetry Study

3.5 Data Analysis

Large-scale, multi-objective passage studies that assess movement of anadromous fish through telemetered river-reaches are complex in nature. Further, analysis is made difficult because of the presence of false positive signals and receivers with overlapping detection zones. Considerable data cleaning is required before an assessment of movement can occur. FirstLight implemented the following protocol to analyze radio telemetry data collected for the ultrasound evaluation:

1. Identify and remove false positive detections with a Naïve Bayes Classifier,
2. Reduce overlap between detection zones,
3. Assess upstream arrival with an open population mark recapture model,
4. Assess movement with time-to-event analysis using a competing risks framework,
5. Assess downstream survival with a Live Recapture Dead Recovery mark recapture model.

A complete synopsis of the data reduction and statistical methods applied, as well as assumptions used, is provided in Appendix B (Statistical Methods).

In short, FirstLight developed competing risks models to describe movement through the project area. Competing risk models assessed movement within the Cabot Station tailrace area and bypass reach using movement data from 2015, 2016, 2018, and 2019. For the purposes of this report, movement occurs between two telemetered reaches. The models always assume movement from an initial location. The initial state for the tailrace model was considered as the Cabot Station tailrace (T04/T05), while the initial state for the bypass movement model was the Conte Discharge (T08). The counting process style data were arranged so that the first detection for every fish was always in the initial state. However, assumptions were relaxed on absorbing states, and we allowed movement back into the initial state to be enumerated as well. These secondary movements were queried out of the initial competing risks assessment using methods of Therneau, Crowson, and Atkinson (2016 and 2017) and with data frame filtering in R. The bypass movement model was also bolstered with data from the 2015, 2016, and 2018 telemetry studies. Random effects associated with the tagging year were controlled with a covariate (*tag year*). We felt it appropriate to combine datasets and bolster statistical power for this assessment and to provide before/after comparisons of movement with and without the ultrasound array present.

The Cox Proportional Hazard regression movement models included several environmental and operational variables that could potentially influence tagged shad movement in the Project area. Many variables are self-explanatory, such as project operations (Cabot discharge, bypass flow, etc). Environmental variables include degree days (day°), which counted the number of days when the mean daily temperature was greater than a threshold. We used a day° of 10° C because American Shad enter the Connecticut River between 10 and 12°C (Collette and Klein-MacPhee 2002). Thus, day represents the potential maximum number of days a fish has been in the river.

FirstLight also conducted a long-run frequency analysis on daily ladder counts at Holyoke and Turners Falls Dams (1989 – 2019) to describe the timing, magnitude and duration of the American Shad run on the Connecticut River. The statistic of interest was the cumulative percentage of run total, which makes it possible to compare the timing of the migratory run between years. In the Connecticut River, mature adults move into the river typically during late March or April, reaching Cabot Station in late April or early to mid-May (Collette and Klein-MacPhee 2002). During the upstream migration, river water temperatures generally range from 12 to 20°C, with spawning occurring from 14 to 23°C (Collette and Klein-MacPhee 2002). River flow is generally declining from the spring peak during the run and water temperature is generally rising. FirstLight used information from the studies conducted in 2015, 2016, 2018 and 2019, as

well as long-term passage count trends and temperature datasets to draw conclusions on the timing of migratory secession.

4 RESULTS AND DISCUSSION

4.1 Shad Tagging

In total, 241 American Shad were collected, tagged, and released upstream via the fish lift exit flume at Holyoke Dam for the upstream portion of the study. Tagging and release dates occurred in three batches: May 14 (n=74), May 17 (n=101), and May 20, 2019 (n=66). An additional 198 shad were captured and tagged at the Cabot fish ladder trap, after ascending the Cabot fish ladder, and released into the power canal on May 31 (n=103), and June 4, 2019 (n=95) for the downstream emigration portion of the study. The third tagging component of the study included tagging 24 euthanized adult American Shad collected from Holyoke and injected into Cabot Station Unit No. 2 to be mobile tracked downstream upon release (Table 4.1-1).

Table 4.1-1: Summary of American Shad tagged for use in the Ultrasound Study

Date	Number of Shad Tagged	Tag Frequency	Capture Location	Release Location	Study Component
5/14/2019	74	148.340 (n=25) 148.380 (n=25) 148.480 (n=24)	Holyoke	Holyoke	Upstream Migration
5/17/2019	101	148.340 (n=25) 148.380 (n=25) 148.480 (n=51)	Holyoke	Holyoke	Upstream Migration
5/20/2019	66	148.340 (n=30) 148.380 (n=30) 148.480 (n=6)	Holyoke	Holyoke	Upstream Migration
5/31/2019	103	148.340 (n=35) 148.380 (n=35) 148.480 (n=33)	Cabot	Cabot Canal	Downstream Emigration
6/4/2019	95	148.340 (n=17) 148.380 (n=37) 148.480 (n=41)	Cabot	Cabot Canal	Downstream Emigration
6/12/2019	12 (dead)	148.340 (n=12)	Holyoke	Cabot Canal	Dead Drift Evaluation
6/13/2019	12 (dead)	148.340 (n=12)	Holyoke	Cabot Canal	Dead Drift Evaluation

4.2 Long Term Migratory Ladder Counts (1989 – 2019)

FirstLight conducted a long run frequency analysis on daily passage counts at Holyoke and Turners Falls Dams (1989 – 2019) to describe the timing, magnitude and duration of the American Shad run on the Connecticut River. The statistic of interest was the cumulative percentage of run total, which makes it possible to compare the migratory run between years. The box and whisker plots shown in Figure 4.2-1 demonstrate that most of the fish arrive and pass between calendar weeks 20 and 24 at both Turners Falls and Holyoke. The highest median counts on average occurred in calendar week 20 at Holyoke and by week 22 at Turners Falls. The box and whisker plots provided an overview of the long-term average counts by calendar week; however, they do not allow for comparison of the runs across years or an understanding of how quickly the run progresses through time at each facility.

The cumulative percentage plot Figure 4.2-2 shows that a majority of the American Shad run occurs within a short amount of time at each passage facility, with heavy tails at either end of the distribution. The tails indicate that the run takes weeks to reach 25% of the total count, while the middle 50% occurs in just days, and the final 25% again takes multiple weeks. From this plot, it appears that on average, over the last 18 years, most of the run occurred between May 9 and June 9. Holyoke's season appears to be better defined

and less variable than that of the Turners Falls facilities. However, when viewing the line color gradation, one may note that the timing of the run at Turners Falls (especially at Gatehouse) appears to have begun earlier in recent years, suggesting that delay has been decreasing with time.

Figure 4.2-3 shows the magnitude of the run at the Gatehouse ladder as a function of the magnitude of the run at Holyoke and depicts a number of management successes. Generally, as the run at Holyoke increases, so does the run at Gatehouse. Passage improvements at Holyoke clearly demonstrate that there are more fish in the Connecticut River between Holyoke and Turners Falls, MA. The figure also shows that passage rates at Cabot have improved over the last 17 years. Note, the points on the figure get lighter as we move farther from the year 2000. In the first few years after 2000, the proportion of fish that passed Cabot was much smaller than in more recent years. For example, in 2002, 335,411 fish passed Holyoke while only 7,922 passed Cabot (2%). In 2017, 303,142 fish passed Holyoke, while 43,269 fish passed Cabot (14%). Over that 15-year range, Cabot station went from passing just 2% of the Holyoke count to passing over 14% of total passage at Holyoke. Management successes have not only increased the magnitude of the run at Cabot, but they have also worked to decrease delay.

Following the visual inspection of the cumulative percentage plots, we divided the adult American Shad run at Cabot and Holyoke into cumulative percentage thresholds of 0 to 25%, 25% to 50%, 50% to 75% , 75% to 90%, and from 90% to 100%. Table 4.2-1 lists the first and last day of each cumulative proportion threshold at Cabot, while Table 4.2-2 lists the dates of the same milestones at Holyoke. It is apparent that some thresholds were reached much faster than others and that on average, the duration of each threshold was shorter at Cabot. From 2000 to 2017, the American Shad run on average starts on April 20 and ends on July 13 at Holyoke, while the run at Cabot ladder on average starts later on May 8 and ends earlier by July 1. The time until the 25th cumulative percentile is reached at Holyoke averages 24.6 while only 13.6 days at Cabot. Then, it only takes another 4.4 days to reach the 50th percentile at Cabot and 6.3 days at Holyoke. The 75th percentile is reached in an additional 5.9 days at Cabot while Holyoke takes on average another 5.8 days to meet the 75th percentile. The 90th percentile occurs 5.6 days later at Cabot and 6.5 days later at Holyoke. The final 10% of the run takes on average 20.9 days at Cabot and 36.3 days at Holyoke.

Most of the American Shad passage (90%) at the Cabot ladder has historically occurred within just 20 days, and it appears to be confined from mid-May to early-June, or more specifically, May 21 to June 9. The proportion of Holyoke fish that pass Cabot Station has increased since 2000, and the timing of run milestones has come earlier at Cabot station, suggesting that delay has also been decreasing since 2000 while the facility has improved passage rates.

Table 4.2-1 Identifies specific run milestones at Cabot Ladder (2000 - 2017)

	25th Percentile			25th - 50th Percentile			50th - 75th Percentile			75th - 90th Percentile			90th - 100th Percentile		
Year	**First Day**	**Last Day**	**Duration (d)**	**First Day**	**Last Day**	**Duration (d)**	**First Day**	**Last Day**	**Duration (d)**	**First Day**	**Last Day**	**Duration (d)**	**First Day**	**Last Day**	**Duration (d)**
2000	May 10	Jun 1	22	Jun 2	Jun 3	1	Jun 4	Jun 12	8	Jun 13	Jun 20	7	Jun 21	Jul 2	11
2001	May 14	May 23	9	May 24	June 28	4	May 29	Jun 1	3	Jun 2	Jun 14	12	Jun 15	Jun 25	10
2002	May 10	May 28	18	May 29	May 31	2	Jun 1	Jun 2	1	Jun 3	Jun 4	1	Jun 5	Jul 1	26
2004	May 5	May 15	10	May 16	May 18	2	May 19	May 22	3	May 23	Jun 9	17	Jun 10	Jun 26	16
2005	May 13	May 22	9	May 23	Jun 6	14	Jun 7	Jun 9	2	Jun 10	Jun 11	1	Jun 12	Jun 17	5
2006	May 6	May 29	23	May 30	May 31	1	Jun 1	Jun 9	8	Jun 10	Jun 19	9	Jun 20	Jun 29	9
2007	May 13	May 26	13	May 27	May 29	2	May 30	May 30	0	May 31	Jun 7	7	Jun 8	Jul 1	21
2008	May 14	May 18	4	May 19	May 26	7	May 27	Jun 1	5	Jun 2	Jun 6	4	Jun 7	Jun 29	24
2009	May 9	May 22	13	May 23	May 24	1	May 25	Jun 5	11	Jun 6	Jun 10	4	Jun 11	Jun 30	19
2010	May 4	May 22	18	May 23	May 26	3	May 27	May 31	4	Jun 1	Jun 7	6	Jun 8	Jul 6	28
2011	May 13	May 23	10	May 24	May 27	3	May 28	Jun 6	9	Jun 7	Jun 8	1	Jun 9	Jul 6	27
2012	Apr 18	May 19	31	May 20	May 23	3	May 24	May 26	2	May 27	May 28	1	May 29	Jun 2	34
2013	May 3	May 8	5	May 9	May 12	3	May 13	May 20	7	May 21	Jun 2	12	Jun 3	Jun 28	25
2014	May 11	May 15	4	May 16	May 26	10	May 27	Jun 5	9	Jun 6	Jun 9	3	Jun 10	Jul 1	21
2015	May 6	May 11	5	May 12	May 18	6	May 19	May 27	8	May 28	May 31	3	Jun 1	Jun 27	26
2016	Apr 26	May 14	18	May 15	May 25	10	May 26	May 30	4	May 31	Jun 3	3	Jun 4	Jul 7	33
2017	May 1	May 20	19	May 21	May 24	3	May 25	Jun 10	16	Jun 11	Jun 15	4	Jun 16	Jul 6	20
Min			4			1			0			1			5
Median			13			3			5			3			21
Mean	May-8	May-21	13.6	May-22	May-27	4.4	May-28	Jun-3	5.9	Jun-4	Jun-9	5.6	Jun-10	Jul-1	20.9
Max			31			14			16			17			34

Table 4.2-2 Identifies specific run milestones at Holyoke (2000 - 2017)

	25th Percentile			25th - 50th Percentile			50th - 75th Percentile			75th - 90th Percentile			90th - 100th Percentile		
Year	**First Day**	**Last Day**	**Duration (d)**	**First Day**	**Last Day**	**Duration (d)**	**First Day**	**Last Day**	**Duration (d)**	**First Day**	**Last Day**	**Duration (d)**	**First Day**	**Last Day**	**Duration (d)**
2000	Apr-17	May-18	31	May-19	May-26	7	May-27	Jun-2	6	Jun-3	Jun-10	7	Jun-22	Jul-7	26
2001	May-7	May-10	3	May-11	May-15	4	May-16	May-22	6	May-23	May-29	6	May-30	Jul-6	37
2003	Apr-18	May-11	28	May-12	May-25	13	May-26	May-30	4	May-31	Jun-2	2	Jun-3	Jul-11	38
2002	Apr-3	May-18	45	May-19	May-24	5	May-25	Jun-2	8	Jun-3	Jun-8	5	Jun-9	Jul-15	36
2004	Apr-21	May-12	21	May-13	May-16	3	May-27	May-20	3	May-21	Jun-3	13	Jun-4	Jul-7	28
2005	Apr-20	May-15	25	May-16	May-19	3	May-20	Jun-03	14	Jun-4	Jun-6	2	Jun-7	Jul-18	41
2006	Apr-4	May-8	34	May-9	May-27	18	May-28	May-30	2	May-31	Jun-14	14	Jun-15	Jul-14	29
2007	May-2	May-23	21	May-24	May-25	1	May-26	May-27	1	May-28	May-31	3	Jun-1	Jul-15	44
2008	Apr-29	May-15	16	May-16	May-19	3	May-20	May-25	5	May-26	May-31	5	Jun-1	Jul-11	40
2009	Apr-23	May-16	23	May-17	May-21	4	May-22	May-29	7	May-30	Jun-6	7	Jun-7	Jul-24	47
2010	Apr-9	May-13	34	May-14	May-17	3	May-18	May-23	5	May-24	May-31	7	Jun-1	Jul-13	42
2011	May-5	May-13	8	May-14	May-24	10	May-25	Jun-2	8	Jun-3	Jun-4	1	Jun-5	Jul-15	40
2012	Apr-5	May-7	32	May-8	May-19	11	May-20	May-25	5	May-26	Jun-1	6	Jun-2	Jul-8	36
2013	Apr-18	May-8	20	May-9	May-16	7	May-17	May-21	4	May-22	Jun-2	11	Jun-3	Jul-17	44
2014	Apr-25	May-16	21	May-17	May-25	8	May-26	Jun-2	7	Jun-3	Jun-7	4	Jun-8	Jul-15	37
2015	Apr-29	May-11	12	May-12	May-17	5	May-18	May-25	7	May-26	May-6	11	Jun-7	Jun-21	14
2016	Apr-1	May-12	41	May-13	May-17	4	May-18	May-25	7	May-26	May-31	5	Jun-1	Jul-15	44
2017	Apr-24	May-21	27	May-22	May-27	5	May-28	Jun-3	6	Jun-4	Jun-12	8	Jun-13	Jul-14	31
Min			3			1			1			1			14
Median			24			5			6			6			37.5
Mean	Apr-20	May-15	24.6	May-16	May-22	6.3	May-23	May-29	5.8	May-30	Jun-5	6.5	Jun-6	Jul-13	36.3
Max			45			18			14			14			47

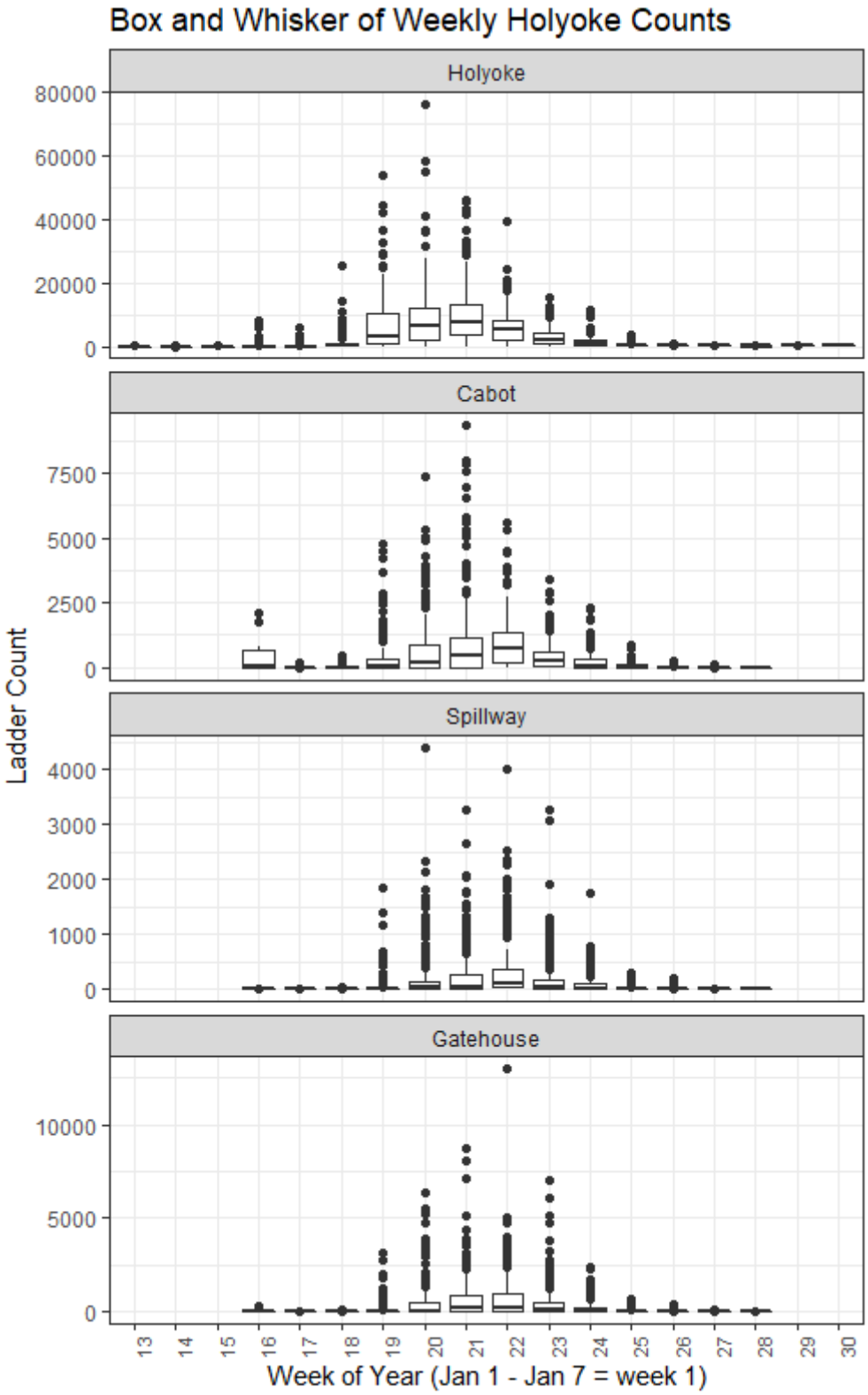

Figure 4.2-1 Box and whisker plots of passage counts by calendar week and fishway. Note a majority of passage occurs within weeks 20 to 24 at all facilities.

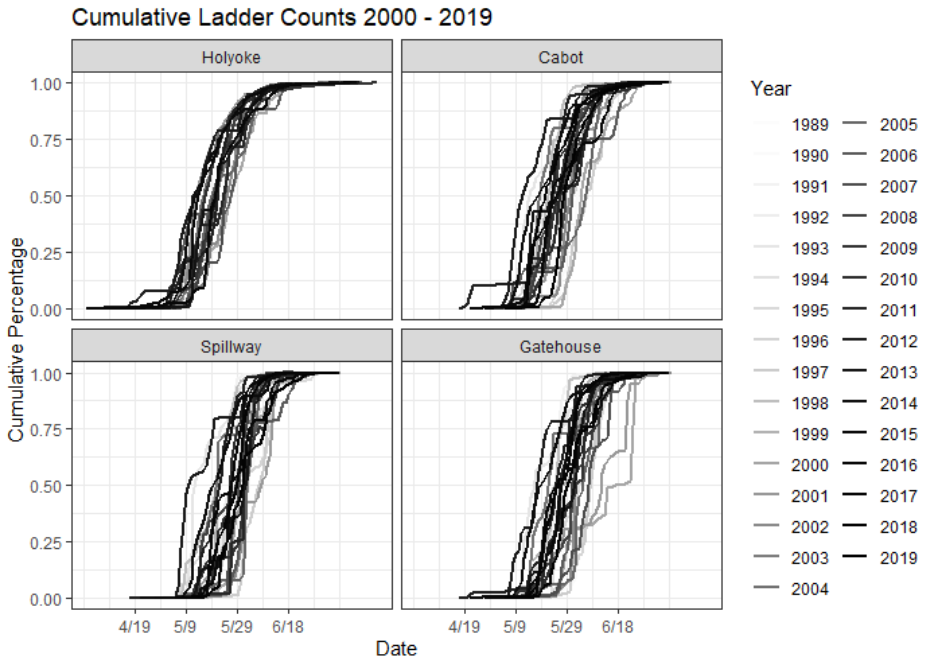

Figure 4.2-2. Cumulative percentage plots at Connecticut River fish passage structures for the past 30 years.

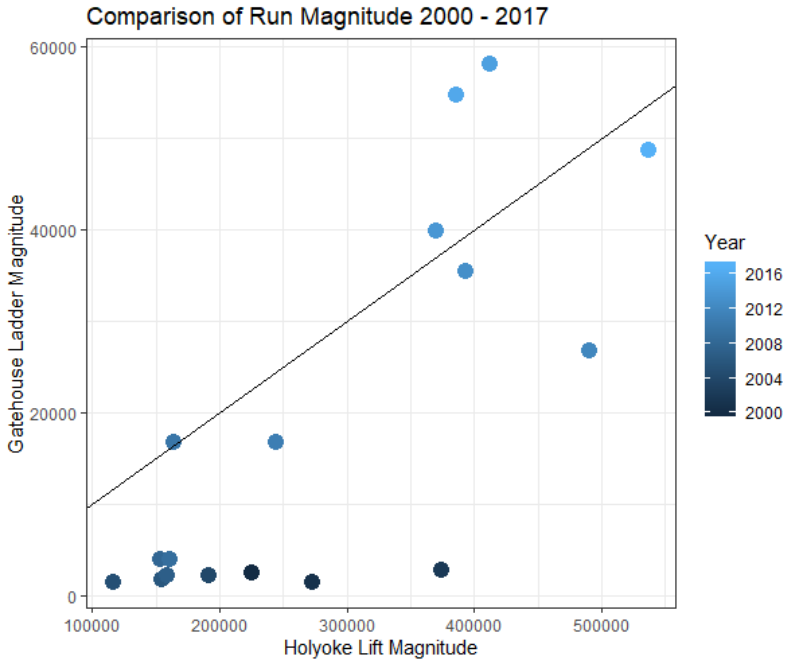

Figure 4.2-3. Gatehouse Ladder counts as a function of Holyoke counts (2000-2017). Note as time progressed and passage at project improved, a much larger percentage of the Holyoke run passed by the project. The diagonal line represents 10% of the Holyoke Run passing Gatehouse.

4.3 Telemetry Analysis: Upstream and Downstream Movement

4.3.1 Project Arrival to TFD Spillway

The probability that a tagged fish will arrive in the spillway was assessed with a combination of CJS mark recapture modeling and time-to-event analysis using a competing risks framework. Recapture histories from 2015, 2018 and 2019 were aggregated to improve the precision of the model's estimate of spillway arrival. Data from 2016 were not used because we lacked a set of receivers that could reliably identify fallback fish. A fish was considered as a "fallback" if it did not reach the Project from the release site while exhibiting downstream movement in the telemetry record. For 2015, 2018 and 2019, the release location was Holyoke. The first recapture occasion was Montague, the second was the tailrace area (including Smead Island and tailrace receivers), the third was the entrance to the bypass reach upstream of the discharge from Conte, and the fourth and final recapture occasion was the spillway area. In every study year, FirstLight had telemetry receivers occupying each of these recapture locations, allowing for comparison of arrival rates across years using a single cohort model with tag-year as a covariate.

In 2015, of the 155 fish that did not fall back, 25 (16%) were recaptured in the spillway. In 2018, 183 fish were released (non-fallback) and 33 (18%) arrived in the spillway. In 2019, 137 fish were released (non-fallback) and 39 (28%) arrived in the spillway. Table 4.3.1-1 contains a list of raw recaptures across study years. Appendix D contains the recapture histories of all fish used in the CJS model. Four models were tested in MARK (Table 4.3.1-2), the model with the lowest AIC had fully dependent location and cohort arrival rates with single year cohort specific recapture rates.

Overall, recapture of non-fallback fish was lowest in 2019 at 83%, while 2018 resulted in the highest rates of recaptured non-fallback fish (98%). Even though recapture at Montague was low in 2015, the study year saw 91% of the fish being recaptured within the Project area. The lowest rate of project arrival occurred in 2015, when only 63% (45 - 78% CI) arrived at Montague. In subsequent years, the rate of project arrival increased to 75% (59 - 86% CI) in 2018 and 73% (63 – 81%) in 2019. Note, in 2015 fish were tagged throughout the passage season at Holyoke, while in 2018-19, only early arrivals were tagged. The probability that a tagged fish recaptured at the Conte discharge will arrive at the spillway ranged from 39% (19 - 63% CI) in 2018 to 49% (20 - 79% CI) in 2015. Note the wide range in CI's suggesting no significant difference between years. Cumulative survival rates (release at Holyoke to spillway arrival) ranged from 18% (2018) to 22% (2019). The rates of spillway arrival, given that a fish has arrived at the project, (Tailrace * Conte * Spillway) was no different between 2019 (30.6%) or 2015 (30.8%). Table 4.3.1-3 lists all arrival rates (φ).

Following the analysis of overall upstream movement to the spillway with a CJS, a competing risks analysis assessed movement from project arrival (Montague WWTP) to the spillway, and regressed against a series of time dependent covariates with Cox Proportional Hazards (CoxPH) regression modeling. Between 2015, 2018 and 2019, 308 fish arrived at the project and 92 transitioned to the spillway (92/308 = 29%). These numbers are in-line with the CJS model, which found between 24% and 31% of the fish that arrive at the project will subsequently arrive at the spillway. Of the fish to transition to the spillway, 50% did so in 42.04 hours or less (Table 4.3.1-4). The Kaplan-Meier survival curve (Figure 4.3.1-1) depicts approximately 50% of the fish remaining within the lower project area after 600 hours, with most of the transitions (to spillway or elsewhere) occurring in 100 hours or less.

A series of CoxPH regression models were fit to time dependent covariates in an effort to understand what factors increased the likelihood that a tagged shad will migrate to the spillway from the entrance of the project. The best model, with the lowest AIC, incorporated additive effects from the Cabot-to-bypass discharge ratio, accumulated thermal units (day° 10°C), the 48-hour rolling variance, and quarter day increments. While the best model did not have a specific flow release component, the Cabot-to-bypass discharge ratio is an important operational variable, because the larger the ratio, the less the bypass reach

will attract fish (HR = 0.76). This ratio is calculated by dividing Cabot discharge by flow through the bypass reach. Figure 4.3.1-2a (histogram) shows a majority of the fish transitioning when this ratio is below 2.5. Figure 4.3.1-2b shows the residence time of each fish according to the Cabot-to-bypass flow ratio where the deeper reds mean a higher ratio. One fish took over 800 hours to move from the project entrance to the spillway and it did so at the highest flow ratio. Figure 4.3.1-2c depicts residence time as a function of day° (10°C). Longer duration transitions appear to be associated with hotter periods (HR = 0.48). Note, day° were transformed with a square root transformation. Figure 4.3.1-2d depicts residence time as a function of the 48-hour rolling variance. The higher the variance, the more volatile the flow has been over the past 48 hours. The last fish to transition did so in over 800 hours, and it appears to be an influential observation, because the estimated hazard ratio for 48-hour rolling variance is 1.03, suggesting the likelihood of a fish migrating to the spillway increases with the variance. However, the previous residencies suggest that higher variance leads to longer transitions. We did not assess this model with the influential observation removed. Finally, the best model was also a function of quarter day increments, which suggests the optimal time of day that transitions occur is between 12:00 and 18:00 (HR = 17.36) (Appendix C).

Table 4.3.1-1: Raw recaptures across study year (2015, 2018, 2019), excluding fallback fish

Year	Release	Project	Tailrace	Conte	Spillway
2015	155	70	89	54	25
2018	183	134	118	85	33
2019	137	106	74	72	39

Table 4.3.1-2: Model selection summary statistics, note best model as the lowest QAIC score.

Model	QAICc	Delta QAICc	AICc Weights	Model Likelihood	Num. Par	QDeviance
{Phi(cxt)p(cx.)}	640.2	0.0	0.9	1.0	14.0	32.9
{Phi(cxt)p(cxt)}	645.9	5.7	0.1	0.1	20.0	26.4
{Phi(cx.)p(cxt)}	649.0	8.8	0.0	0.0	14.0	41.7
{Phi(cx.)p(cx.)}	664.3	24.1	0.0	0.0	6.0	73.1

Table 4.3.1-3: Summary statistics from the best model showing rate of arrival

{Phi(cxt)p(cx.)}	Parameter	Estimate	Standard Error	Lower 95% CI	Upper 95% CI
	1:Project Arrival	0.73	0.05	0.63	0.81
	2:Tailrace	0.89	0.04	0.77	0.95
	3:Bypass Reach	0.72	0.06	0.58	0.83
Cohort1: 2019	4:Spillway	0.48	0.08	0.32	0.64
	5:Project Arrival	0.75	0.07	0.59	0.86
	6:Tailrace	0.87	0.07	0.68	0.95
	7:Bypass Reach	0.72	0.09	0.51	0.86
Cohort2: 2018	8:Spillway	0.39	0.12	0.19	0.63
	9:Project Arrival	0.63	0.09	0.45	0.78
	10:Tailrace	1.00	0.00	1.00	1.00
	11:Bypass Reach	0.63	0.13	0.37	0.83
Cohort3: 2015	12:Spillway	0.49	0.18	0.20	0.79

Table 4.3.1-4: Transit times (hrs) from Project to Spillway arrival (2015, 2018, 2019, n = 92)

	Min	25%	50%	75%	Max
Spillway Arrival	3.89	20.90	42.04	71.1	835.12

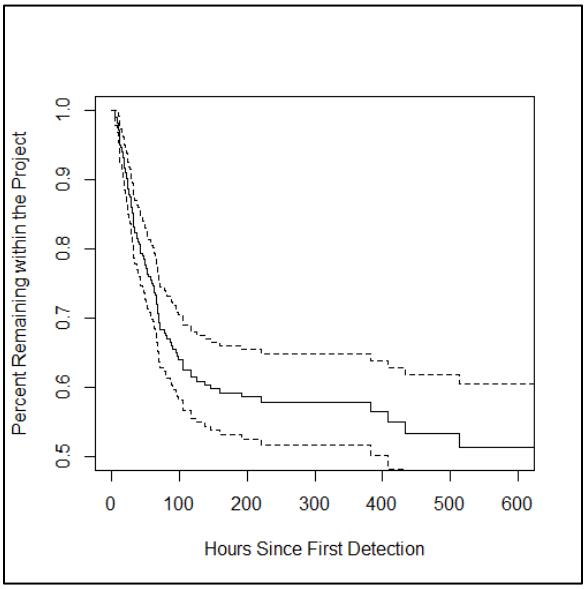

Figure 4.3.1-1: Kaplan-Meier plot showing hours since first detection at the Project and movement to the Spillway

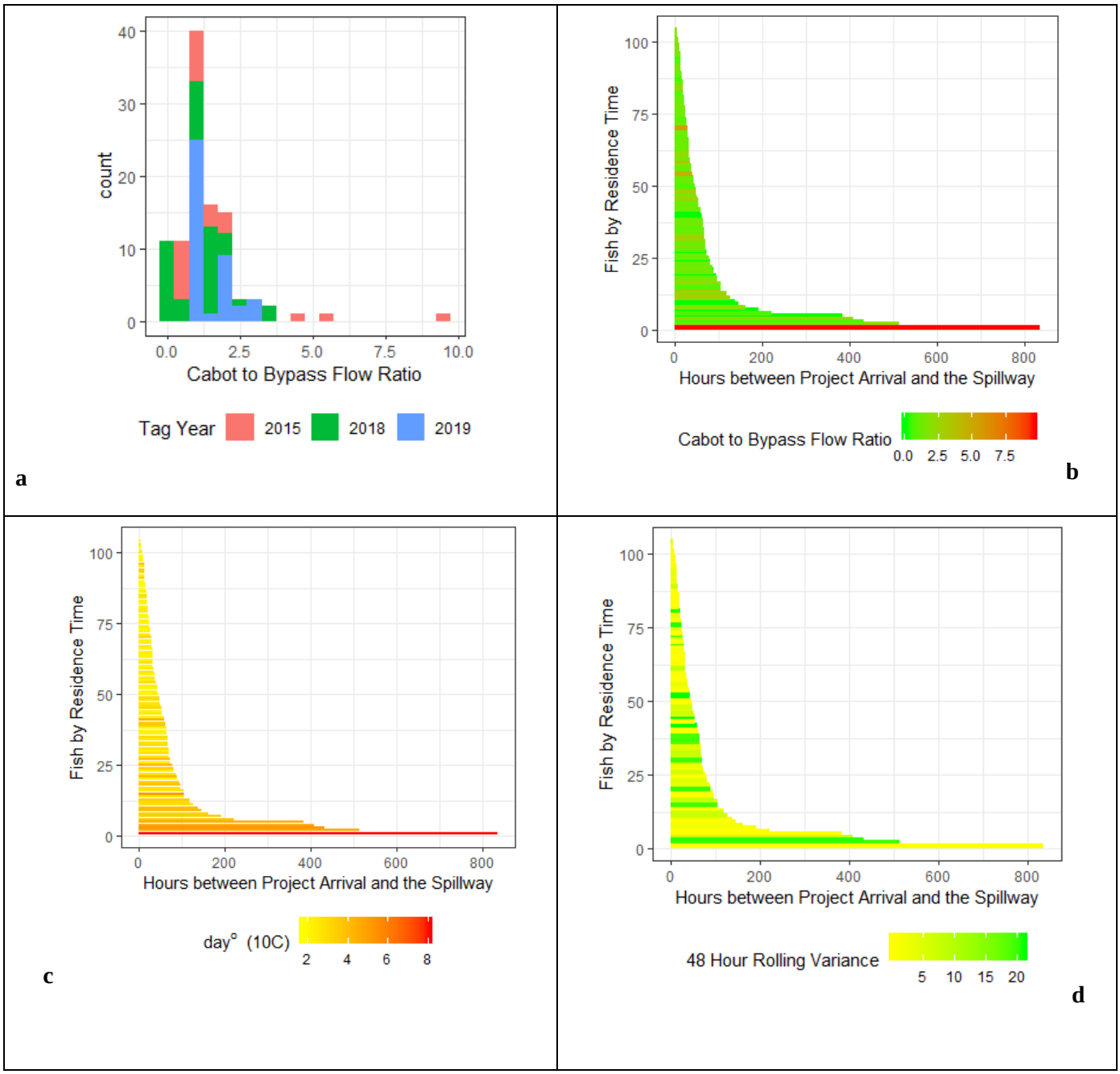

Figure 4.3.1-2(a, b, c, d): Project arrival to Spillway movement: Instantaneous Cabot to Bypass flow ratio (a), transit times (b), day° (10°C) (c), and 48-hour rolling variance (d)

4.3.2 Cabot Tailrace Movement

Movement within the Cabot tailrace was assessed with a time-to-event analysis using a competing risks framework. There were four receivers that encompassed the Cabot Station tailrace (T04, T05, T06, and T07). Of the 137 non-fallback fish that were tagged and released at Holyoke Dam fish lift in 2019, 74 (54%) arrived to the Cabot Station tailrace. From there, 49 (66%) of those fish moved to the bypass reach (Conte Discharge) and 51 (69%) fish were detected at the Cabot Station fish ladder entrance (Table 4.3.2-3). In 2015, there were 66 fish detected in the Cabot tailrace and 30 (45%) of those made it to the bypass reach

(Table 4.3.2-1). In 2018, there were 112 fish detected in the Cabot tailrace and 85 (76%) of those fish made it the bypass reach (Table 4.3.2-2). The state tables display the number of unique fish (n) to make a particular number of movements (m), as well as the minimum, median, and maximum number of movements made for each transition. Movements are read on the state table from a column to a row.

Movement analysis within the Cabot tailrace for three years of telemetry studies (2015, 2018 and 2019) was aggregated. A series of CoxPH regression models were fit to time dependent covariates in an effort to understand what factors increased the likelihood that a tagged shad will migrate from Cabot tailrace to the Cabot ladder and from the tailrace to the bypass reach. For movement from the tailrace to the Cabot ladder, the single covariate models that were significant included accumulated thermal units (10°C), and bypass flow (kcfs) rolling variance for 2-hr and 5-hr intervals. The 2-hr and the 5-hr bypass flow rolling variance models suggest that as the near-term flow volatility increases in the bypass reach, the likelihood of fish movement from the tailrace to the Cabot Ladder decreases (HR = 0.58 and 0.73, and p values = 0.05 and 0.01, respectively) (Appendix C). The model including tag year was also significant, with hazard ratio values of 2.29 and 2.35 for 2018 and 2019, respectively, suggesting that fish were much more likely to move from the tailrace to the ladder in those years as compared to 2015. The single covariate model with the lowest AIC (5261.9) included day° (10°C). A hazard ratio of 0.71 suggests that for every day the mean daily temperature begins to rise above the 10° C threshold, fish are less likely to move from the tailrace to the ladder.

For movement from the Cabot tailrace to the bypass reach, there were several single covariate models that were significant, including Cabot discharge (kcfs), the number of operational units at Cabot Station, bypass flow (kcfs), Cabot rolling average flow (1hr, 2 hr, 5 hr and 24 hr), bypass rolling average flow (1 hr, 2 hr, 5 hr), cumulative average bypass flow and Cabot discharge (kcfs), day° and the ultrasound array operational. In total, there were 27 models that were created to describe movement in this reach (Appendix C). The single covariate model with the lowest AIC (2208.6) included operation of the ultrasound array. The HR was 3.9 and the model was highly significant ($p<0.001$), suggesting that when the array was operational in 2018, fish were much more likely to move from the Cabot tailrace to the bypass reach as compared to 2015 and 2019 when there was no ultrasound array present. Multivariate models including the operation of the ultrasound array with bypass flow, and the operation of the ultrasound array with the Cabot-to-bypass flow ratio were tested. In both cases, no interactions were significant and the flow components on their own within those multivariate models were not significant. Only significant component in either model was the ultrasound array being operational.

However, the proportional hazard assumption was significant, meaning the effect of the ultrasound array changed with the duration of exposure. A model was constructed that incorporated an interaction effect between the operation of the ultrasound array and the duration a fish remained in the tailrace. The model had the lowest AIC (2078.1) of all models, and both the operation of the array and duration were significant ($p <0.001$), with hazard ratios of 3.82 and 0.98, respectively. The interaction effect between the operation of the array and duration was not significant ($p=0.09$). As fish remain in the tailrace for a longer period of time when the array is operational, they are less likely to move up to the bypass reach (Appendix C).

Figure 4.3.2-1a shows the transit times of fish that transitioned from the Cabot tailrace to the bypass reach when the ultrasound array was operating (blue) and not operating (red). The figure shows that the majority of fish that transitioned in less than 5 hours did so when the array was on, whereas the majority of fish that transitioned in more than 5 hours did so when the array was off. Figure 4.3.2-1b depicts the transit times with the ratio of Cabot discharge to bypass flow. As the ratio of Cabot to bypass discharge increases it takes longer for fish to transition into the bypass reach. Figure 4.3.2-1c depicts the day° (10°C) as it relates to the transit times from the tailrace to the bypass reach. As the day° increases past 10°C, it takes fish longer to transition from the tailrace to the bypass reach (Figure 4.3.2-1c).

Table 4.3.2-1: 2015 Cabot Tailrace Movement

	Cabot Tailrace	Cabot Ladder	Bypass Reach	Downstream
Cabot Tailrace	n = 66	n = 23 m = 87 min = 1 med = 3 max =13	n = 30 m = 40 min = 1 med =1 max =4	n = 19 m = 31 min = 1 med = 1 max =5
Cabot Ladder	n = 22 m = 86 min = 1 med = 3 max =13	n = 23	n = 0 m = 0 min =0 med =0 max =0	n = 0 m = 0 min = 0 med = 0 max =0
Bypass Reach	n = 30 m = 14 min = 1 med = 1 max = 3	n = 1 m = 1 min =1 med = 1 max =1	n =30	n = 3 m = 4 min =1 med = 1 max = 2
Downstream	n = 15 m = 26 min = 1 med = 1 max =5	n = 0 m = 0 min = 0 med = 0 max = 0	n = 2 m = 3 min =1 med = 1.5 max =2	n = 20

Table 4.3.2-2: 2018 Cabot Tailrace Movement

	Cabot Tailrace	Cabot Ladder	Bypass Reach	Downstream
Cabot Tailrace	n = 112	n = 53 m = 117 min = 1 med = 2 max =7	n = 72 m = 135 min = 1 med = 1 max = 6	n = 73 m = 94 min = 1 med = 1 max = 5
Cabot Ladder	n = 52 m = 114 min = 1 med = 2 max =7	n =55	n = 3 m = 3 min = 1 med = 1 max = 1	n = 11 m = 12 min = 1 med = 1 max = 2
Bypass Reach	n = 53 m = 89 min = 1 med = 1 max =4	n = 3 m = 3 min =1 med = 1 max =1	n = 85	n = 38 m = 51 min = 1 med = 1 max = 3
Downstream	n = 29 m = 40 min = 1 med = 1 max =5	n = 7 m = 9 min =1 med = 1 max =3	n = 29 m = 37 min = 1 med = 1 max = 3	n = 92

Table 4.3.2-3: 2019 Cabot Tailrace Movement

	Cabot Tailrace	Cabot Ladder	Bypass Reach	Downstream
Cabot Tailrace	n = 74	n = 51 m = 260 min = 1 med = 3 max = 28	n = 47 m = 60 min = 1 med = 1 max = 3	n = 56 m = 109 min = 1 med = 1 max = 11
Cabot Ladder	n = 51 m = 260 min = 1 med = 3 max =	n = 51	n = 0 m = 0 min = 0 med = 0 max = 0	n = 0 m = 0 min = 0 med = 0 max = 0
Bypass Reach	n = 34 m = 43 min = 1 med = 1 max = 3	n = 0 m = 0 min = 0 med = 0 max = 0	n = 49	n = 20 m = 27 min = 1 med = 1 max = 4
Downstream	n = 27 m = 65 min = 1 med = 1 max = 10	n = 0 m = 0 min = 0 med = 0 max = 0	n = 11 m = 12 min = 1 med = 1 max = 2	n = 63

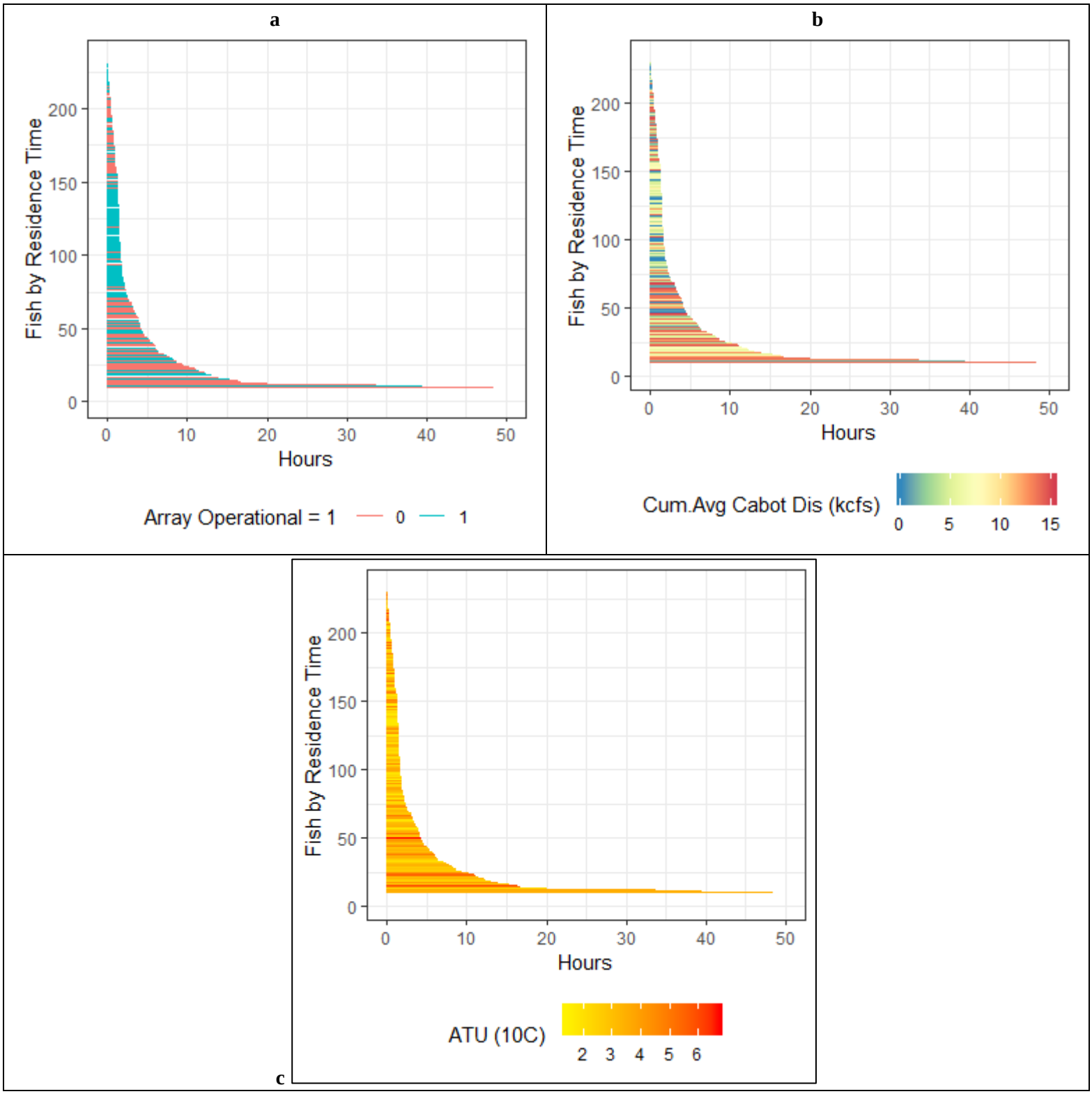

Figure 4.3.2-1(a,b,c): Cabot station tailrace to bypass movement variables with transit times. Ultrasound array operational (a), cumulative average Cabot discharge (b), and day° 10°C (c)

4.3.3 Bypass Reach Movement: Conte Discharge to Spillway

FirstLight tracked the movements of American Shad within the bypass reach in 2015, 2016, 2018 and 2019. Each year, the fixed telemetry monitoring station upstream of the Conte discharge was designated as the entrance to the bypass reach. Raw movement suggested that 37%, 46%, 35% and 50% of fish detected at the Conte receiver successfully arrived to the TFD spillway in 2015, 2016, 2018, and 2019, respectively (Tables 4.3.3-1-4.3.3-4). The median transit time for all fish that moved from Conte discharge to the TFD spillway was 19.8 hours, with a minimum of 2.24 hours and a maximum of 307.8 hours. Table 4.3.3.5 describes bypass movement timing summary statistics by study year. Note on average, fish transitioned between Conte discharge and TFD spillway much quicker in 2015 and 2016 than in 2017 and 2018. While the highest proportion of fish successfully migrated in 2019 (50%), that year had the longest on average travel times (29.3 hours). Figure 4.3.3-1 shows proportion of fish remaining at Conte (Kaplan-Meier survival curve) before transitioning to the spillway over time. The x-axis is in increments of 24 hours. All fish transitioned within 72 hours in 2016, while fish remained in the bypass reach for much longer in other years. The global p-value was significant (p = 0.007) suggesting a difference between years. However, when a pairwise comparison was performed, the only significant difference was between 2016 and 2019 (Table 4.3.3-6). With few observations in 2016 and very wide confidence intervals, there is likely no difference between years.

Figures 4.3.3-2– 4.3.3-5 depict the presence history (blue, horizontal) of each successful Conte – Spillway migrant over the bypass flow in kcfs. Each line starts when the fish arrives at Conte and ends when it arrives at the spillway. The first grey dotted vertical line shows when the spillway ladder count achieved 50% of its total (50th percentile). The second dotted line shows when the spillway ladder achieved the 90th percentile. The thick red line indicates when the Connecticut River reached 18.5°C, which has been shown to correspond with peak spawning (Collette and Klein-MacPhee 2002). This statistic was corroborated with the 2015 spawning study which found peak splash counts occurred when the water temperature reached 18.5°C (Relicensing Study No. 3.3.6). During all study years, this temperature threshold occurred at the end of May except in 2019 (Table 4.3.3-7). With the exception of 2016, the majority of the successful bypass migrations occur before the peak spawning threshold. The thick green line indicates when shad could be in the river for 20 days based upon a 10°C threshold.

A series of CoxPH regression models were fit to time dependent covariates in an effort to understand what factors increased the likelihood a tagged shad will migrate from Conte discharge to the TFD Spillway. The models in Appendix C are ordered from lowest AIC to highest AIC and include both single covariate models and multi-covariate interactions. The single covariate model that best described movement (lowest AIC) within the bypass reach included day^{o} (10°C). The model incorporating day^{o} had the lowest AIC (993.8) and was highly significant (p=<0.001) with a hazard ratio of 0.57, suggesting that as day^{o} increases past 10°C, the likelihood of fish moving up to the TFD spillway decreases. Note that day^{o} was transformed using a square root transformation. The second lowest AIC (1013.5) for single covariate models included 24-hour bypass flow variance. The model was significant (p<0.001) and the hazard ratio of 1.05 suggests that as flow variability in the bypass reach increases over a 24-hr period, fish are less likely to transition up to the TFD spillway. The models including instantaneous bypass flow (kcfs) and cumulative average bypass flow were also highly significant (p = 0.001 and <0.001, respectively), with hazard ratios of 1.05 and 1.06, respectively. This suggests that as bypass flow increases by 1,000 cfs, shad are more likely to move up to the spillway.

Figure 4.3.3-6a is a histogram of the bypass flows experienced when a fish arrives at the TFD spillway. In 2019, only 3 out of the 36 fish that made this transition did so under 5,000 cfs; all other fish moved up to spillway between ~7,000 and 25,000 cfs. Flow duration curves were developed for the bypass reach during the fish passage season (Reach 1 - May 15 to July 15) for all study years (Appendix E). Table 4.3.3-8 displays the bypass flow exceedance percentages for each year. In 2019, the majority of the fish moved from the entrance of the bypass reach to the TFD spillway when flows were above 7,000 cfs, which was

only met or exceeded 10% of the time. The high flow events in 2019 have not been indicative of the seasonal trends at the project. Seasonality and temperature seem to be more important than particular flows, as multiple years of telemetry studies show fish moving through the bypass reach at a range of flows, while movement starts to drop off when peak spawning temperatures are reached around Memorial Day. A histogram of the temperature at transition was also plotted (Figure 4.3.3-6b). The majority of movements made in 2019 and 2016 occurred when water temperature was below 15°C, whereas the majority of movements in the bypass reach made in 2018 and 2015 occurred over when water temperature was above 15°C (Figure 4.3.3-6b).

One of the objectives of the study was to determine whether or not adult shad migrate by the Station No.1 tailrace at a bypass flow of 4,400 cfs with 2,190 cfs from TFD and 2,210 cfs from Station No.1. A ratio between Station No.1 discharge and spill at TFD was calculated to assess this flow split (50%:50%). If the flow ratio was greater than 1, more water was being discharged from Station No.1 than was spilling over TFD; when the ratio is less than 1, more water was spilling than discharged at Station No.1. The Cox Proportional Hazard model constructed to evaluate Station No.1 to bypass flow ratio with movement to the TFD spillway was not significant ($p = 0.07$). Figure 4.3.3-7a shows the instantaneous Station No.1 to bypass flow ratio while fish were transitioning from the entrance of the bypass reach to the TFD spillway for each tagging year (2015, 2016, 2018 and 2019). In 2019, no fish made this movement when the ratio was above 0.5. In other words, all of the fish made their movements toward TFD spillway when the spill exceeded Station No.1 discharge. In all study years, there were only 2 fish in 2015 that transitioned to the TFD spillway when there was a 50%:50% flow split (ratio = 1) (Figure 4.3.3-7a). Figure 4.3.3-7b shows the Station No.1 to bypass flow ratio during the study period (May 15 to July 15, 2019). Station No.1 flow was rarely higher than bypass flow in the 2019 study period (May 15 to July 15, 2019). From May 15 to June 30, there were only 8 total hours where Station No.1 discharge exceeded spill in the bypass reach. After June 30, Station No.1 discharge remained higher than spill to the bypass reach; however, there were no tagged fish that moved from the bypass reach to TFD spillway this late in the season.

Table 4.3.3-1: 2015 Bypass Movement

	Conte Tailrace	TFD Spillway	Downstream
Conte Tailrace	n = 54	n = 20 m = 23 min = 1 med = 1 max = 2	n = 18 m = 26 min = 1 med = 1 max = 3
Turners Falls Spillway	n = 4 m = 4 min = 1 med = 1 max = 1	n = 20	n = 0 m = 0 min = 0 med = 0 max = 0
Downstream	n = 13 m = 20 min = 1 med = 1 max = 3	n = 1 m = 1 min = 1 med = 1 max = 1	n = 18

Table 4.3.3-2: 2016 Bypass Movement

	Conte Tailrace	TFD Spillway	Downstream
Conte Tailrace	n = 28	n = 11 m = 11 min = 1 med = 1 max = 1	n = 24 m = 30 min = 1 med = 11 max = 3
Turners Falls Spillway	n = 8 m = 8 min = 1 med = 1 max = 1	n = 13	n = 0 m = 0 min = 0 med = 0 max = 0
Downstream	n = 28 m = 34 min = 1 med = 1 max = 3	n = 2 m = 2 min = 1 med = 1 max = 1	n = 58

Table 4.3.3-3: 2018 Bypass Movement

	Conte Tailrace	TFD Spillway	Downstream
Conte Tailrace	n = 85	n = 30 m = 38 min = 1 med = 1 max = 4	n = 66 m = 152 min = 1 med = 2 max = 9
Turners Falls Spillway	n = 8 m = 8 min = 1 med = 1 max = 1	n = 30	n = 14 m = 20 min = 1 med = 1 max = 4
Downstream	n = 49 m = 121 min = 1 med = 2 max = 9	n = 0 m = 0 min = 0 med = 0 max = 0	n = 70

Table 4.3.3-4: 2019 Bypass Movement

	Conte Tailrace	TFD Spillway	Downstream
Conte Tailrace	n = 72	n = 33 m = 35 min = med = max =	n = 65 m = 101 min = 1 med = 1 max = 4
Turners Falls Spillway	n = 29 m = 30 min = 1 med = 1 max = 2	n = 36	n = 6 m = 6 min = 1 med = 1 max = 1
Downstream	n = 25 m = 37 min = 1 med = 1 max = 3	n = 3 m = 3 min = 1 med = 1 max = 1	n = 69

Table 4.3.3-5 Bypass reach travel times by study year

Tag Year	Min	25%	50%	75%	100%
2015	2.25	4.38	7.52	20.4	97.1
2016	4	5.42	8.11	24.4	71.3
2018	3.72	8.25	19.7	26.3	74.8
2019	7.53	19.8	29.3	47.0	308.0

Table 4.3.3-6. Matrix of Kaplan-Meier survival curve pairwise comparison p-values by year. Note the only significant pairing occurred between 2016 and 2019, with 2019 having much longer time-to-spillway movement.

	2015	2016	2018
2016	0.051	-	-
2018	0.060	0.257	-
2019	0.305	***0.032***	0.06

Table 4.3.3-7: American Shad migration and spawning activities by temperature range

Temperature Range (ºC)*	Activity	2015	2016	2018	2019
10 - 12	Enter natal rivers	May 3 – May 5	May 1 – May 11	May 4 – May 9	May 16 – May 19
13 - 18	Onset of spawning in CT River	May 6 – May 26	May 12 – May 27	May 11 – May 26	May 20 – June 10
18.5	Peak Spawning	May 27	May 28	May 29	June 11
20	Cease Migration	May 29	May 30	June 1	June 26
15.5 – 21.5	Maximum hatch and survival of eggs	May 10 – May 31	May 25 – June 2	May 17 – June 11	June 3 – June 28

*Collette and Klein-MacPhee 2002.

Table 4.3.3-8: Bypass Flow (Reach 1) Percent exceedance (2015, 2016, 2018, and 2019)

	Percent Exceedance				
Year	**10%**	**25%**	**50%**	**75%**	**90%**
2019	11,759	7,112	4,857	768	418
2018	6,151	4,467	2,135	456	399
2016	4,765	2,577	2,484	1,482	1,003
2015	9,733	6,181	3,710	2,458	1,440
All years	**8,271**	**5,687**	**3,249**	**996**	**420**

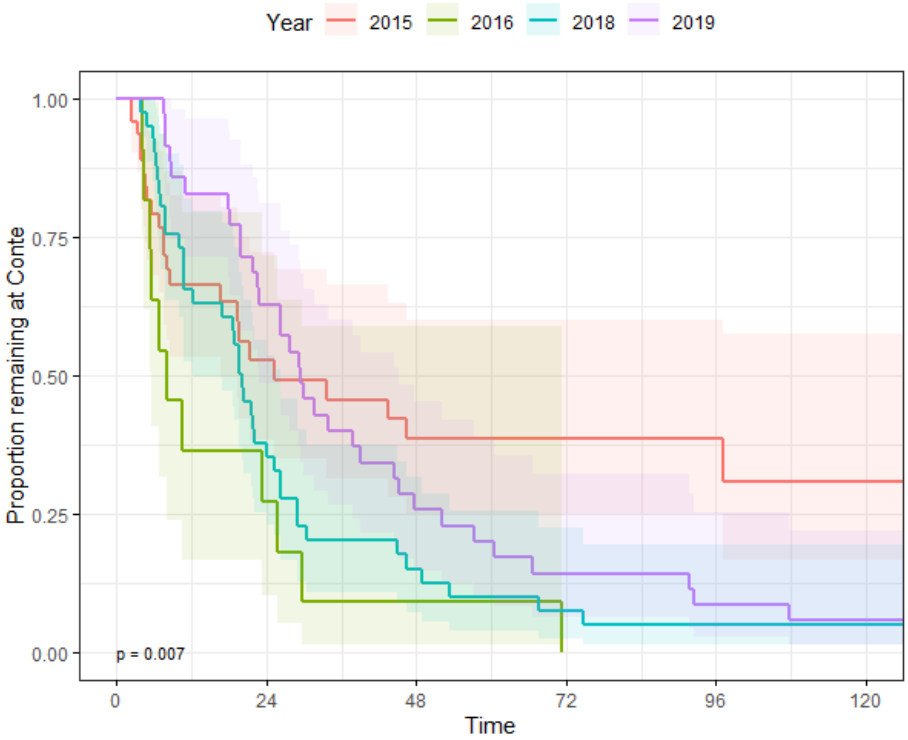

Figure 4.3.3-1: Kaplan-Meier survival curves for Conte to Spillway movement by tag-year.
Note, in all years more than 50% of the successful migrants will reach the spillway in 48 hours.

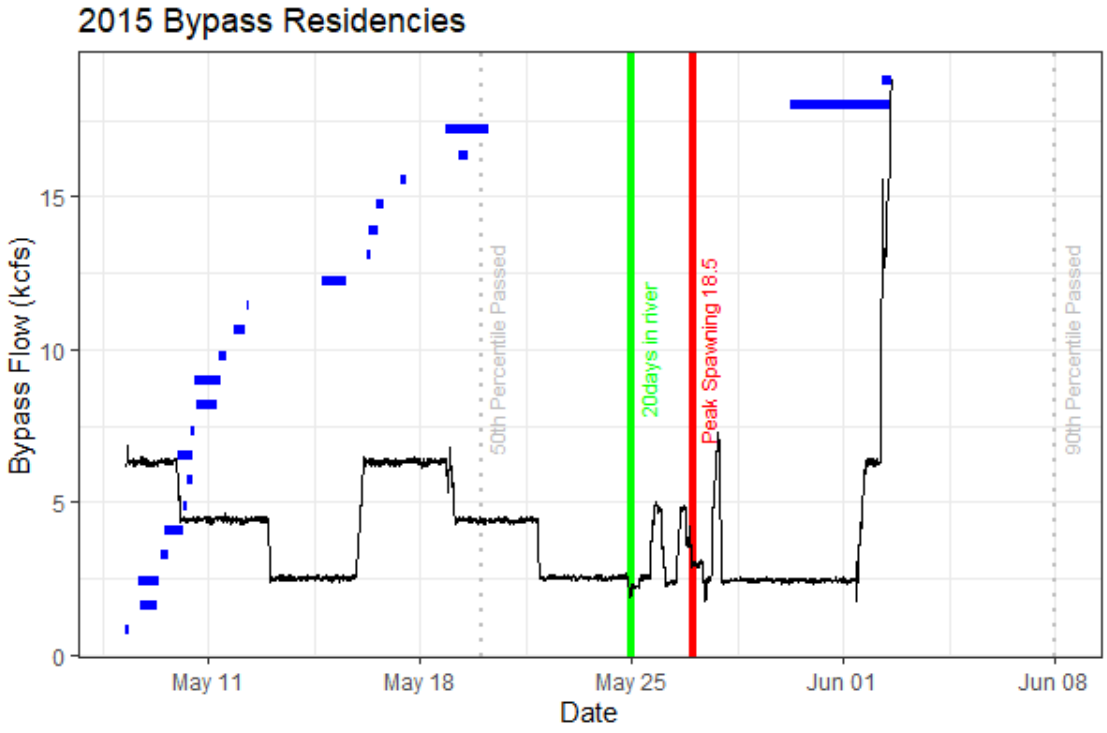

Figure 4.3.3-2. 2015 bypass reach residencies over bypass flow (kcfs) with showing an estimated 20 days in river, peak spawning temperature threshold, and cumulative percent of run at TFD spillway milestones.

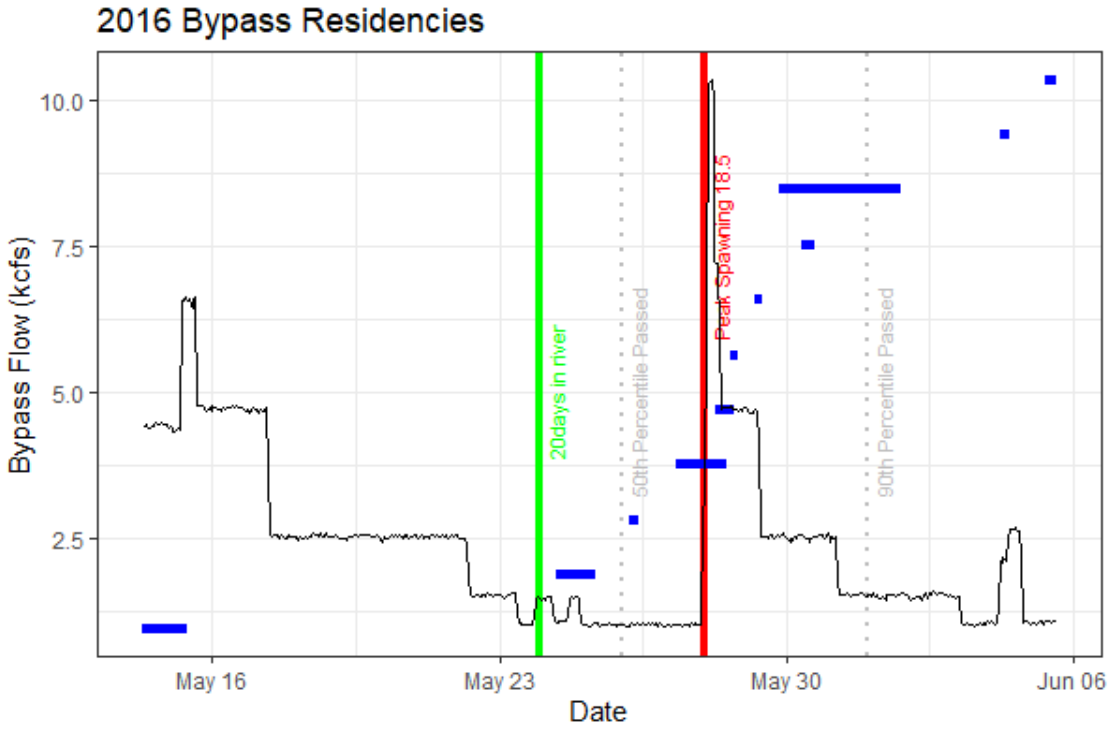

Figure 4.3.3-3. 2016 bypass reach residencies over bypass flow (kcfs) with showing an estimated 20 days in river, peak spawning temperature threshold, and cumulative percent of run at TFD spillway milestones.

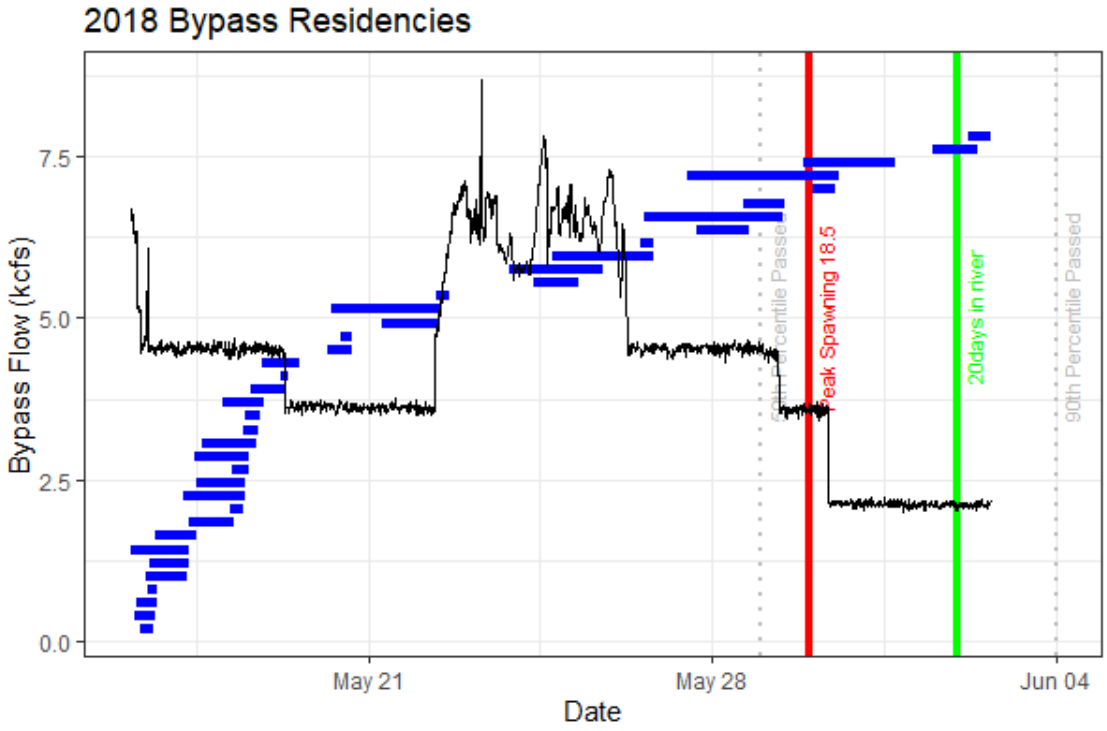

Figure 4.3.3-4. 2018 bypass reach residencies over bypass flow (kcfs) with showing an estimated 20 days in river, peak spawning temperature threshold, and cumulative percent of run at Spillway milestones.

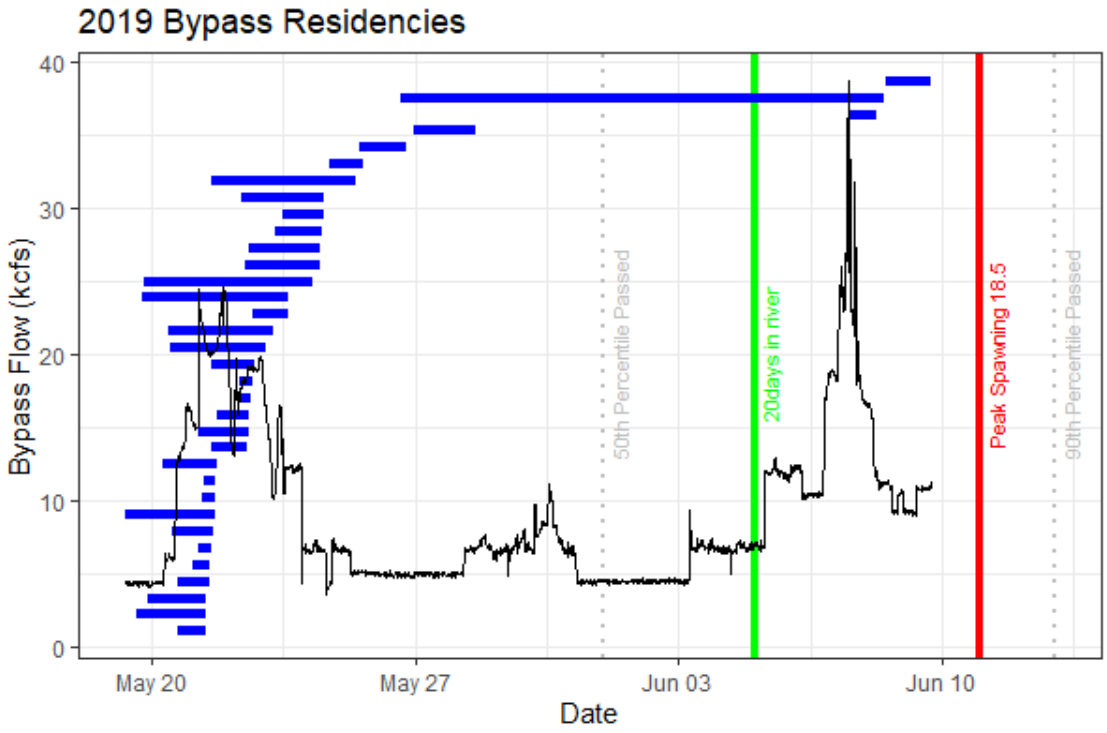

Figure 4.3.3-5. 2019 bypass reach residencies over bypass flow (kcfs) with showing an estimated 20 days in river, peak spawning temperature threshold, and cumulative percent of run at TFD spillway milestones.

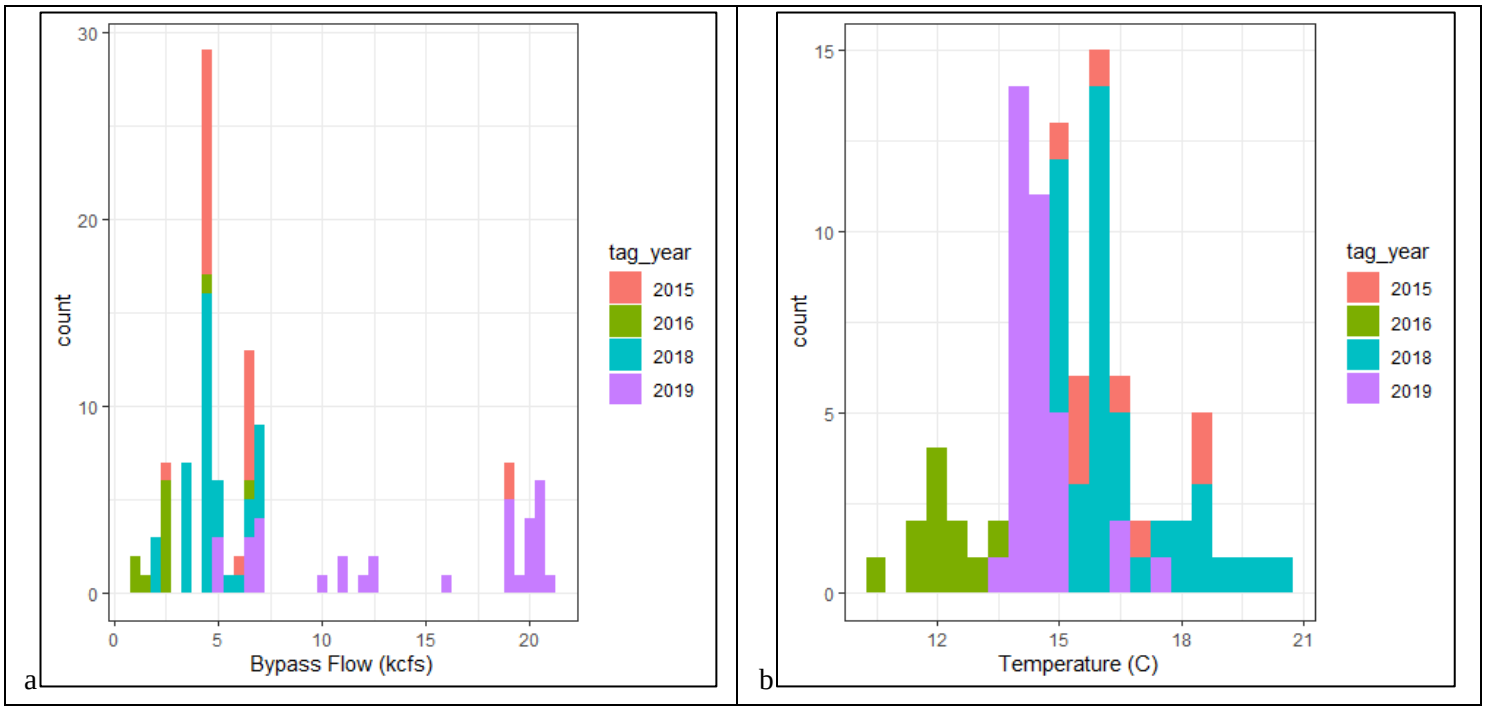

Figure 4.3.3-6. Instantaneous bypass flow (kcfs) (a) and instantaneous water temperature (b) during Conte – TFD spillway movement

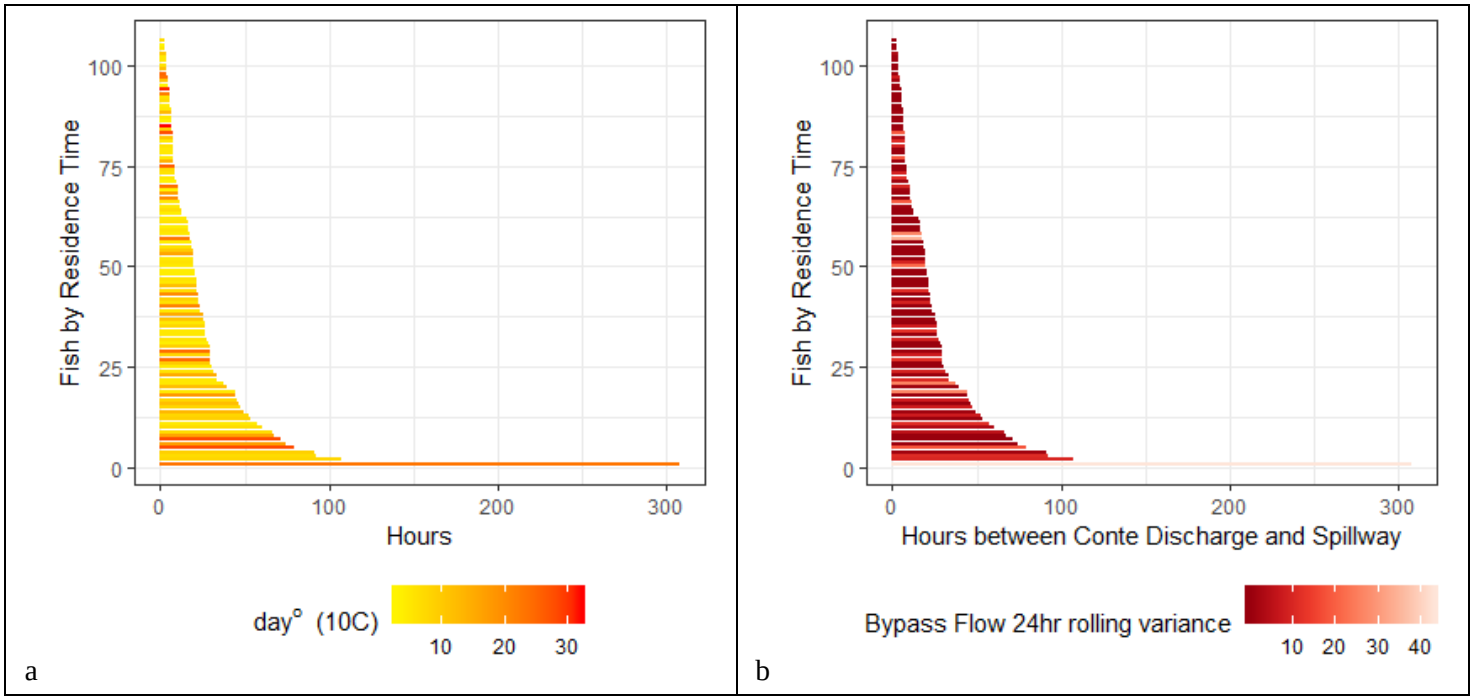

Figure 4.3.3-7. Degree days at transition by transition length (a) and bypass flow 24-hour rolling variance at transition by transition length.

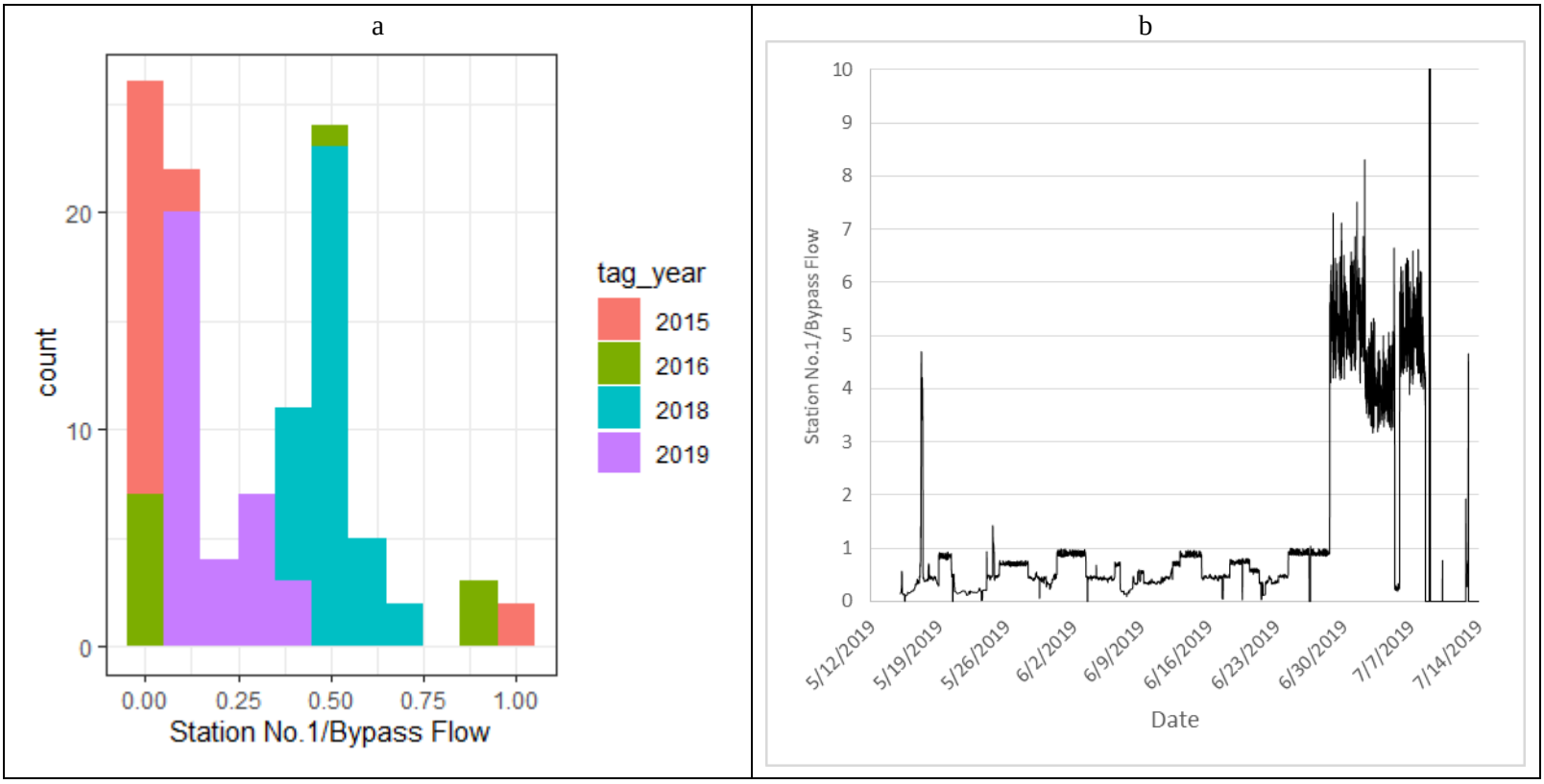

Figure 4.3.3-8 (a and b): Station No. 1 discharge to bypass flow ratio during transition from Conte discharge to TFD spillway (a), Station No.1 to bypass flow ratio for the 2019 study period (b)

4.3.4 Rawson Island Complex

In 2019, fixed telemetry receivers were installed around Rawson Island (T09, T10, T11, T12 and T24) in mid-May, before any fish were tagged at Holyoke. After the island receivers were installed, they were not accessed again for maintenance until May 29, 2019 due to river flows at Montague USGS gage averaging 27,200 cfs from May 15 to May 29, 2019. Technicians were prohibited from accessing the island locations due to boating safety concerns. Upon first arrival at the island locations on May 29, all receivers were out of service due to low power issues and/or inundation from high flows. As a result, any movement from fish during that time period was undetected; the results below reflect movements made after May 29, 2019.

The Rawson Island movement model included all fish that were tagged and released at Holyoke Fish Lift (n = 241, non-fallback n = 137). The initial state for the model was the Conte tailrace where 72 fish were detected. From there, fish could make the following movements; to state 2 (Rock Dam pool), state 3 (lower west channel), state 4 (west channel), state 5 (middle channel), or state 6 (upstream to TFD) (Table 4.3.4-1).

For this model, 72 fish were detected at Conte tailrace, and 40 were detected upstream of Rawson Island. In total, 20 fish were detected in the Rock Dam pool, 15 in the lower west channel, 8 in the west channel and no fish detected in the middle channel. Unfortunately, there was no way to determine the routes of passage utilized by the 40 fish that passed Rawson Island prior to May 29 due to the receiver outages as 23 fish moved undetected from the Cabot tailrace to upstream of Rawson Island. However, it is evident that fish were detected at all routes except for the middle channel of Rawson Island.

Table 4.3.4-1: Rawson Island movement state table

	Conte Tailrace	**Rock Dam Pool**	**Lower West Channel**	**West Channel**	**Middle Channel**	**Upstream of Rawson**
Conte Tailrace	n = 72	n = 13 m = 18 min = 1 med = 1 max = 4	n = 7 m = 9 min = 1 med = 1 max = 3	n = 4 m = 4 min = 1 med = 1 max = 1	n = 0 m = 0 min =0 med = 0 max = 0	n = 39 m = 40 min = 1 med = 1 max = 2
Rock Dam Pool	n = 15 m = 21 min = 1 med = 1 max = 4	n = 20	n = 4 m = 4 min = 1 med = 1 max = 1	n = 0 m = 0 min = 0 med = 0 max = 0	n = 0 m = 0 min = 0 med = 0 max = 0	n = 3 m = 3 min = 1 med = 1 max = 1
Lower West Channel	n = 11 m = 14 min = 1 med = 1 max = 2	n = 3 m = 4 min = 1 med = 1 max = 1	n = 15	n = 1 m = 1 min = 1 med = 1 max = 1	n = 0 m = 0 min = 0 med = 0 max = 0	n = 2 m = 2 min = 1 med = 1 max = 1
West Channel	n = 1 m = 1 min = 1 med = 1 max = 1	n = 1 m = 1 min = 1 med = 1 max = 1	n = 6 m = 7 min = 1 med = 1 max = 2	n = 8	n = 0 m = 0 min = 0 med = 0 max = 0	n = 0 m = 0 min = 0 med = 0 max = 0
Middle Channel	n = 0 m = 0 min = 0 med = 0 max = 0	n = 0 m = 0 min = 0 med = 0 max = 0	n = 0 m = 0 min = 0 med = 0 max = 0	n = 0 m = 0 min = 0 med = 0 max = 0	n = 0	n = 0 m = 0 min = 0 med = 0 max = 0
Upstream of Rawson	n = 23 m = 23	n = 6 m = 7	n = 2 m = 2	n = 4 m = 4	n = 0 m = 0	

	Conte Tailrace	Rock Dam Pool	Lower West Channel	West Channel	Middle Channel	Upstream of Rawson
	min = 1 med = 1 max = 1	min = 1 med = 1 max = 2	min = 1 med = 1 max = 1	min = 1 med = 1 max = 1	min = 0 med = 0 max = 0	n = 40

4.4 Downstream Passage

In 2019, FirstLight assessed downstream passage with a combination of observational studies. As part of the telemetry study, FirstLight released 198 fish into the canal to further evaluate delay within the forebay, choice of route of passage, and downstream passage survival. After observing that all fish were recaptured in the forebay, we excluded fish that exhibited a mortality signal. Therefore, only fish known to be alive were used in modeling. FirstLight also conducted a dead drift study by injecting euthanized fish into the penstock at Cabot Station Unit No. 2 and compared both the total distance traveled for 48 hours after passage and rate of travel to fish known to have passed through the powerhouse while still alive. FirstLight used a combination of live recapture dead recovery (LRDR) mark recapture modeling and time-to-event analysis within a competing risks framework to understand movement. Dead drift fish were compared to their live counterparts with non-inferential comparisons.

4.4.1 Live Recapture Dead Recovery

The survival estimates generated from LRDR mark recapture modeling are an improvement over those generated with traditional CJS modeling because information from known mortalities are incorporated. With traditional CJS modeling, we do not know if a fish has died or if it has emigrated from the study area. By incorporating information from dead recoveries, we are able to partition true survival from those fish known to be dead and those that emigrated. Fish that are not recovered dead or recaptured alive are assumed to have emigrated from the study reach. The LRDR method has more output than the CJS, including an estimate of site fidelity. Fidelity estimates the probability that a tagged shad remained within the study reach for the 48-hour window. Thus, the higher the site fidelity, the better the estimate of true survival. Aside from the traditional CJS survival and recapture probabilities, the LRDR method also estimated a recovery probability, which is the probability of recovering a dead shad during mobile tracking and reporting it. The LRDR mark recapture estimates were generated in MARK.

Latent mortality was estimated at 48 hours after known passage. Passage was deemed to occur at the time of the final recapture in the forebay (or log sluice entrance). Information from live recaptures at stationary receivers were censored after 48 hours.

Three LRDR models were constructed: (1) powerhouse passage survival, (2) log sluice passage survival, and (3) whole project downstream survival (Table 4.4.1-1). The MARK input files are found in Appendix D. In total, 76 fish were known to have passed through the powerhouse alive, and 47 were recaptured alive at Nourse Farms. No fish were recovered dead within one week in the stretch of river from Fourth Island to the Hatfield WWTP. During mobile tracking, 6 fish that passed via the powerhouse were recovered dead including 4 in the Deerfield confluence and two between Montague WWTP and Fourth Island. Immediate survival to the tailrace was high (100%). Aside from dead recoveries during mobile tracking, we also examined Orion receivers in the tailrace to note if any fish exhibited a mortality pulse. No fish recaptured at the tailrace Orions exhibited a pulse rate of 11 seconds. Once fish transitioned to the tailrace, the median travel time to Montague was only 0.62 hours (37.2 minutes). However, a latent mortality event occurred in the Deerfield confluence with only 69% surviving until Montague WWTP. Of those fish that survived until reaching Montague, 96% survived to the southern tip of Fourth Island at Nourse Farms. Of those fish that reached Fourth Island, 50% did so in 18 minutes or less. The LRDR model also found that 99% of the fish

that survived to Nourse Farms survived to reach Hatfield WWTP. Overall, the cumulative survival rate (48 hr after passage) of fish known to pass via the powerhouse was 65.5%. Those fish that do eventually pass downstream, pass quickly.

The cumulative survival (48-hr) via the log-sluice (n = 38) was higher at 89%. A latent mortality event occurred in the Deerfield confluence with 92% of the fish expected to survive until the WWTP at Montague. The cumulative whole project estimate was 65%. Our confidence in these survival estimates are high, because our estimate of site fidelity for dead fish was also high. Estimated fidelities for the whole project, powerhouse and log sluice were 100%, 96% and 100%, respectively.

Mortality was observed in the Cabot Station forebay with 58 of the 198 fish released (29%) exhibiting an 11-second mortality pulse rate before transitioning into the tailrace; these fish were excluded from the initial and latent survival analysis. A Nelson-Aalen plot (Figure 4.4.1-1) was created to assess the transit times for the downstream running fish released in the power canal for each route of downstream passage (through the powerhouse or through the log sluice). The median time for transitioning from the Cabot forebay through the powerhouse was 264.3 hours, with a minimum of 0.02 hours and a maximum of one fish remaining in the forebay for 754.9 hours. In contrast, the median time to transition from the Cabot forebay through the log sluice was 119.1 hours, with a minimum of 0.003 hours and a maximum of 405.5 hours (Figure 4.4.1-1).

Table 4.4.1-1: Survival estimates for LRDR downstream survival Mark Recapture model

	Whole Project	Powerhouse	Log Sluice
Forebay - Tailrace	0.95 (0.87 – 1.0)	1 (0.97 – 1.0)	1 (1.0 – 1.0)
Tailrace - Confluence	0.71 (0.61 – 0.81)	0.69 (0.57 – 0.88)	0.92 (0.81 – 0.98)
Confluence - Montague	0.97 (0.91 – 0.99)	0.96 (0.89 – 0.99)	0.97 (0.88 – 0.99)
Nourse Farms - Hatfield	1 (0.0 – 1.0)	0.99 (0.0 – 0.99)	1 (1.0 – 1.0)
Cumulative	0.654265	0.655776	0.8924

Table 4.4.1-2: Initial and 48hr survival of downstream Cabot canal released shad

Survival	Powerhouse	Log Sluice
Initial Passage	100%	100%
48hr	65.5%	89.2%

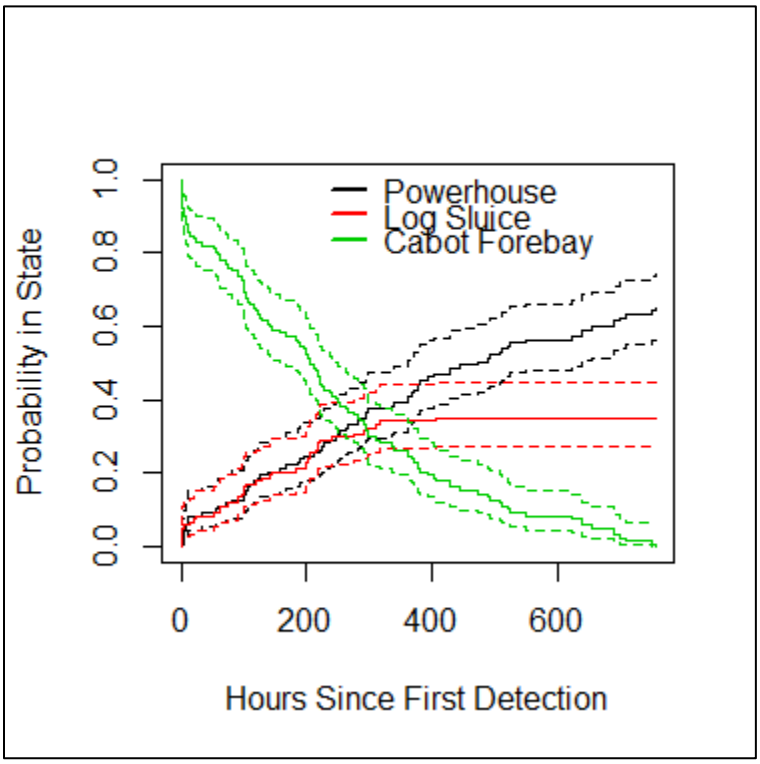

Figure 4.4.1-1: Nelson-Aelen plot of Cabot Canal released fish

4.4.2 Cabot Station Dead Drift Study

A total of 24 euthanized shad were tagged and released into the Cabot Unit 2 turbine in two batches on June 12 (n=12) and June 13, 2019 (n=12). The fish that were released on June 12 experienced a "low" flow scenario where only one unit (Cabot Unit No. 2) was running at the time fish were released (13:30 – 14:04). The fish that were released on June 13 experienced a "high" flow scenario where 5 units (Cabot Units No. 1, 2, 3 ,4, 5) were running at the time fish were released (08:33 – 09:04) (Tables 4.4.2-1 and 4.4.2-2). All euthanized shad (n=24) that were released directly into Unit No. 2 were recovered by mobile tracking in the Cabot tailrace shortly after release (Tables 4.4.2-1 and 4.4.2-2).

The fish released on June 12 took an average time of 1 minute and 18 seconds to be recaptured in the tailrace, with a minimum time of 55 seconds and a maximum time of 3 minutes (Table 4.4.2-1). The fish released on June 13 took an average time of 1 minute and 50 seconds to be recaptured in the tailrace, with a minimum of 30 seconds and a maximum of 6 minutes and 22 seconds (Table 4.4.2-2).

Once all euthanized shad were mobile tracked downstream of Cabot Station on their release dates, additional mobile tracking efforts occurred weekly on four occasions (June 18, June 25, July 2 and July 11). After four weeks of tracking, the median distance traveled for all euthanized shad was 1,090.6 ft, with a minimum of 45.1 ft and a maximum of 13,442.8 ft (Figure 4.4.2-1). There was only one fish that traveled more than 10,000 ft downstream of Cabot Station; 90% of fish that were tracked on more than one occasion (n = 23) only traveled 4,337 ft or less (approximately to Montague WWTP) in one month of tracking (Figure 4.4.2-2). After June 18, the majority of euthanized fish settled and were observed in approximately the same locations (Cabot tailrace to the Deerfield River confluence) for the next three weeks (Figure 4.4.2-2).

FirstLight then assessed time of downstream movement from the tailrace until arrival at the lower end of Smead Island and Montague WWTP for both alive and dead cohorts. Figure 4.4.2-3 displays the Kaplan-

Meier survival curves for alive and dead fish that moved between the tailrace and Smead Island. Eventually, dead fish will float or become entrained in flow and arrive at this location; however, the majority of alive fish (~ 75%) will transition immediately while the first dead fish arrived in 3.7 hours. Further, only approximately 25% of the dead fish will arrive at Smead Island. Figure 4.4.2-4 displays the Kaplan-Meier curve for time until Montague WWTP arrival from the tailrace. Only 1 known dead fish made this transition. Approximately 75% of the fish known to be alive at the time of powerhouse passage transitioned to Montague WWTP. The minimum time for this transition was 11 minutes, while the slowest fish transitioned in 317 hours. Figure 4.4.2-5 displays the time until Montague WWTP arrival for the fish that passed via the powerhouse in the 2015 study. All 2015 fish transitioned within one month (720 hours), and about 75% transitioned almost immediately. Given the patterns of time until movement for the 2015 fish and the Kaplan-Meier curve for known alive fish in 2019, it is likely that a majority, if not all of the 2015 fish were alive at the time they arrived at Montague. When emigrating, American Shad move through the project very quickly.

Table 4.4.2-1: Euthanized tagged shad (n=12) released into Cabot Unit No. 2 on June 12, 2019

Fish Number	Frequency and Code	Sex	Length (mm)	Drop Time (hh:mm:ss)	Detection Time (hh:mm:ss)	Time Elapsed
1	148.340 152	F	525	13:30:30	13:33:30	3 m
2	148.340 154	F	504	13:36:57	13:38:22	1 m 25 s
3	148.340 151	F	494	13:38:46	13:39:43	57 s
4	148.340 155	M	451	13:40:12	13:41:08	56 s
5	148.340 153	F	503	13:42:07	13:43:27	1 m 20 s
6	148.340 156	F	514	13:43:44	13:44:44	1 m
7	148.340 158	F	502	13:45:45	13:46:57	1 m 12 s
8	148.340 157	M	468	13:47:30	13:48:30	1 m
9	148.340 159	F	525	13:49:18	13:51:26	2 m 8 s
10	148.340 162	F	472	13:55:30	13:57:00	1 m 30 s
11	148.340 163	M	455	13:59:10	14:01:18	2 m 8 s
12	148.340 160	F	531	14:04:05	14:05:00	55 s

Table 4.4.2-2: Euthanized tagged shad (n=12) released into Cabot Unit No. 2 on June 13, 2019

Fish Number	Frequency and Code	Sex	Length (mm)	Drop Time (hh:mm:ss)	Detection Time (hh:mm:ss)	Time Elapsed
13	148.340 167	F	526	08:33:15	08:35:00	1 m 45 s
14	148.340 161	F	520	08:35:55	08:37:10	1 m 15 s
15	148.340 165	F	457	08:38:40	08:40:25	1 m 45 s
16	148.340 164	M	453	08:41:15	08:42:05	50 s
17	148.340 166	M	444	08:43:55	08:45:15	1 m 20 s
18	148.340 168	M	466	08:45:45	08:51:58	6 m 13 s
19	148.340 170	F	482	08:54:40	08:55:58	1 m 28 s
20	148.340 172	F	409	08:56:25	08:56:55	30 s
21	148.340 169	F	503	08:57:00	08:57:45	45 s
22	148.340 171	M	390	08:59:50	09:00:50	1 m
23	148.340 174	F	545	09:01:45	09:04:05	2 m 20 s
24	148.340 173	F	489	09:04:38	09:06:25	1 m 47 s

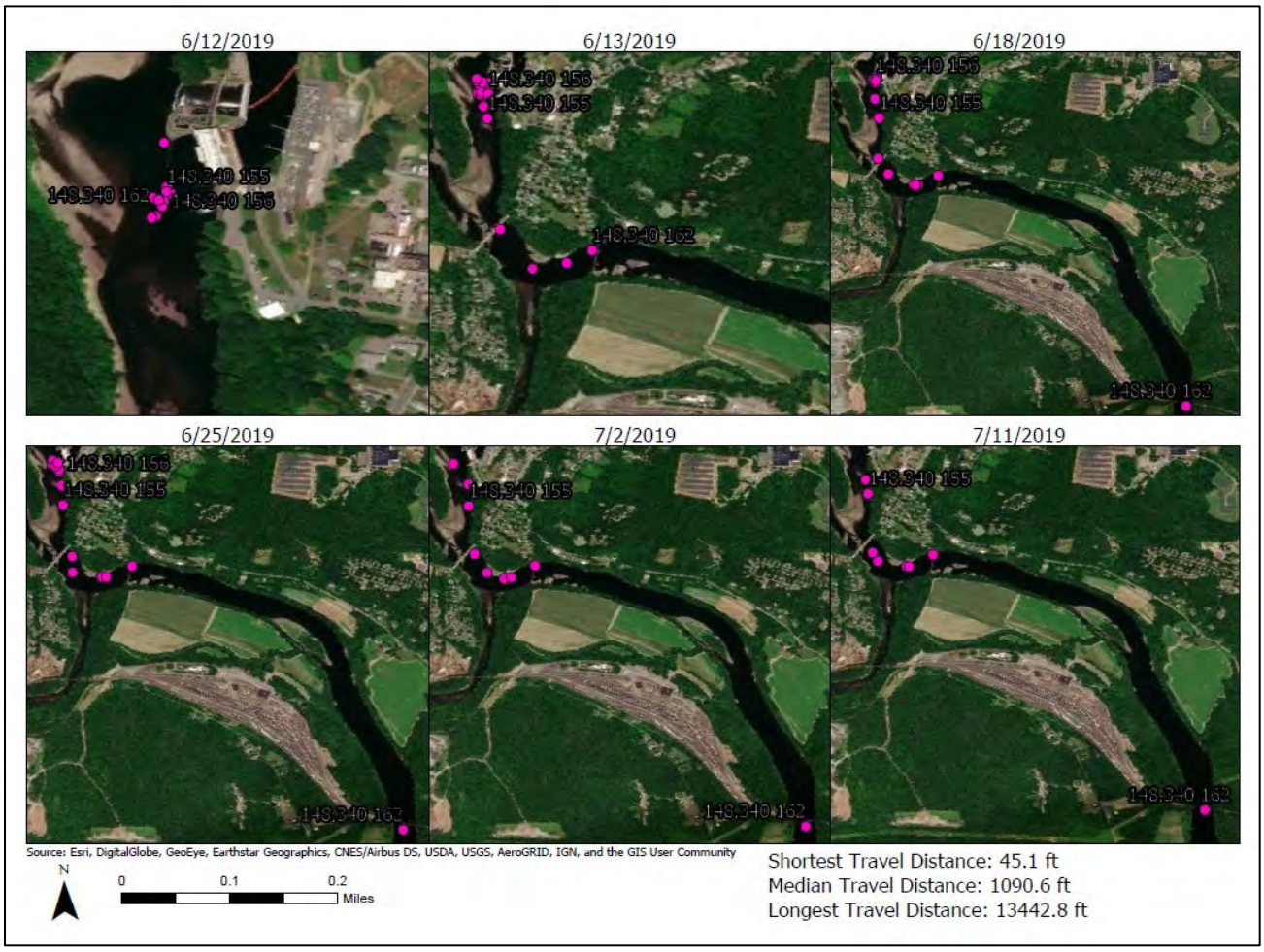

Figure 4.4.2-1: Locations of euthanized shad during six mobile tracking events

Figure 4.4.2-2: Distance traveled for euthanized shad (n = 24)

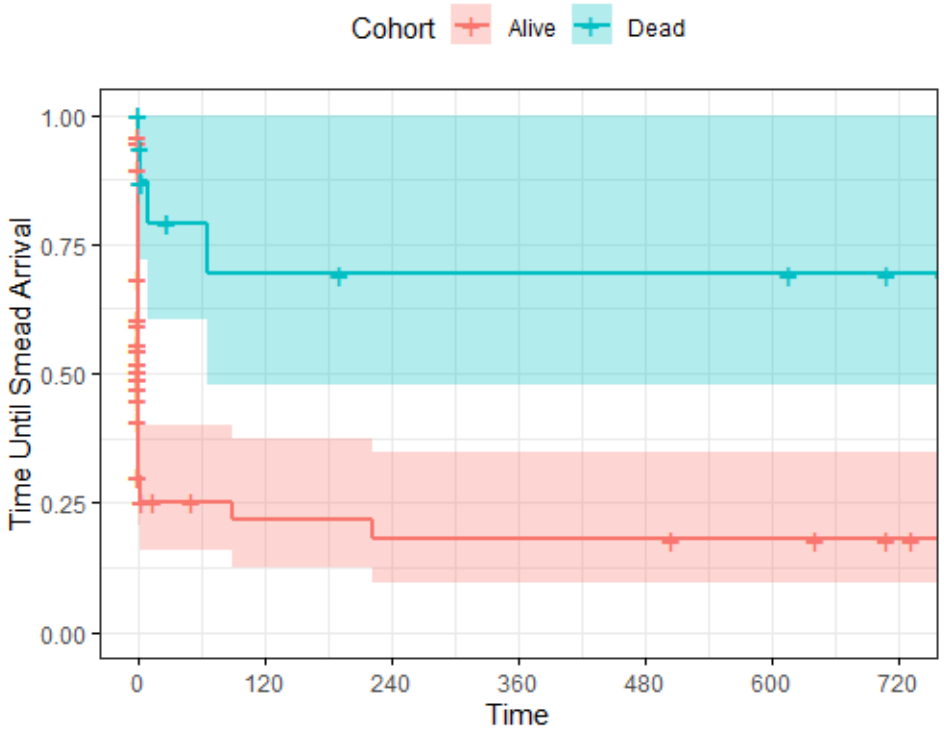

Figure 4.4.2-3. Time until Smead Island arrival for fish with known status when passing via Cabot Powerhouse.

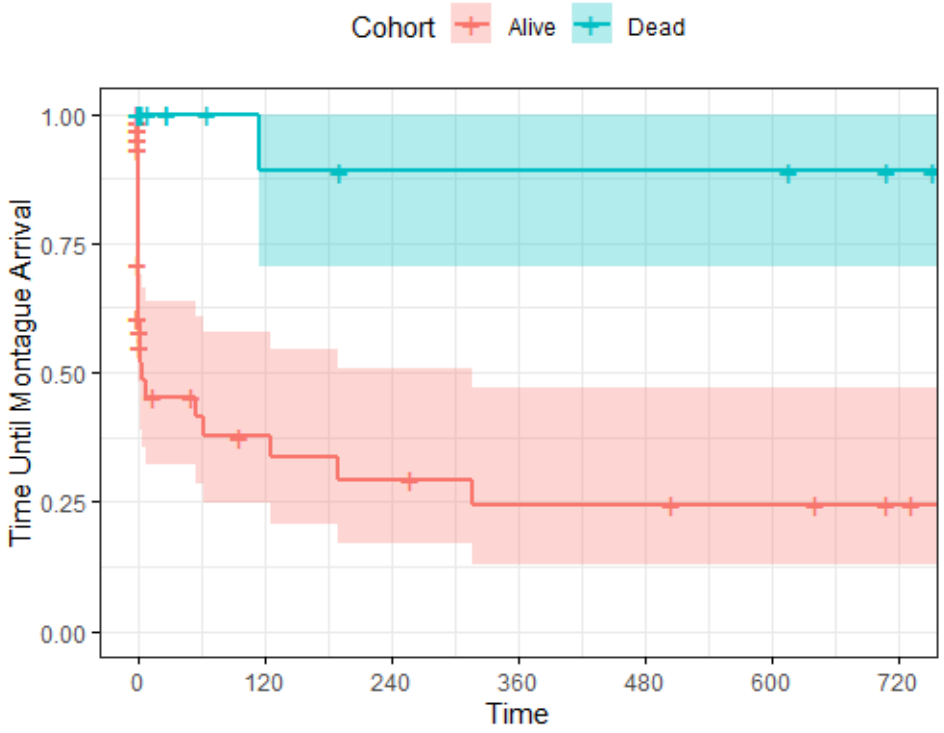

Figure 4.4.2-4. Time until Montague arrival for fish with known status when passing via Cabot Powerhouse.

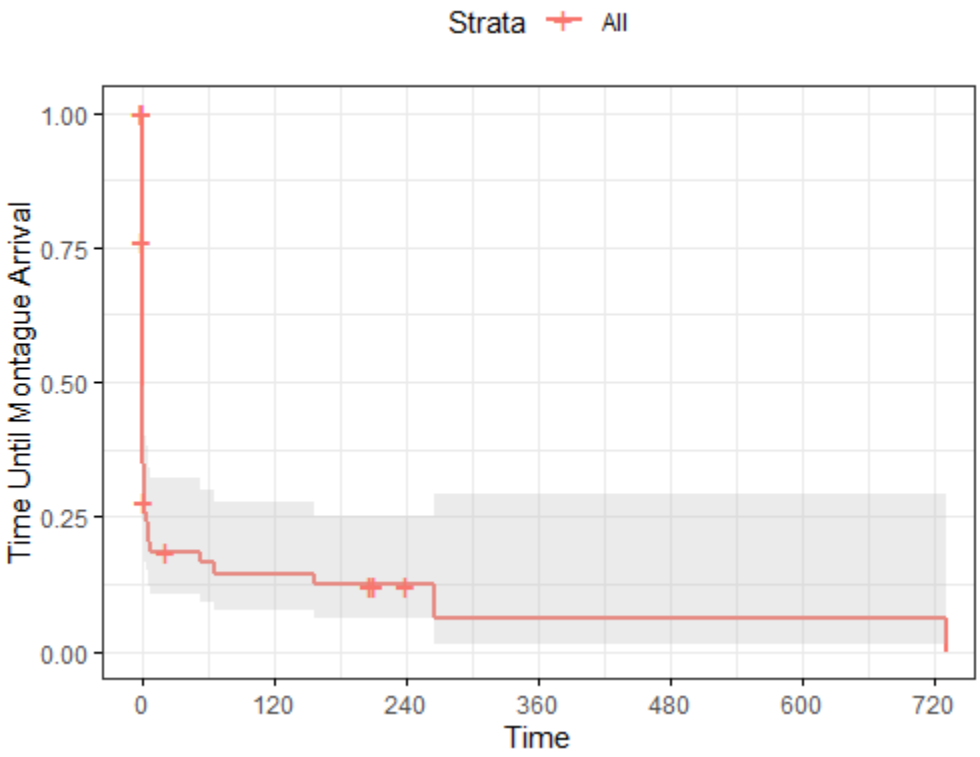

Figure 4.4.2-5. Time until Montague arrival for downstream migrants in the 2015 study.

5 CONCLUSIONS

Based on passage studies in 2015, 2018 and 2019, FirstLight determined that when the ultrasound array was present in the Cabot Station tailrace, fish were more likely to move into the Bypass Reach. The majority of fish that transitioned in less than 5 hours did so when the ultrasound array was operational. We also identified day° (10°C) to be a driving factor in many reaches. The more days with mean temperatures greater than 10°C, the less likely fish will move upstream. In every study year but 2016, a majority of the fish migrated through the bypass reach by the time passage at the Spillway ladder reached its 50th percentile, suggesting that the run through the bypass reach is short and limited by temperature. One would expect the run to conclude earlier on warmer, drier years as compared to colder, wet years. Interestingly, the study year with the largest proportion of fish to arrive at the spillway from Conte discharge was 2019 (50%), but 2019 had the longest on average travel time (29.3 hours to reach the TFD spillway) and was an exceptionally high flow year as compared to others. For all study years, water temperature appeared to be a more important driver of movement since fish moved through the bypass reach over a range of high and low flow conditions. Further, overall movement upstream in all study years began to decrease when water temperature reached 18.5 °C, which coincides with peaking spawning temperature (Collete and Klein-MacPhee 2002), regardless of flow conditions. Water temperatures generally reached 18.5 °C by the end of May, except in 2019 when water temperature reached 18.5 °C on June 11.

This study attempted to assess adult shad migration in the area of Rawson Island and Rock Dam by placing telemetry receivers in all routes of passage through the island complex. There were high flows (>20,000 cfs) in the bypass reach during the last two weeks of May that prohibited access to these receivers for regular maintenance. As a result, all of the receivers around Rawson Island experienced a power outage during this time. Late May was also when many of the tagged fish were moving through this reach. Therefore, the detections at those receivers were limited and determination of route of passage through the Rawson Island complex is inconclusive.

To determine if adult shad migrate by the Station No.1 tailrace under a flow split of 50% spill from the TFD and 50% from Station No.1 discharge, a ratio was calculated (Station No.1 discharge: bypass flow). A CoxPH model comparing movement and the ratio of Station No.1 to bypass flow for all years of telemetry studies (2015, 2016, 2018, and 2019) was found to be insignificant, suggesting that the Station No. 1 discharge does not influence movement when bypass flow and Station No. 1 discharge are equal. Station No. 1 discharge rarely exceeded spill to the bypass reach during the 2019 passage season; it only did so after June 30, which was about 2.5 weeks after movement had already began to decrease.

FirstLight assessed the survival of adult shad as they passed downstream through the Turners Falls Project, and found that immediate survival was 100% while 65.5% of the fish known to pass via the powerhouse were expected to survive to the 48-hour threshold and beyond. Shad exiting via the log sluice also had 100% initial survival while 89% of the fish that passed via the log sluice survived after 48 hours. Adult shad that passed downstream through the Project and survived, migrated downstream quickly, whereas dead fish remained between the Project and the Deerfield River confluence. The results of the LRDR model are supported by the dead drift study, which found that a majority of the known-dead fish only drifted as far as the Deerfield confluence in one month's time.

6 LITERATURE CITED

Amstrup, S.C., McDonald, T.L., and Manly, F.J. (2005). Handbook of Capture – Recapture Analysis. Princeton University Press, Princeton and Oxford.

Beeman, J. W., & Perry, R. W. (2012). Telemetry Techniques: A User Guide for Fisheries Research. In N. Adams, J. Beeman, & J. Eiler (Eds.). American Fisheries Society.

Beyersmann, J., Allignol, A., & Schumacher, M. (2011). Competing Risks and Multistate Models with R. New, York, NY: Springer.

Blaxter, J.H.S., and Hunter, J.R. (1982). The biology of the Clupeid fishes. Advances in Marine Biology Advances in Marine Biology Volume, 20:1-223.

Carlson, T. J. & Popper, A. N. (editors) (1997). Using sound to modify fish behavior at power-production and water-control facilities. A workshop held December 12-13, 1995, Portland, Oregon. Published by Bonneville Power Administration, Portland Oregon, 362 pp.

Castro-Santos, T. (2004). Quantifying the combined effects of attempt rate and swimming capacity on passage through velocity barriers. Canadian Journal of Fisheries and Aquatic Sciences, 61, 1602-1615.

Castro-Santos, T. (2005). Optimal swim speeds for traversing velocity barriers: an analysis of volitional high-speed swimming behavior of migratory fishes. Journal of Experimental Biology, 208, 421-432.

Castro-Santos, T. (2006). Modeling the effect of varying swim speeds on fish passage through velocity barriers. Transactions of the American Fisheries Society, 135, 1230-1237.

Collette, B.B. and G. Klein-MacPhee. (2002). Bigelow and Schroeder's Fishes of the Gulf of Maine. 3rd edition. Smithsonian Institution Press, Washington. 748 p.

Cooch, E., & White, G. (2006). Program MARK: A Gentle Introduction. Available in. pdf format for free download at http://www. phidot. org/software/mark/docs/book.

Denton, E. J., and Blaxter, J. H. S. (1976). The mechanical relationships between the Clupeid swimbladder, inner ear and lateral line. Journal of the Marine Biological Association of the United Kingdom, 56(3):787-807.

Frank, H.J., Mather, M.E., Smith, J.M., Muth, R.M., Finn, J.T. and McCormick, S.D. (2009). What is "fallback"?: metrics needed to assess telemetry tag effects on anadromous fish behavior. Hydrobiologia 635, 237–249.

Gibson, A., Jamie, F., and Myers, R.A. (2002). Effectiveness of a high-frequency-sound fish diversion system at the Annapolis Tidal Hydroelectric Generating Station, Nova Scotia. North American Journal of Fisheries Management 22(3):770-84.

Gurshin, C.W. D., Balge, M.P., Taylor, M., and Lenz, B. (2014). Importance of ultrasonic field direction for guiding juvenile blueback herring past hydroelectric turbines. North American Journal of Fisheries Management 34(6):1242-1258.

Guindon, A. and D. Desrochers. (2016a). Rivière des Prairies generating station – Monitoring downstream migration shad -2016 and evaluation of a guidance system, [by] MEDIUM Inc.

[pour] l'unité Environnement, Gestion des actifs et conformité réglementaire, Hydro-Québec [for] Environment, Asset Management and Regulatory Compliance Unit, Hydro-Québec Production, 56 p.Production, 56 p. et annexes. and annexes.

Guindon, A. and D. Desrochers. (2016b). ESSAI DE GUIDAGE DE L'ALOSE SAVOUREUSE DANS LA RÉGION DE MONTRÉAL, [by] MEDIUM Inc. [pour] l'unité Environnement, Gestion des actifs et conformité réglementaire, Hydro-Québec[for] Environment, Asset Management and Regulatory Compliance Unit, Hydro-Québec Production, 52 p. Production, 52 p.

Higgs, D. M. (2004). Development of ultrasound detection in American Shad (Alosa Sapidissima). Journal of Experimental Biology 207(1):155-163.

Higgs, D. M, D. T. T. Plachta, A. K. Rollo, M. Singheiser, M. C. Hasting and A. N. Popper. (2004). Development of ultrasound detection in American Shad (Alosa sapidissima). The Journal of Experimental Biology 207, 155-163.

Kynard, B., and Taylor, R. (1984). Studies of downrunning adult alosids in the Holyoke Dam Canal System. Final Report. Northeast Utilities. 29 pp.

Lebreton, J.-D., Burnham, K. P., Clobert, J., & Anderson, D. R. (1992). Modeling Survival and Testing Biological Hypotheses Using Marked Animals: A Unified Approach with Case Studies. Ecological Monographs, 62(1): 67-118.

Marsland, S. (2009). Machine Learning: An Algorithmic Perspective. Boca Raton, Florida: CRC Press, Taylor and Francis Group.

Richert, W., & Pedro-Coelho, L. (2013). Building Machine-Learning Systems with Python. Birmingham, UK: Packt Publishing.

Sibly, R., H. Nott. and D. Fletcher. (1990). Splitting behavior into bouts. Anim. Behavior 39: 63-69.

Steffler, P. & Blackburn, J. (2002). River2D: Two-dimensional depth-averaged model of river hydrodynamics and fish habitats. University of Alberta, Edmonton, Canada.

Stone, J. V. (2013). Bayes' Rule: A Tutorial Introduction to Bayesian Analysis. Lexington, KY: Sebtel Press.

Therneau, T., Crowson, C., & Atkinson, E. (2016, October). Multi-state models and competing risks. From https://cran.r-project.org/web/packages/survival/vignettes/compete.pdf

Therneau, T., Crowson, C., & Atkinson, E. (2017). Using Time Dependent Covariates and Time Dependent Coefficients in the Cox Model.

APPENDIX A – TELEMETRY STATION CALIBRATION RESULTS

APPENDIX A:

2019 TELEMETRY CALIBRATION

APPENDIX A: Telemetry Network Calibration and Equipment Effectiveness

Radio Telemetry Calibration:

Each telemetry station was tested with a radio transmitting tag prior to any Shad being released to ensure adequate power readings, range and proper calibration of equipment. One tag, programed with code 13, was used as a '*test tag*' during the calibration period. This code was not used for any tags inserted into Shad during the study. The test radio tag was attached to fishing line and tested at a water depth of approximately 4 to 5 ft to mimic the swimming depth of adult American Shad. One member of the field crew remained on land monitoring the receiver output signals and two field staff used a boat to test the targeted detection zone at each telemetry station. Communication via handheld two-way-radios allowed transfer of power signals at different locations that were recorded on a map for calibration purposes.

A list of the receivers used for this study is provided in Table 1 of the main report. Orion receivers output an average power number for each contact, which is recorded in decibel levels (db). These numbers are negative, with less negative numbers being higher in signal strength. Lotek receivers output an average power number for each contact, which is also recorded in decibel levels (db). These numbers are positive, with high numbers signifying a stronger signal.

All station figures listed below show the position of the 'test tag' and the average power levels associated within the detection zones recorded during testing (noted in white). Several test detections were recorded at each location.

Station 1: Montague Wastewater Treatment

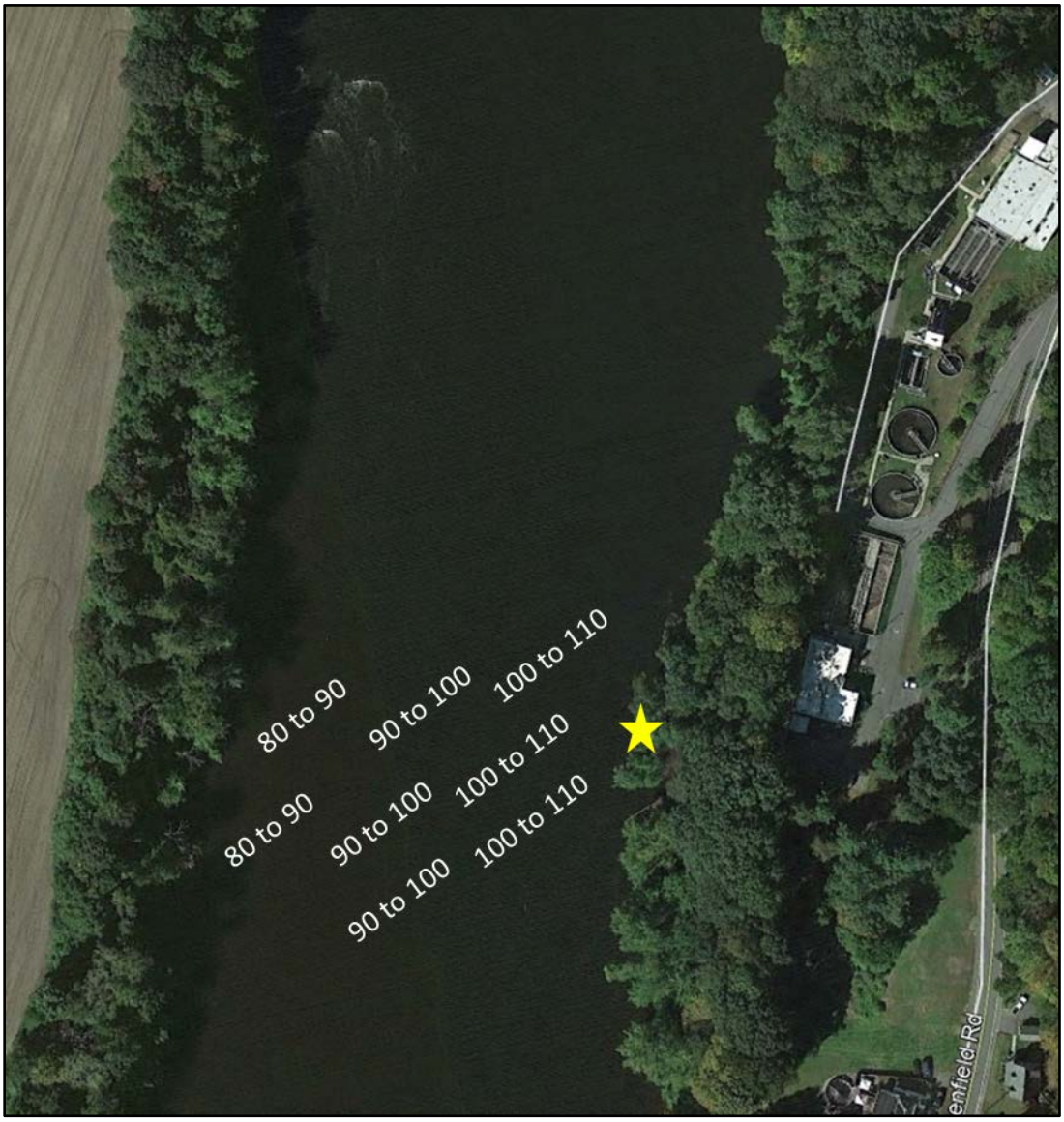

Figure 1: The yellow star marks the approximate placement of the yagi antenna and the Lotek receiver used to detect fish moving across the width of the river at River Mile 119.5. The radio test tag produced power levels ranging from 80s to 110 db with highest powers located near the bank of the river closest to the yagi antenna and attenuating slightly toward the far bank.

Station 2: Entrance to the Deerfield River

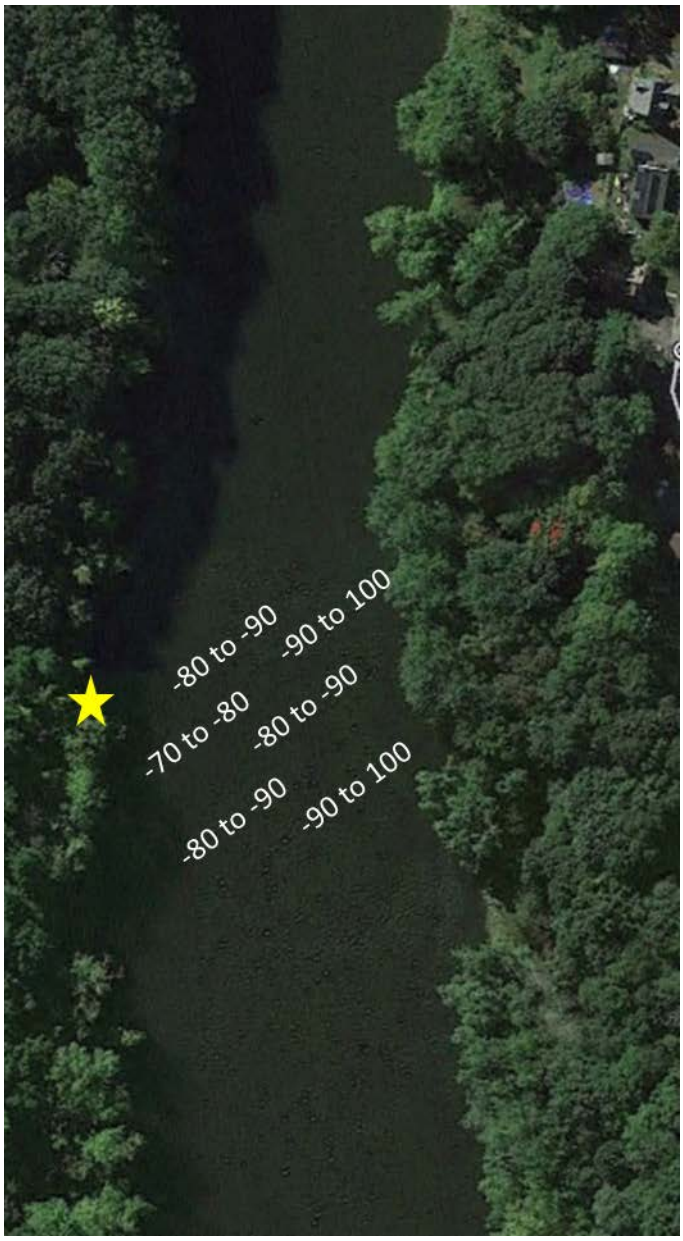

Figure 2: The yellow star marks the approximate location of the Yagi antenna and the Orion receiver used to detected fish moving across the width of the Deerfield River at River Mile 119.5. The radio test tag produced power levels ranging from -70s to -100s db with highest powers located near the bank and attenuating slightly toward the far bank of the river.

Station 3E: Downstream Smead Island East Channel

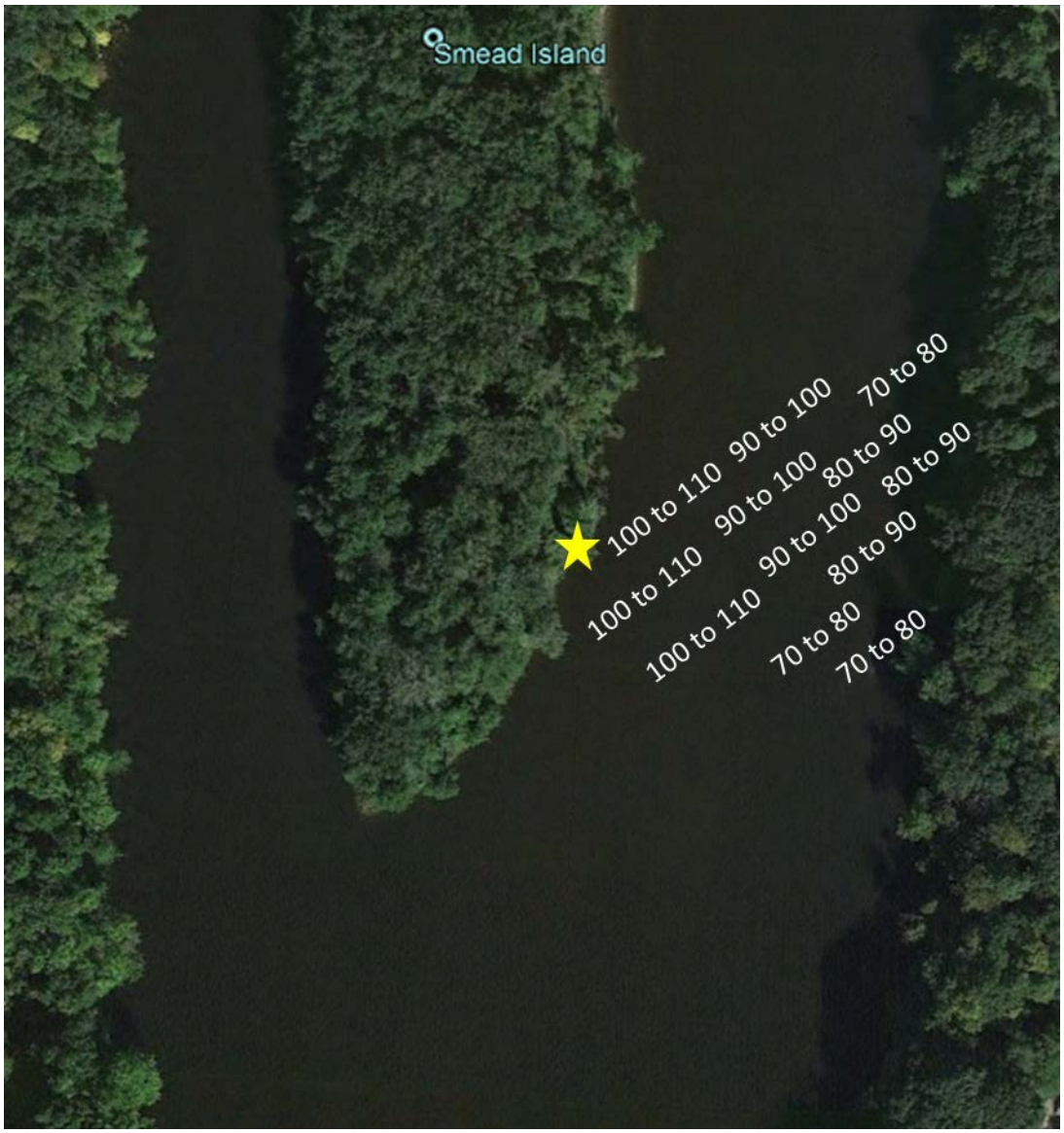

Figure 3: The yellow star marks the approximate placement of the yagi antenna and receiver used to detect fish moving across the width of the river at River Mile 120. An Lotek receiver was used to monitor the eastern channel. The radio test tag produced power levels ranging from 70s to 110s db at the Lotek receiver, with highest powers located near the bank of the river on the East channel of Smead Island closest to the yagi antenna and attenuating slightly toward the far bank.

Station 3W: Downstream Smead Island West Channel

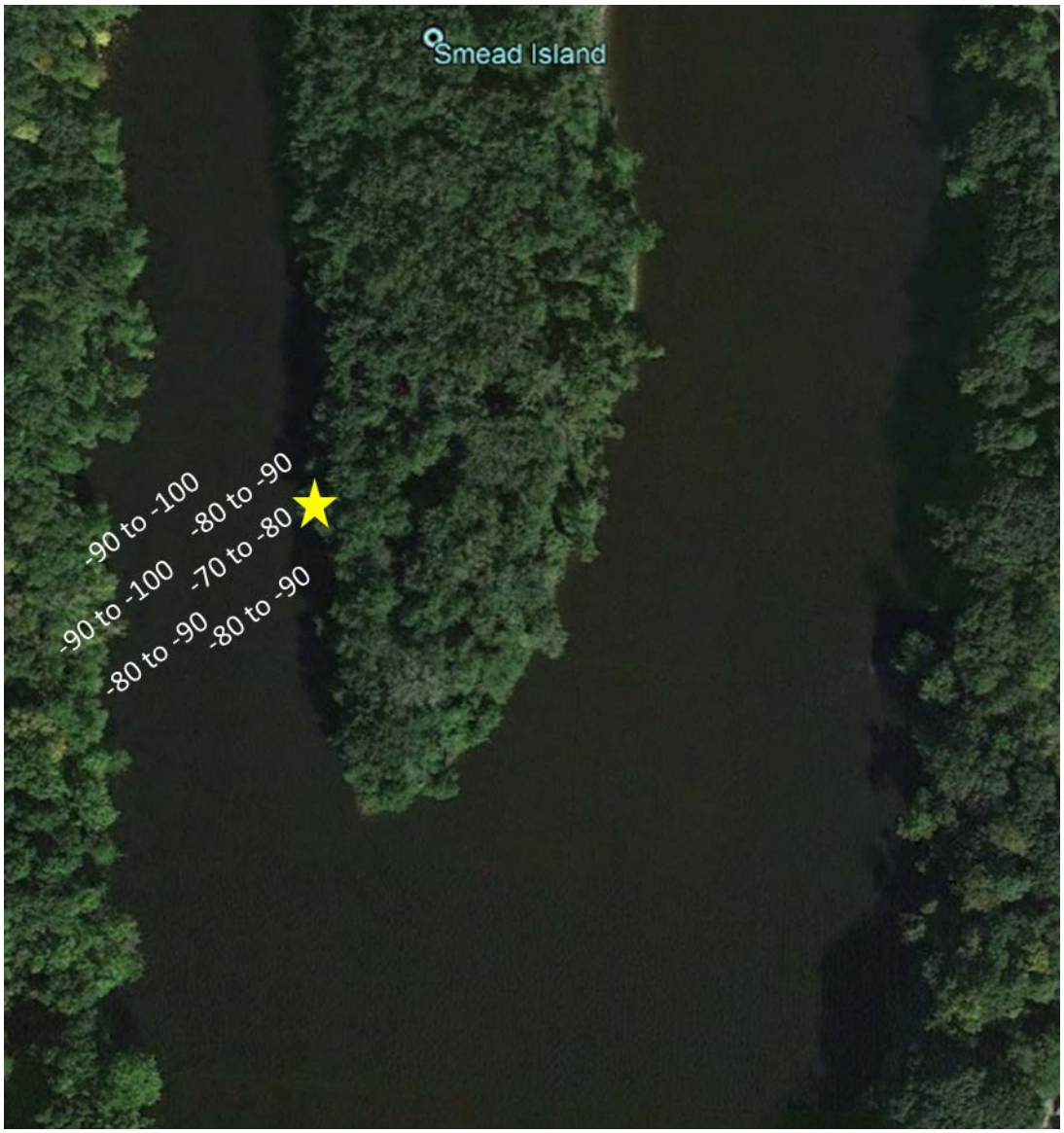

Figure 4: The yellow star marks the approximate placement of the yagi antennaa and receiver used to detect fish moving across the width of the river at River Mile 120. An Orion receiver was used to monitor the western channel. The radio test tag produced power levels ranging from -70 to -100 db at the Orion receiver, with highest power levels read near the island bank, closer to the yagi antenna, and attenuating toward the western bank. The test tag was not detected downstream of the islands point.

Station 4**:** Cabot Tailrace Left

Figure 5: The yellow star marks the approximate placement of the yagi antenna and the Orion receiver used to detect fish moving in the Cabot Tailrace at River Mile 120. The radio test tag produced power levels ranging from -70s to -110 db at both locations with highest powers located closest to the yagi antennas and attenuating slightly toward the opposite bank.

Station 5**:** Cabot Tailrace Right

Figure 6: The yellow star marks the approximate placement of the yagi antenna and the Orion receiver used to detect fish moving in the Cabot Tailrace at River Mile 120. The radio test tag produced power levels ranging from -70s to -110 db at both locations with highest powers located closest to the yagi antennas and attenuating slightly toward the opposite bank.

Station 6: Cabot Ladder Entrance Dipole

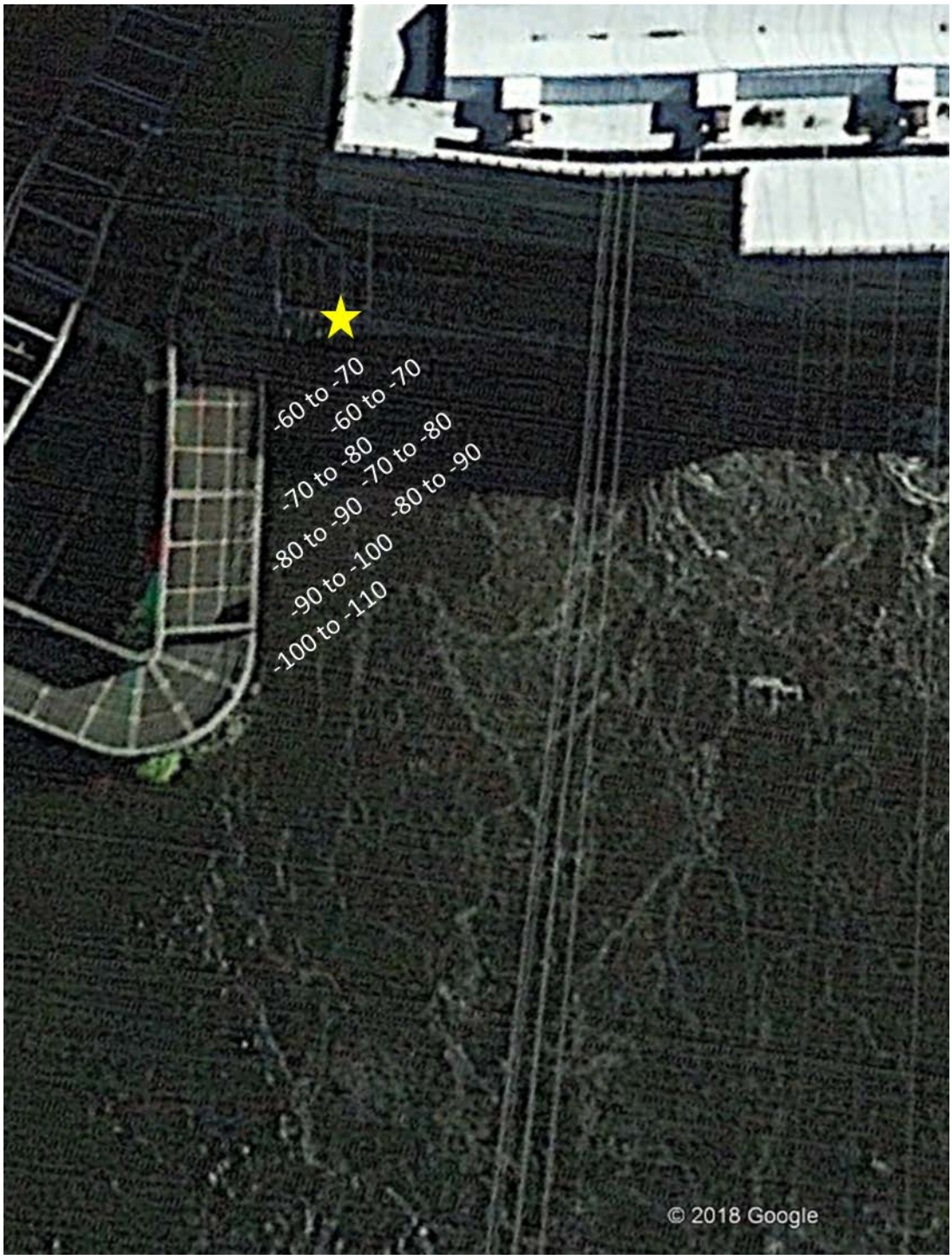

Figure 7: The yellow star marks the approximate placement of the dipole antenna and the Orion receiver used to detect fish moving to the Cabot Ladder entrance at River Mile 120. The radio test tag produced power levels ranging from -60s to -110s db with highest powers located near Cabot Fish ladder entrance and attenuating slightly farther out.

Station 7: Cabot Far-field

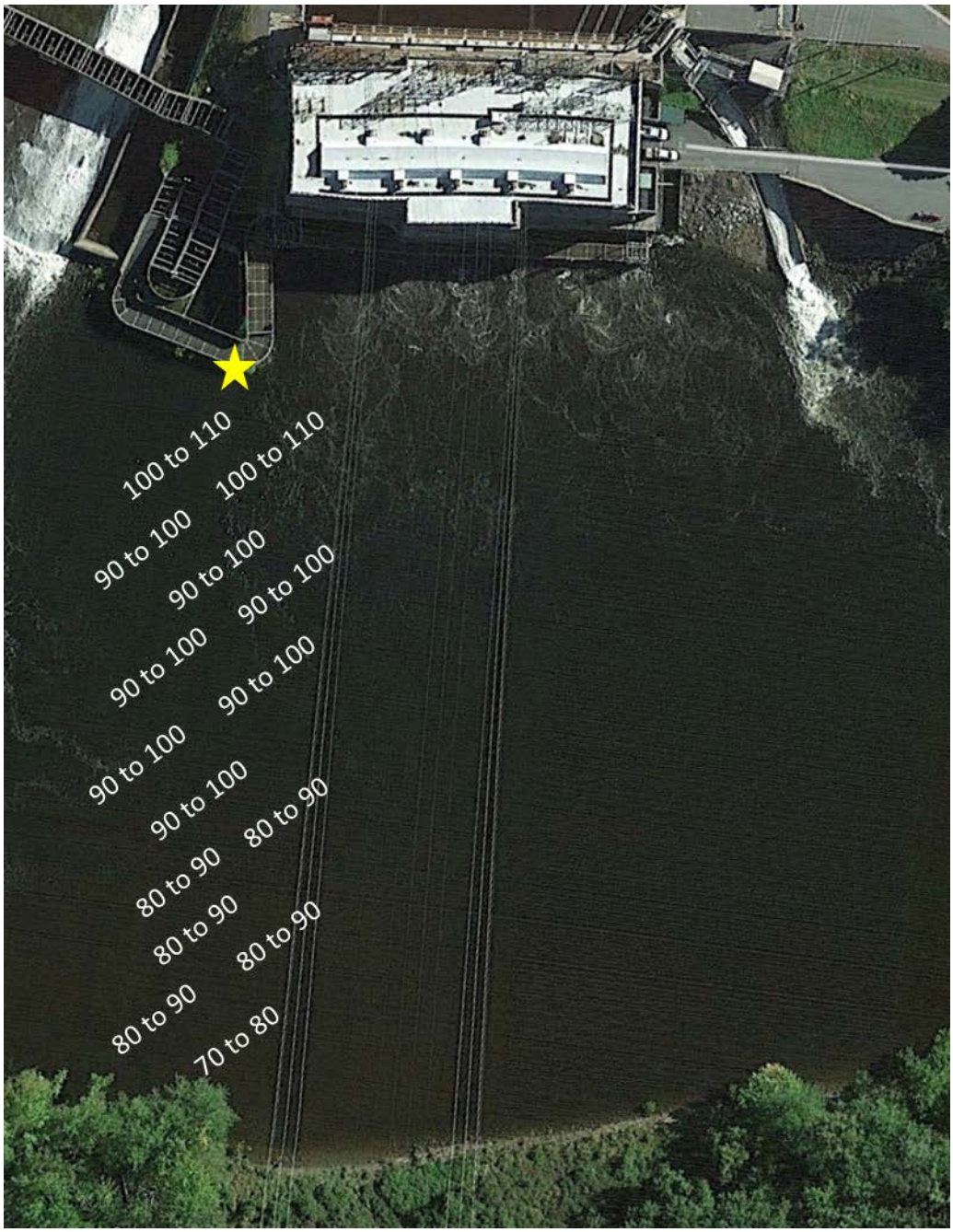

Figure 8: The yellow star marks the approximate placement of the Yagi antenna and the Lotek receiver used to detect fish moving passed the upstream end of Smead Island at River Mile 120. The radio test tag produced power levels ranging from high 70s to mid-110s db with highest powers located near the yagi antenna and attenuating toward the bank of Smead Island.

Station 8: Bypass Reach- Conte Discharge

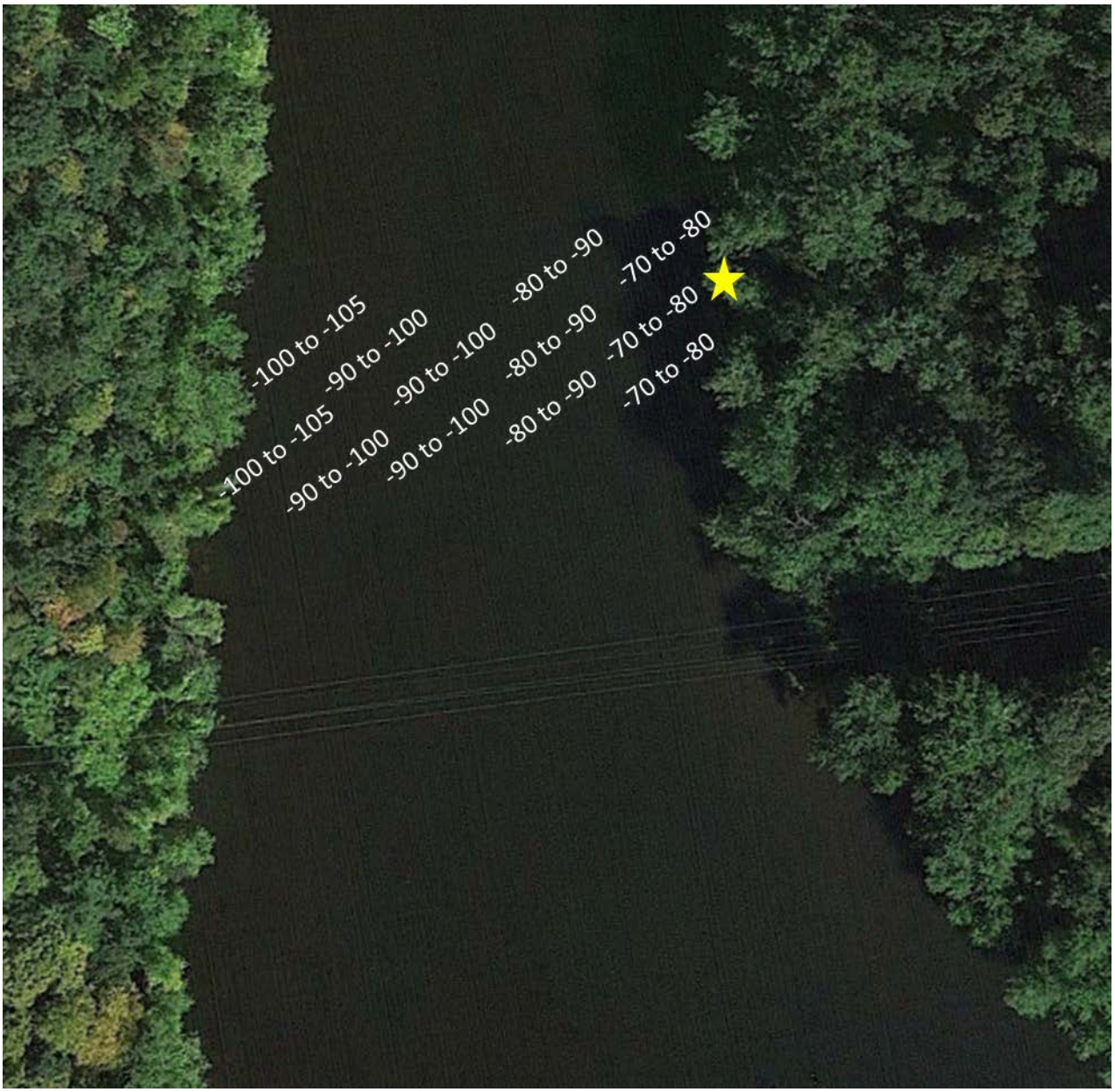

Figure 9: The yellow star marks the approximate placement of the Yagi antenna and the Orion receiver used to detect fish moving upstream through the Bypass Reach at River Mile 120, near the Conte Lab Discharge. The radio test tag produced power levels ranging from -70s to -105 db with highest powers located near the yagi antenna and attenuating toward the opposite bank of the river.

Station 9: Rock Dam

Figure 10: The yellow star marks the approximate placement of the Yagi antenna and the orion receiver used to detect fish moving upstream through the Bypass Reach, up to and past Rock Dam.. The radio test tag produced power levels ranging from -70s to -105 db with highest powers located near the yagi antenna and attenuating toward the opposite bank of the river.

Station 10: Lower Left Channel Rawson Island

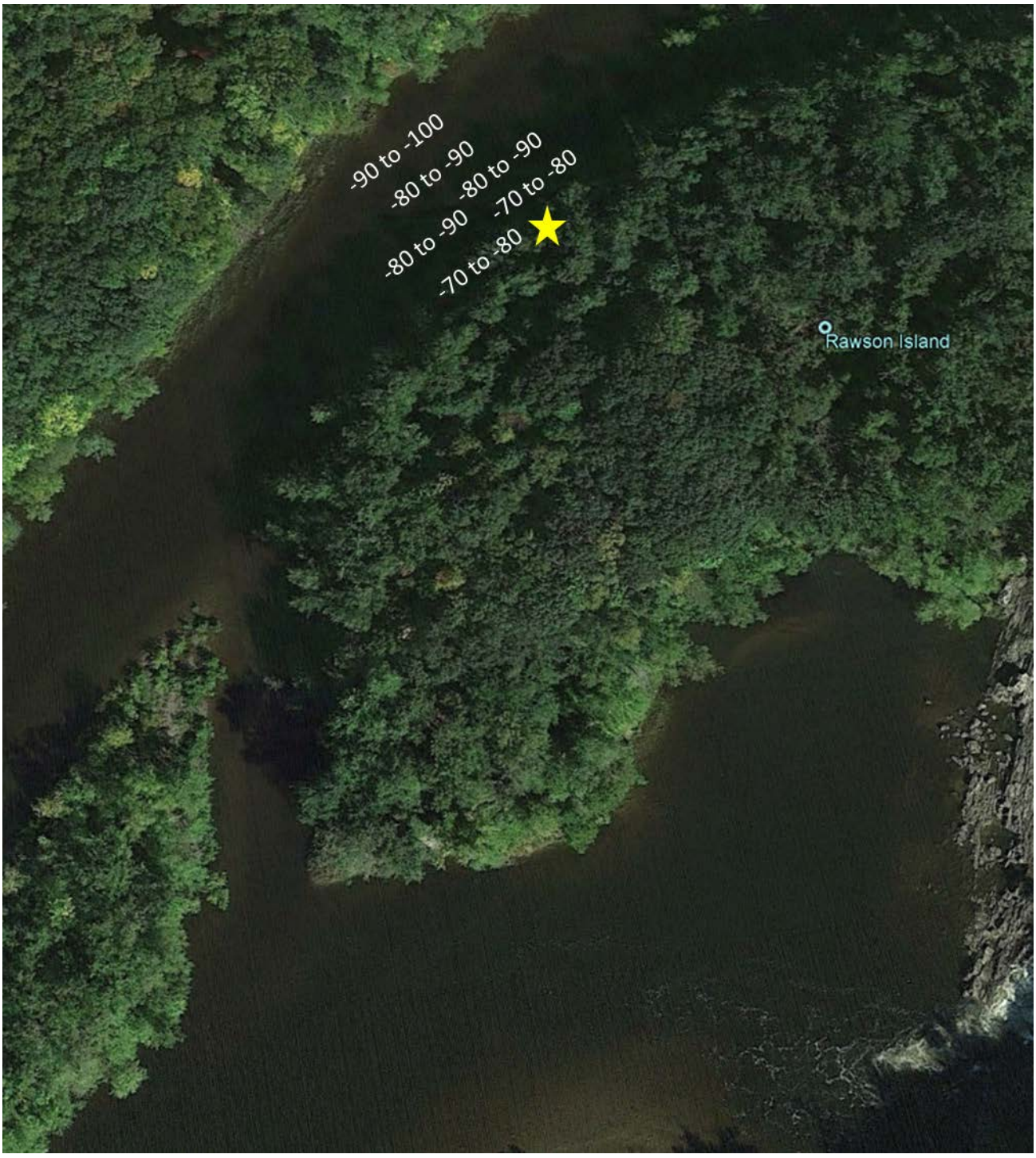

Figure 11: The yellow star marks the approximate placement of the Yagi antenna and the orion receiver used to detect fish moving upstream through the Bypass Reach, up to the left channel of Rawson Island. The radio test tag produced power levels ranging from -70s to -100 db with highest powers located near the yagi antenna and attenuating toward the opposite bank of the river.

Station 11: Middle Channel Rawson Island

Figure 12: The yellow star marks the approximate placement of the Yagi antenna and the orion receiver used to detect fish moving upstream through the Bypass Reach, up the middle channel of Rawson Island. The radio test tag produced power levels ranging from -70s to -100 db with highest powers located near the yagi antenna and attenuating toward the opposite bank of the river.

Station 12: Left Channel Rawson Island

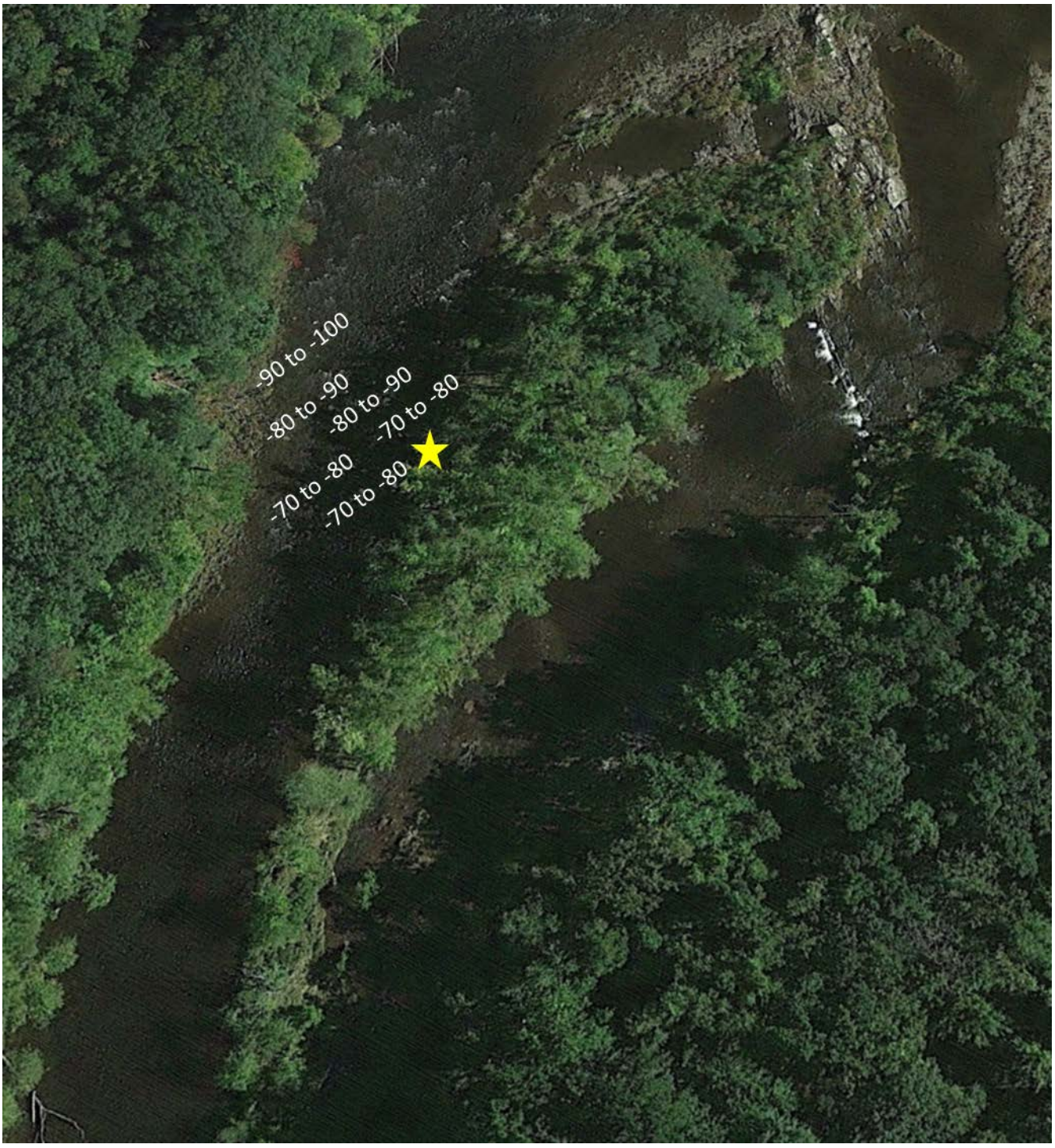

Figure 13: The yellow star marks the approximate placement of the Yagi antenna and the orion receiver used to detect fish moving upstream through the Bypass Reach, up the left channel of Rawson Island. The radio test tag produced power levels ranging from -70s to -100 db with highest powers located near the yagi antenna and attenuating toward the opposite bank of the river.

Station 13: Bypass Reach, Upstream of Rawson

Figure 14: The yellow star marks the approximate placement of the 6-Element Yagi antenna and the Lotek receiver used to detect fish moving upstream through the Bypass Reach, upstream of Rawson Island. The radio test tag produced power levels ranging from 90s to 110 db with highest powers located near the yagi antenna and attenuating toward the opposite bank of the river.

Station 14: Bypass Reach, Downstream Station 1

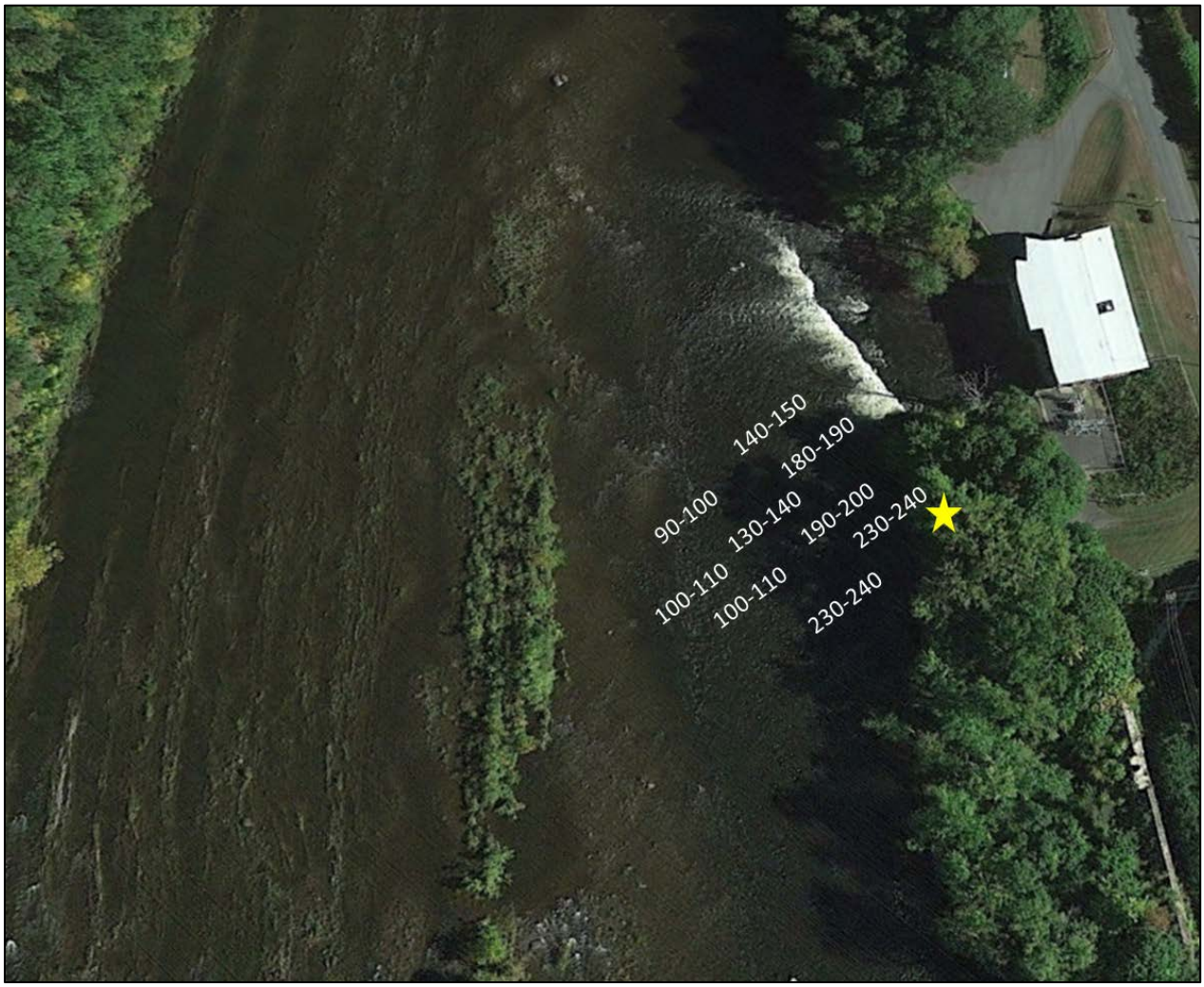

Figure 15: The yellow star marks the approximate placement of the 6-Element Yagi antenna and the Lotek receiver used to detect fish moving upstream through the Bypass Reach, downstream of Station 1. The radio test tag produced power levels ranging from 90 to 240 db with highest powers located near the yagi antenna and attenuating toward the opposite bank of the river.

Station 15: Bypass Reach, Upstream Station 1

Figure 16: The yellow star marks the approximate placement of the 6-Element Yagi antenna and the Lotek receiver used to detect fish moving upstream through the Bypass Reach, downstream of Station 1. The radio test tag produced power levels ranging from 100 to 210 db with highest powers located near the yagi antenna and attenuating toward the opposite bank of the river.

Station 16: Spillway Ladder Entrance

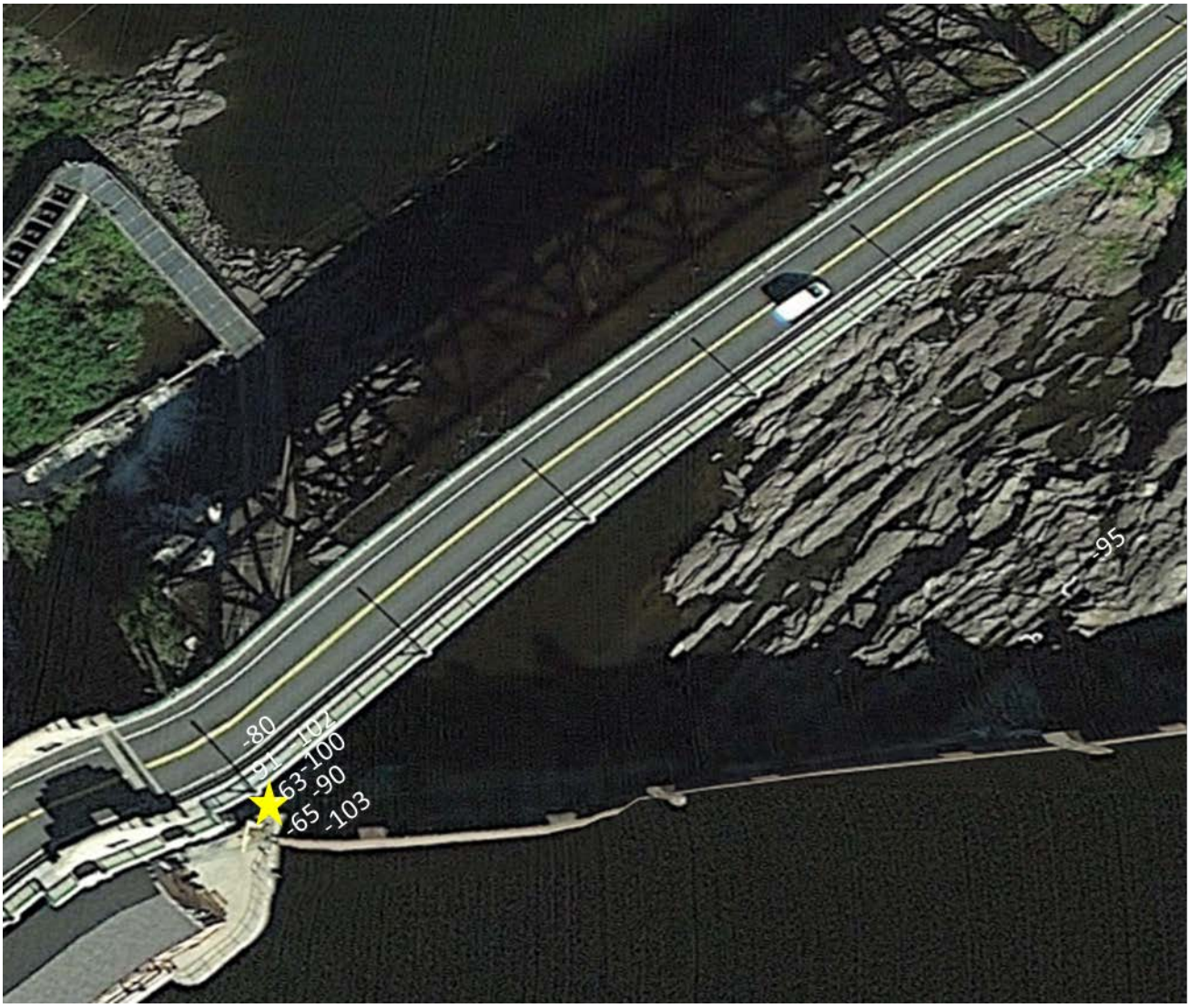

Figure 17: The yellow star marks the approximate placement of the dipole antenna and the orion receiver used to detect fish moving upstream through the spillway fish ladder entrance. The radio test tag produced power levels ranging from -63 to -102 db with highest powers located near the dipole antenna and attenuating away from the dipole.

Station 17: Spillway Ladder Vicinity

Figure 18: The yellow star marks the approximate placement of the yagi antenna and the Lotek receiver used to detect fish moving upstream towards the spillway fish ladder entrance. The radio test tag produced power levels ranging from 130 to 140 db with highest powers located near the yagi antenna and attenuating toward the opposite bank of the river.

Station 18: Cabot Station Forebay

Figure 19: The yellow star marks the approximate placement of the yagi antenna and the orion receiver used to detect fish moving downstream towards the Cabot station forebay. The radio test tag produced power levels ranging from -70 to -110 db with highest powers located near the yagi antenna and attenuating toward the opposite bank of the river.

Station 19: Cabot Log Sluice

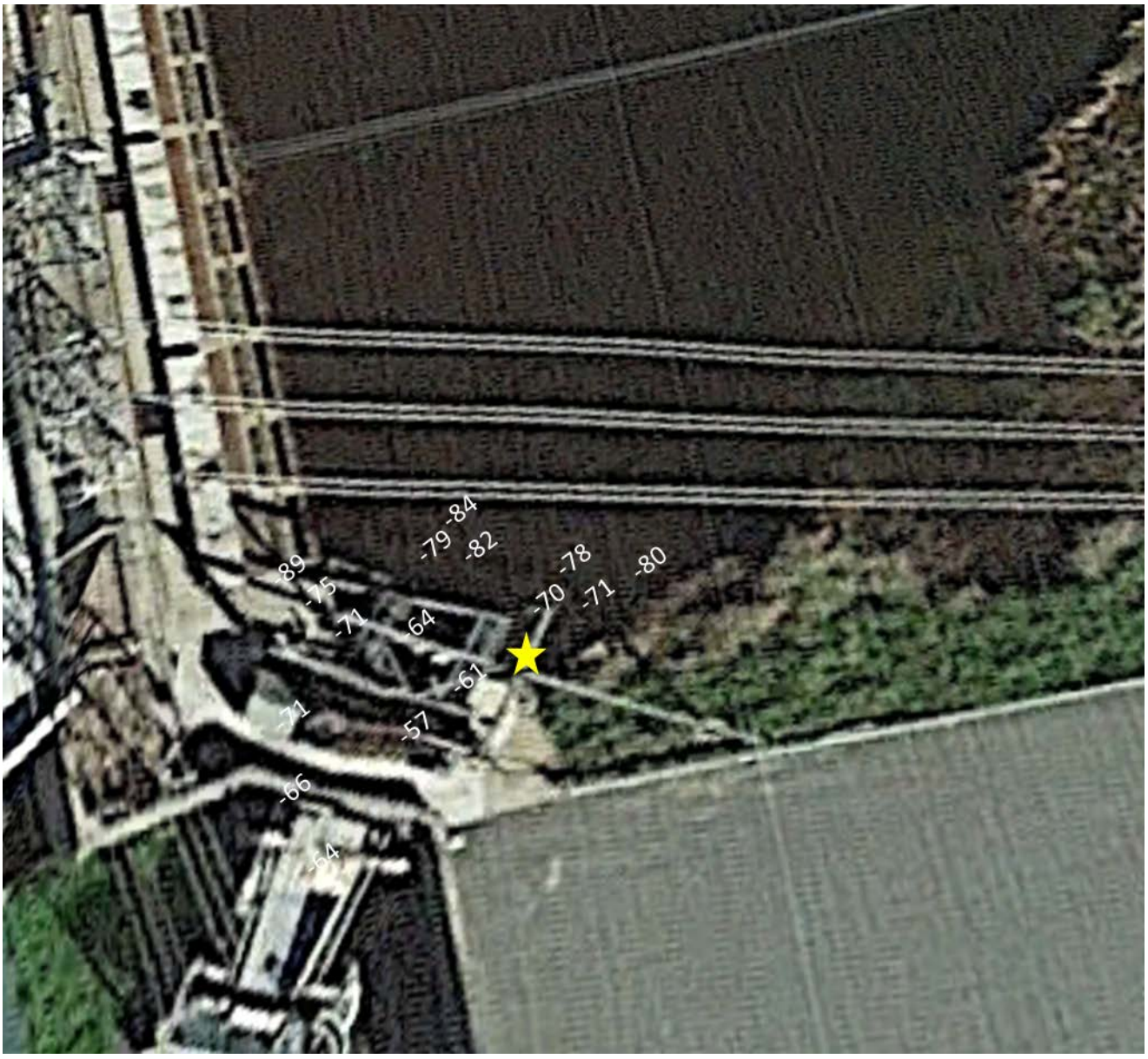

Figure 20: The yellow star marks the approximate placement of the dipole antenna and the orion receiver used to detect fish moving downstream towards the Cabot station log sluice. The radio test tag produced power levels ranging from -57 to -89 db with highest powers located near the dipole antenna and attenuating away from the antenna.

Station 20: Copley Tunnel

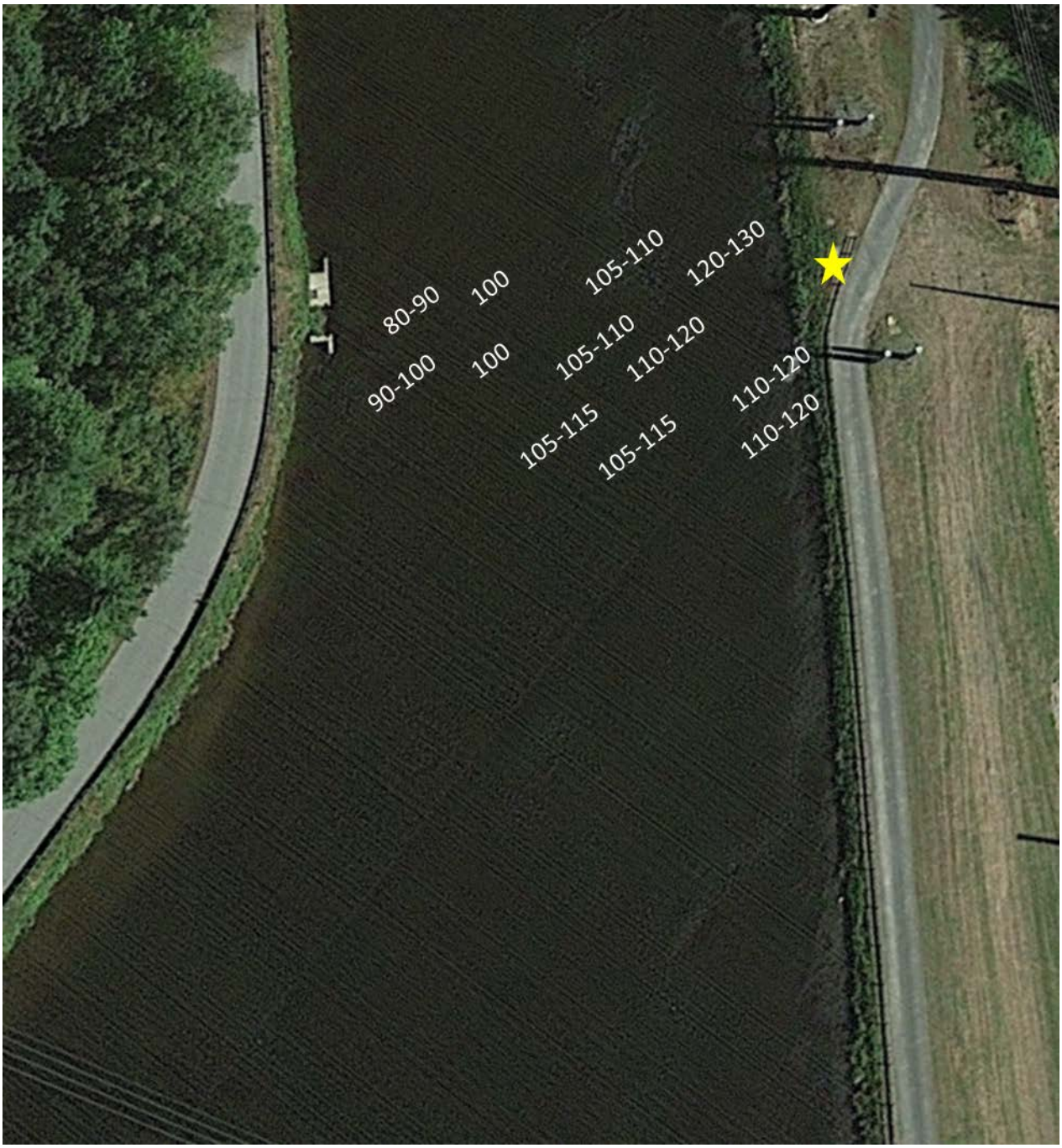

Figure 21: The yellow star marks the approximate placement of the yagi antenna and the Lotek receiver used to detect fish moving downstream towards Cabot station. The radio test tag produced power levels ranging from 80 to 130 db with highest powers located near the yagi antenna and attenuating towards the opposite bank.

Station 21: Nourse Farms

Figure 22: The yellow star marks the approximate placement of the yagi antenna and the Lotek receiver used to detect fish moving upstream towards Cabot station. The radio test tag produced power levels ranging from 60s to 140s db with highest powers located near the yagi antenna and attenuating towards the opposite bank.

Station 22: Hatfield Wastewater Treatment

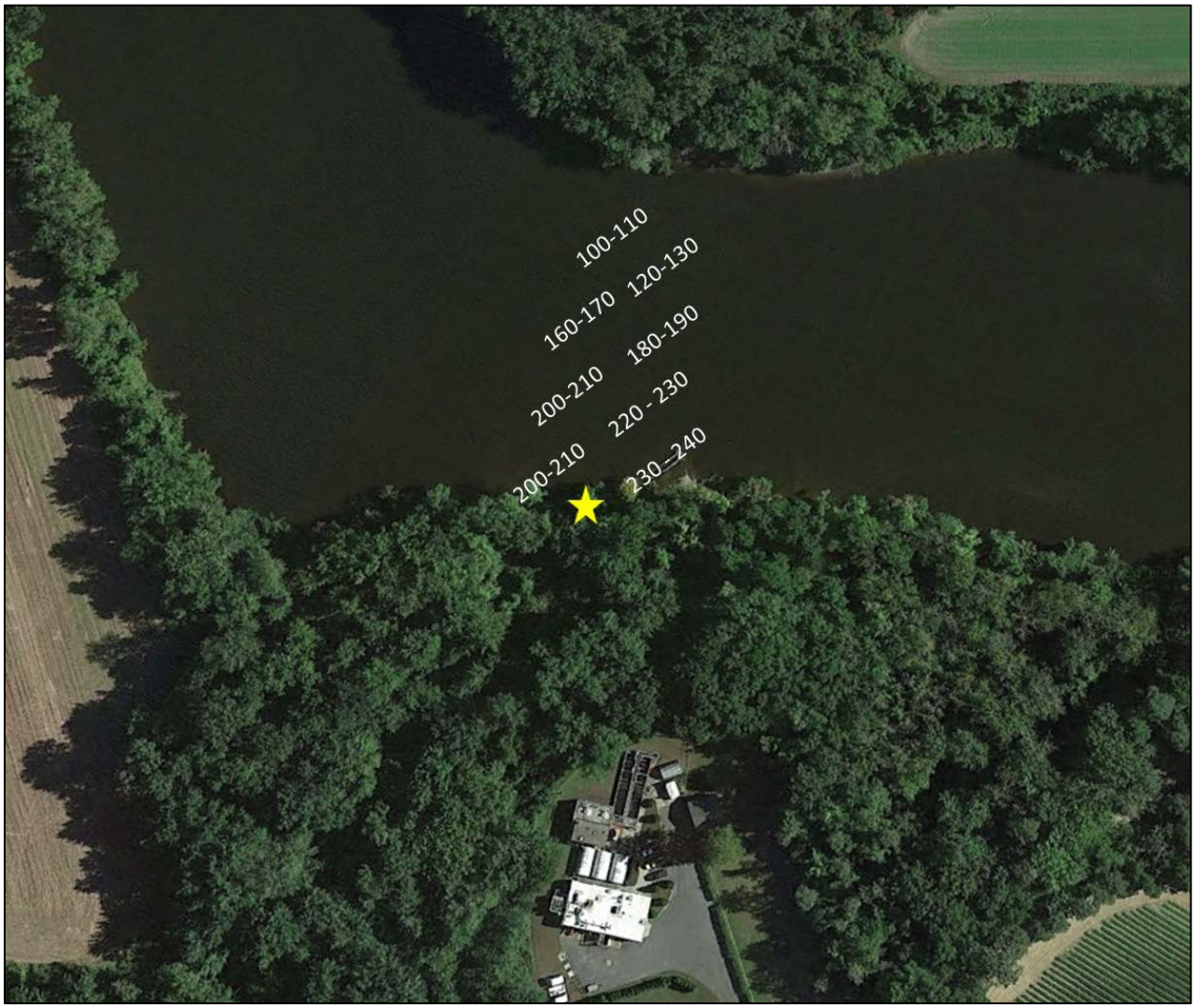

Figure 23: The yellow star marks the approximate placement of the yagi antenna and the Lotek receiver used to detect fish moving upstream towards Cabot station. The radio test tag produced strong power levels ranging from 100 to 240 dbs near the antenna.

Station 23: Rt.202 Bridge Holyoke

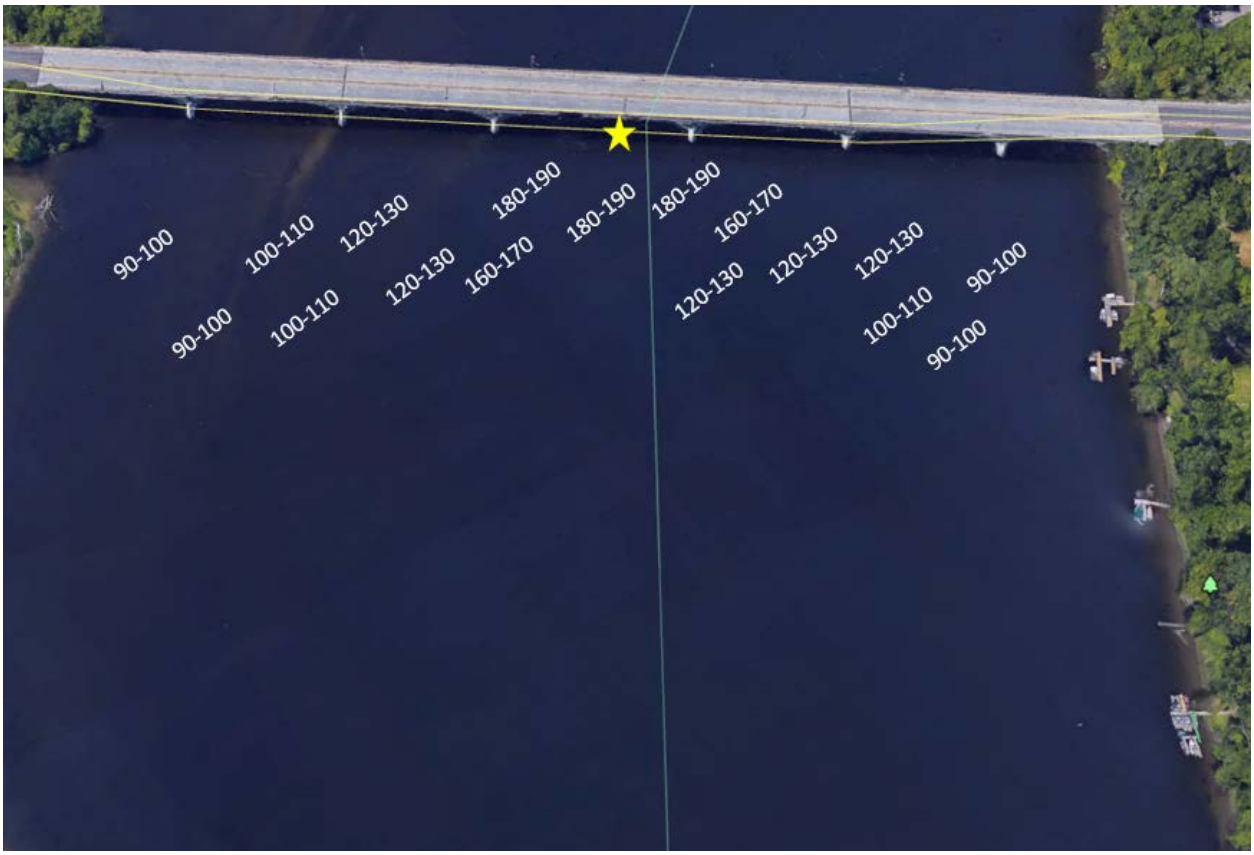

Figure 24: The yellow star marks the approximate placement of the yagi antenna and the Lotek receiver used to detect fish moving upstream towards Cabot station from the Rt.202 Bridge in Holyoke, MA. The radio test tag produced strong power levels ranging from 90 to 190 dbs near the antenna.

APPENDIX B – ADDITIONAL STATISTICS FROM TELEMETRY ANALYSES

APPENDIX B:

STATISTICAL METHODS

1 METHODS

This appendix contains the unabridged statistical methods used to assess movement of radio-tagged American shad at the Turners Falls Project. Statistical assessments of movement with radio telemetry are complex due to the amount of data produced, inclusion of false positives and significant overlap between receiver detection zones. Prior to analyzing movement within a competing risks or mark recapture framework, we implemented an algorithm that identifies and removes false positive detections while not being so strict as to introduce false negatives into the dataset, then we implemented an overlap reduction algorithm that reduced ambiguity in a fish's position. Both of these steps are necessary as they reduce bias and ambiguity that have traditionally plagued assessments of movement with radio telemetry.

1.1 False Positive Data Reduction

Radio telemetry receivers record four types of detections based upon their binary nature; true positives, true negatives, false positives and false negatives (Beeman and Perry, 2012). True positives and true negatives are valid data points that indicate the presence or absence of a tagged fish. A false positive is a detection of a fish's presence when it is not there, while a false negative is a non-detection of a fish that is there. False negatives arise from a variety of causes including insufficient detection areas, collisions between transmitters, interference from ambient noise, or weak signals (Beeman & Perry, 2012). Inclusion of false negatives may negatively bias statistics as there is no way to know if a fish's absence from a receiver was because it truly wasn't there or if it was not recaptured by the receiver. While the probability of false negatives can be quantified from sample data as the probability of detection, quantifying the rate of false positives (type I error) is more problematic (Beeman & Perry, 2012). Inclusion of false positives in a dataset can bias study results in two ways: they can favor survivability through a project by including fish that weren't there, or increase measures of delay when a fish has already passed. There are no statistical approaches that can reduce bias associated with false positives, therefore they must be identified and removed *a priori*. For the purposes of this study, false positive reduction methods relied upon a Naïve Bayes classifier and an overlap reduction algorithm inspired by nested Russian dolls.

1.1.1 Probabilistic Data Reduction – Weight of Evidence

Bayes Rule is a rigorous method for interpreting evidence in the context of previous experience or knowledge (Stone, 2013). Bayes Rule cannot guarantee the correct answer, but rather provides the probability that each alternative answer (either true or false positive) is correct. Bayes theorem updates conditional probabilities (probability of a record being true positive given some data) and is particularly useful when evaluating diagnostic tests (false positives and false negatives).

Specifically, Bayes Rule calculates the posterior probability, or the probability of a hypothesis occurring given some information about its present state, and is written with $P(\theta_i|x_j)$; where θ_i is the hypothesis (true or false positive) and x_j is observed data. Formally, Bayes Rule is expressed as:

$$P(\theta_i|x_j) = \frac{P(x_j|\theta_i)P(\theta_i)}{P(x_j)} \qquad \textit{Equation 1}$$

Where $(x_j|\theta_i)$ is referred to as the likelihood of the j^{th}data occurring given the hypothesis (θ_i); $P(\theta_i)$ is the prior probability of the i^{th}hypothesis (θ); and $P(x_j)$ is the marginal likelihood or evidence. In most applications, including this one, the marginal likelihood is ignored as it has no effect on the relative magnitudes of the posterior probability (Stone, 2013). Therefore, there is no need to waste computational effort by calculating the joint probability. We can state that the posterior probability is approximately equal to the prior probability times the likelihood or:

$$posterior \propto prior * likelihood$$ *Equation 2*

The prior probability is estimated by looking at how often each class (true or false positive) occurs in the training dataset, while the likelihood is estimated from the histogram of the values of each predictor (observed data) in the training dataset given each hypothesis (true or false positive) (Marsland, 2009). A kernel density function was fit for continuous predictors while qualitative predictors replied upon a multinomial probability distribution.

In most circumstances, the data (x) are usually vectors of feature values or predictor variables with n levels (x_n). As the dimensionality of x increases (number of predictor variables increase), the amount of data within each bin of the histogram of related variables shrinks, and it becomes difficult to estimate the posterior probability without more training data (Marsland, 2009). For example, long strings of continuous detections in series may only occur when the power of a detection is fairly high. Therefore, a simplifying assumption, the Naïve Bayes classifier, was employed.

1.1.2 Naïve Bayes Classifier

The Naïve Bayes classifier assumes that the elements (j) of the feature vector x (predictor variables) are conditionally independent of each other given the classification (Marsland, 2009). Therefore, the probability of getting a particular string of feature values of predictor variables is equal to the product of multiplying all of the individual probabilities (Marsland, 2009). The likelihood is given with:

$$P(x_1, \dots, x_n|\theta_i) = \prod_{j=1}^{n} P(x_j|\theta_i)$$ *Equation 3*

Where n is equal to the number of features or predictor variables in x and θ_i is the hypothesis (either true or false positive). The classifier rule for Naïve Bayes is to select the detection class θ_i for which the following computation is maximized:

$$argmax\left\{ P(\theta_i|x_n) \propto P(\theta_i) * \prod_{j=1}^{n} P(x_j|\theta_i) \right\}$$ *Equation 4*

The detection class $\theta_j$with the maximum posterior probability classifies every line of data belonging to a study tag into one of two classes: true or false positive. This is known as the maximum a posteriori or MAP hypothesis (Marsland, 2009).

The Naïve Bayes classifier was nothing more than a database application designed to keep track of which feature gives evidence to which class (Richert & Pedro-Coelho, 2013). However, there were circumstances where a particular feature variable level did not occur for a given detection class in the feature dataset (e.g., false positive detection with very high power and many consecutive hits in series), meaning that the likelihood for that feature given a detection class is zero. When multiplied together, the posterior probability was zero and uninformative. Therefore, the Naïve Bayes classifier used add-one smoothing, which simply adds 1 to all histogram counts (Richert & Pedro-Coelho, 2013). The underlying assumption here is that even if the feature value was not seen in the training dataset for a particular detection class, the resultant likelihood probability would be close to zero allowing for an informative posterior.

The training dataset consists of known true and false positive detections. By placing study tags at strategic locations throughout the study area for the duration of the study, these beacon tags give the algorithm information on what a known true positive detection looks like. On the other hand, known false positive detections are generated by the telemetry receivers themselves, and consist of detections coded toward tags that were not present in the list of tags released for the study.

Following the completion of the study, several predictor features were calculated for each received line of data. Predictor features include a detection history of pulses, the consecutive record hit length, hit ratio, miscode ratio, consecutive detection, detection in series, and power. The pulse detection history consists of a string of 1s and 0s that look forwards and backwards in time from the current detection in series, and identifies whether or not a pulse from that particular tag was detected. For example, if a particular tag had a 3-second burst rate, the algorithm will look forwards and backwards in time 3 seconds, query the entire dataset, and then return 1 if it was detected or 0 if it was not. The algorithm looks forwards and backwards for a user-defined set of detection intervals. Consecutive detection length and hit ratio are derived from this detection history. Consecutive detection length simply counts the number of detections in series, while hit ratio is the ratio of the count of heard detections to the length of the detection history string (Table B1).

Note from Table B1 that both detection history events are considerably different, but they have the same hit ratios. The hit ratio counts the number of correctly assigned detections to the total number of detections within a user-defined set of time. The hypothesis behind this predictor stipulates that a detection is more likely to be true when there are less miscoded detections. Consecutive detections and detections in series are binary in nature and quite similar, but the consecutive detection feature was stricter. For consecutive detection to return as true, either the previous or next detection must occur within the next pulse (i.e., 3-second interval). Detections in series allow the previous or next detection to occur at intervals greater than the first pulse; however, recaptures need to be in series. For example, if the pulse rate is 3 seconds and the next consecutive detection was missed, series hit would return true if the next recorded transmission occurred on the 6^{th} or 9^{th} second. In other words, the pulse rate must be a factor of the difference in time between the present detection and next detection for a series hit to return true. The last predictor, power, is hypothesized to be higher for true detections than false positives.

Prior to classification, FirstLight assessed the accuracy of the Naïve Bayes false positive detection algorithm with a k-fold cross validation procedure. The cross validation procedure randomly assigned folds (1,…,10) to each row of data. Then, the procedure iterates over each fold. The data assigned to the current fold are classified while the remaining rows served as the training data. Then, the classifications were compared against the known states, compiled into a cross validation table, and assessed with accuracy statistics. FirstLight assessed the accuracy of the classifier with the positive predictive value, negative predictive value, sensitivity, and specificity.

Table B-1. Example detection histories with their derived consecutive record length and hit ratio predictor feature levels.

Detections in series originating at the present detection (T_0)							Consecutive Record Length	Hit Ratio
T_{-3}	T_{-2}	T_{-1}	T_0	T_1	T_2	T_3		
0	1	0	1	0	1	0	1	3/7
0	0	1	1	1	0	0	3	3/7

1.1.3 Overlap Reduction

The radio telemetry network for this assessment was complex due to the nature of the questions asked and small scale of movement in and around the tailrace. In order to assess the efficacy of the ultrasound array in deflecting movement away from the Cabot Station ladder entrance and into the bypassed reach, the study required an assessment of movement into and out of small discrete locations. Unfortunately, discretizing fish presence into a single location and time was difficult because of the amount of overlap between receiver detection zones. To reduce the amount of overlap, FirstLight utilized multiple antenna types, including using stripped coaxial cable, dipole antennas, and large aerial Yagi antennas where appropriate. The detection ranges on these antennas vary greatly, but it was assumed that the regions increase in size from stripped coaxial cable up to large aerial Yagis. An algorithm inspired by nested-Russian Dolls was developed to reduce overlap and discretize positions in time and space within the telemetry network. If a

fish can be placed at a receiver with a limited detection zone (stripped coaxial cables or dipole), then it can be removed from the overlapping detection zone (Yagi) if it is also recaptured there.

Fish will often visit a limited range antenna for a certain amount of time, then leave that detection zone only to return sometime later. This behavior is commonly referred to as a "bout" in the ecological literature (Sibly, Nott, and Fletcher, 1990). FirstLight followed the method of Sibly, Nott and Fletcher (1990) to fit a three-process broken-stick model (piecewise-linear regression with two knots ($k = 2$)). We first calculated the lag between detections for each fish within each discrete detection zone. Then, we binned the lag time into 10-second intervals and counted the number of times a lag interval occurred within each bin. After log-transforming the counts, the three-process broken-stick model was fit using a brute-force procedure that tested every bout-length combination with an ordinary least squares regression. The best three-process model was the one that minimized the total residual error (sum of squares). The first bout process describes a continuous string of detections indicative of a fish being continuously present, the second bout process describes milling behavior at the edge of a detection zone where lags between detections may be 20 – 30 seconds or more, and the third bout process describes the lags between detections where a fish leaves one detection zone completely for another only to come back sometime later.

After deriving the bout criteria for each discrete telemetry location, presences were enumerated. We assumed that a fish left a detection zone at the start of the third process. Therefore, the second knot location in the piecewise linear process model (a.k.a. broken-stick model) described this lag-time. If the lag between detections is equal to or greater than this duration, a fish has left the telemetry location only to return much later. In other words, the fish experiences a new presence. We iterated over every detection, for every fish, at every receiver, applied this logic to each lag time, and then enumerated and described presences at each location with start and end time statistics.

After describing presences at each receiver (time of entrance, time of exit) it is possible to reduce the overlap between receivers that traditionally plague statistical assessments of movement. If we envision overlapping detection zones as a series of nested-Russian Dolls, we can develop a hierarchical data structure that describes these relationships. If a fish is present in a nested antenna while also present in the overlapping antenna, we can remove coincident detections in the overlapping antenna and reduce bias in our statistical models. This hierarchical data structure is known as a directed graph, where nodes are detection zones and the edges describe the hierarchical relationships among them. For this assessment, edges were directed from a larger detection zone towards a smaller. Edges identify the successive neighbors (smaller detection zones) of each parent node (larger detection zone).

Movement within the tailrace was very complex and overlapping detection zones added to the complexity. Each node on the telemetry network consisted of one or more telemetry receivers (Table B2). We described the hierarchical relationships between nested receivers with the directed graph depicted in. Here, the edges between nodes indicate successors, or nodes with successively smaller detection zones. In cases where aerial Yagi antennas overlap, removal was conservative and favored those receivers closer to the tailrace. In other words, if statistics are biased after overlap removal, they will favor delay within the tailrace.

The Russian Doll algorithm iterated over each detection at each node in (Figure B1). Then, the algorithm iterated over each presence at each successor node and asked a simple question: Was the fish detected at the child node while it was also detected at the parent node? If the answer is yes, then the detection at the parent node overlaps the detection at the child node. The algorithm is nothing more than an iterative search over a directed graph that applies a simple Boolean logic statement. However, it is very powerful in its ability to simplify movement and place fish in discrete spatial locations at discrete points in time. Following false positive and overlap removal, we created detection histories for a Cormack-Jolly-Seber survival model and processed strings of detections into counting-format style for analysis with time-to-event modeling.

Table B-2: Example of node to telemetry receiver relationship

Node	Telemetry Antennas
S01	T02
S02	T01
S03	T03O
S04	T03L
S05	T07
S06	T04, T05, T06
S08	T08
S09	T09
S10	T10
S11	T11
S12	T13
S13	T12

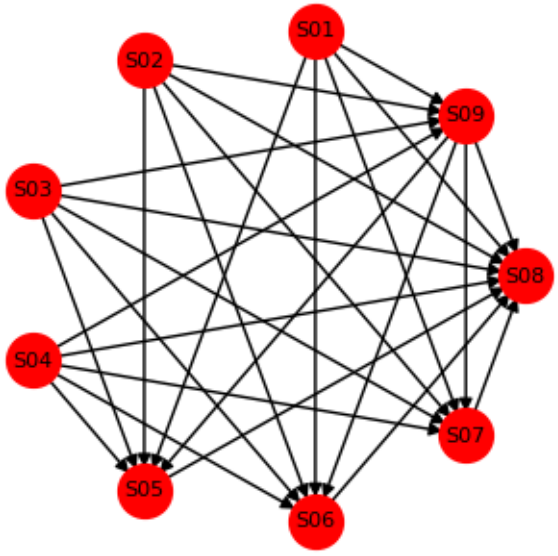

Figure B-1: The hierarchal relationships used to reduce overlap between Cabot Station tailrace antennas. Note edges show which nodes are successors (i.e., have successively smaller detection zones).

1.2 Cormack-Jolly-Seber Open Population Mark-Recapture Model

Mark-recapture survival analysis is typically used to assess passage effectiveness of fish ladders (Beeman and Perry, 2012). Use of the term "survival" is standard for mark-recapture analysis, which is predominantly used to assess the actual survival of marked animals over time. Survival in this context simply means successful passage, it should not convey mortality. Given that the temporal and spatial horizon is very short for those stretches studied with mark-recapture techniques (on the order of hours to less than 1,000 ft), mortality was not tested using a mark-recapture framework. Therefore, to reduce confusion, we will refer to the estimate as arrival. To estimate arrival parameters in the field under natural or anthropogenic conditions, one must follow individually marked animals through time (Lebreton et al., 1992). However, it is rarely possible to follow all individuals of an initial sample over time (Lebreton et al.,

1992) as is evident by varying recapture rates at each telemetry receiver location. Open population mark-recapture models allow for change (emigration and mortality) during the course of a study (Armstrup, McDonald, and Manly, 2005). The Cormack-Jolly-Seber (CJS) model is based solely on recaptures of marked animals and provides estimates of arrival and capture probabilities only (Armstrup, McDonald, and Manly, 2005). The CJS model has the following assumptions:

- Every marked animal present in the population at time (t) has the same probability of recapture (p_t).
- Every marked animal in the population immediately after time (t) has the same probability of surviving to time $(t + 1)$.
- Marks are not lost or missed.
- All samples are instantaneous, relative to the interval between occasion (t) and $(t + 1)$.
- Each release is made immediately after the sample (Cooch and White, 2006).

An animal that has not been observed for some time may have survived and escaped recapture by chance or for biological reasons its recapture might occur if the study were to continue (Lebreton et al., 1992). With this binary state of nature in mind, the presence and absence of animals at each location along a telemetry network is encoded with a string of 1s or 0s denoting presence and absence respectively. To properly assess arrival with variability in recapture, more parameters are required.

Under the assumption of independence of fates and identity of individuals, the observed detection history strings are observations of a multinomial probability distribution (Lebreton et al., 1992). The method of maximum likelihood estimation was used to estimate the parameters in the model (Lebreton et al., 1992). The statistical likelihood is the product of the probability of observing a particular detection history given release over those capture histories actually observed (Lebreton et al., 1992). More than one animal may have the same recapture history; therefore, the number observed in each recapture history appears as an exponent in its corresponding probability likelihood statement (Lebreton et al., 1992). MARK uses the profile likelihood estimation of variance to construct the confidence intervals (Cooch & White, 2006). Consequently, the shape of the log-likelihood function estimated by the maximum likelihood procedure provides information on the precision of the estimators (Lebreton et al., 1992). Profile likelihood intervals have better coverage with small samples and because the distribution of estimators is often very non-normal and the parameter space has boundaries (e.g., 0 and 1) (Lebreton et al., 1992).

The following lists the steps of the procedure for model creation and selection, which relied on methods from Lebreton et al. (1992) and Cooch and White (2006):

1. Build a global model compatible with the biology of the species studied and with the design of the study.
2. Assess model fit using appropriate goodness-of-fit (GOF) measures.
3. Select a more parsimonious model using Akaikes Information Criteria (AIC) to limit number of formal tests.
4. Test for the most important biological questions by comparing this model with neighboring ones using likelihood ratio tests.
5. Obtain maximum likelihood estimates of model parameters with estimates of precision.

The first step was to build a saturated model, which is loosely defined as the model where the number of parameters equals the number of data points or data structures (Cooch and White, 2006). The saturated model estimated a survival (ϕ) between each facility location and recapture (p) probability at each facility relocation (Figure B2). It is not possible to differentiate between the final survival (ϕ_5) and recapture station (p_4) because it is not known if an animal died or was simply not recaptured at the final telemetry station. Following the creation of the saturated model, GOF testing was performed.

GOF procedures tested the assumptions underlying the models that the data are being fit to. GOF is a necessary first step to ensure that the most general model adequately fits the data (Cooch and White, 2006). To accommodate for lack of fit, we needed a measure of how much extra binomial noise (variation) is in the data, which is known as the variance inflation factor or $\hat{c}$ (Cooch and White, 2006). The internal MARK program RELEASE assessed GOF for CJS model and consists of two important tests, Test 2 and 3. Test 2 deals with those animals known to be alive between time t and $t+1$ and tests the assumption that all marked animals should be equally detectable at location $t+1$ independent of whether or not they were captured at occasion t. Test 3 analyzes the assumption that all marked animals alive at t have the same probability of surviving to $t+1$. If the resultant χ^2 tests are significant, the assumptions are violated. Further, if the overall GOF test proves significant, it is necessary to assume the assumptions are violated. If the assumptions were violated, the Median-$\hat{c}$ procedure within MARK estimated the variance inflation factor and the models were adjusted accordingly. After adjustment or non-significant GOF, a series of reduced models were created: reduced survival and individual recapture ($\phi.\,p(t)$), individual survival and reduced recapture($\phi(t)p.$)), reduced time and reduced recapture($\phi.\,p.$).

Following model creation, model selection starts with comparing AIC values and then computing likelihood ratio tests. Model selection is important as parsimony is desired. Therefore, models relating sample data and population parameters should contain enough parameters to account for all of the significant variation (Lebreton et al., 1992). An important tradeoff exists between the number of parameters in the model and sampling variance (Lebreton et al., 1992). The goal in model selection is to identify a biologically meaningful model that explains the variability in the data but excludes unnecessary parameters. The AIC is a measure of the relative quality of statistical models for a given set of data and provides a means for model selection. The lower the AIC, the more parsimonious the model (best fit with fewest parameters). However, the AIC value should not be the deciding factor, especially when hypothesis testing is available with other techniques. The likelihood ratio test compares a restricted model nested within the full model. If the likelihood ratio test is significant, there is evidence to suggest for variance in survival between stations. Once the final model was chosen, MARK provided estimates of critical survival (ϕ) and recapture (p) ratios.

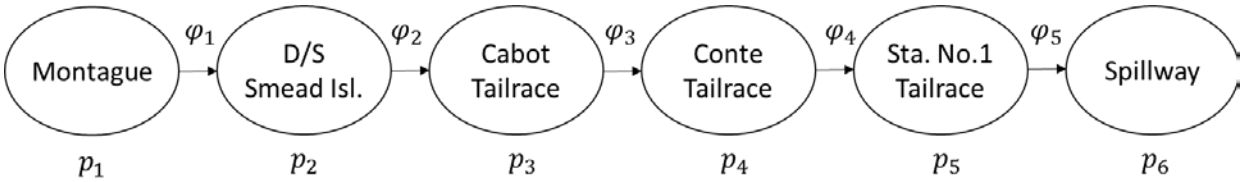

Figure B-2. Graphical schematic of the CJS model used in 2018 to assess the arrival rate of fish at the Turners Falls spillway having been recaptured at Montague. Survival probabilities (φ_i) are assessed between stations while recapture rates (p_i) are measured at a station.

1.3 Time-to-Event Analysis

A multi-state model is used to understand situations where a tagged animal transitions from one state to the next (Therneau, Crowson, & Atkinson, 2016). A standard survival curve (Kaplan-Meier) can be thought of as a simple multi-state model with two states (alive and dead) and one transition between those two states (Therneau, Crowson, & Atkinson, 2016). For the purpose of this assessment, these two states are staging and passing. Competing risks generalize the standard survival analysis of a single endpoint (as described above) into an investigation of multiple first event types (Beyersmann, Allignol, & Schumacher, 2011). Competing risks are the simplest multi-state model, where events are envisioned as transitions between states (Beyersmann, Allignol, & Schumacher, 2011). For competing risks, there is a common initial state for all models (Beyersmann, Allignol, & Schumacher, 2011). For example, with the assessment of time to move either upstream or downstream of the ultrasound array, the common initial state is within the array. When fish move upstream or downstream of the array, they enter an absorbing state. The baseline hazard

is measured with the Nelson-Aalen cause specific cumulative incidence function. One can think of the hazard as the probability of experiencing an event (passage) within the next time unit conditional on still being in the initial state (Beyersmann, Allignol, & Schumacher, 2011). The Nelson-Aalen ($\hat{A}(t)$ is computed with (Beyersmann, Allignol, & Schumacher, 2011):

$$\hat{A}(t) = \sum_{k=1}^{K} \frac{number\ of\ individuals\ observed\ to\ transition\ into\ state\ i\ at\ t_k}{number\ of\ individuals\ at\ risk\ just\ prior\ to\ t_k}$$

Where t is a time of interest, K is the number of event times for fish entering state i, and k is an event (duration an animal took to transition from the array into a passing state). This formula is simple, it counts the number of individuals to experience the event of interest (i.e., movement upstream from within the array) at t_k divided by the number of individuals still in the array just prior to t_k. The sum term simply adds the probability across all discrete event times K. Therefore, the end probability is the probability of an animal traversing from the array into an absorbing state i. If we lose track of an animal, it is not censored at its last event time, rather it enters an unknown state. By attributing each tagged animal to a state at all times, we are ensured our final probabilities match empirical expectations. In other words, if 50 out of 100 animals transitioned upstream of the array, and 25 of 100 animals transitioned downstream, and we lost track of 25 animals, the Nelson-Aalen cumulative incidence estimators will result in 50% transitioning upstream of the array, 25% transitioning downstream of the array, and 25% within a state-unknown at the final event time. Animals are only censored if they are still being tracked within the array until the end of study. If we happen to lose track of a fish before the end of the study, they enter an unknown state. After computing the Nelson-Aalen estimators for each route of passage (competing event) and plotting the survival function (Kaplan-Meier) for those fish still remaining in the tailrace, we generated the probability of being in a state (across all times) while summing to 1.0.

Following the computation of cause-specific Nelson-Aalen estimators, an assessment of delay was carried out with Cox Proportional Hazards regression analysis for each separate event. Therneau, Crowson, & Atkinson (2016) state that a common mistake with competing risks is to use the Kaplan-Meier separately on each event type while treating other event types as censored. When this occurs, the probability of transitioning into the absorbing state of interest is positively biased, and the reason why competing risk curves may sum to less than 1.0. When analyzed in the frameowrk proposed by Therneau, Crowson, and Atkinson (2016), each separate Cox model ignores the other absorbing events and assesses the cause-specific transition. Here, rates depend only on the set of subjects who are at risk (fish in staging state) at a given moment. The Cox models for a competing risk assessment were fit in a procedure analogous to multiple regression modeling, where individual time-dependent covariates were added in an iterative fashion constructing ever more complex models. Model quality was assessed with the omnibus likelihood ratio test statistic, the null hypothesis of which states that the model is not better than chance. If this statistic is rejected at the $\alpha = 0.05$ level, then the model is considered to be better than chance, and we observe the estimated hazard ratio associated with the covariate of interest and its significance. If the covariate is significant at the $\alpha = 0.05$ level, then we conclude that the estimated hazard ratio is significant, and interpret the results. When the hazard ratio is greater than 1, a unit increase in the covariate (i.e., flow) would increase the instantaneous risk (or hazard) of the event occurring and delay is reduced. If for example, the model described attraction towards a ladder with a time varying covariate of flow and the hazard ratio greater than 1.0, then the risk of the event occurring (passage towards the ladder) increases with a unit increase in flow as compared to baseline. One would conclude that the population appears to experience less delay as flow is increased. If the hazard ratio is less than 1.0, then the instantaneous risk decreases, and the proportion of fish that have passed into the structure at time (t) decreases, thus delay is incurred. The "best" model minimized AIC scores and/or had a significant omnibus statistic ($p < 0.05$) and informative hazard estimate ($HR \neq 1.0$).

FirstLight diagnosed the fit of the CoxPH models by testing for the proportional hazard assumption using the R software Survminer. If the p-value of Schoenfeld Individual test was less than 0.05, the proportional

hazards assumption was not met. If the test statistic comes back significant, a model was built where the covariate of interest interacts with time.

1.4 Treatment of Time-Series Data

At each event time, Cox Proportional Hazard (CoxPH) regression compares the current covariate values of a subject who had an event, to the current values of all others who were at risk at that time (Therneau, Crowson, & Atkinson, 2017). The event in question being movement from one location to another, and the number at risk being the number of fish remaining at the original location when the movement in question occurs. One of the drawbacks of CoxPH is that it regresses on the value of the covariate of interest immediately before an event occurs, and we are forced to assume that this was the value that affected movement. However, a fish that has been in the Cabot Station tailrace for a few hours, or in the river for a few weeks, has likely experienced a range of flows and conditions that will also affect movement. This information is lost if we only regress on the level of the covariate in the instant before an animal moves. Therefore, FirstLight also derived a number of statistics that incorporated greater amounts of information from time series data (flow, temperature, etc.) with moving window averages.

A rolling or moving average analyzes time series data by creating a series of averages at different subsets of the full timeseries. Rolling averages simply look behind the current time stamped measurement for a certain length of time. FirstLight chose window lengths that were biologically meaningful for migrating shad (1 hour, 2 hours, 5 hours and 24 hours). FirstLight also calculated the rolling variance, or volatility at these same window lengths. Volatility is a key variable, it either describes the short term or long-term variance (depending on window length) in flow. If volatility is high, the river is unsettled and is indicative of changing flows due to a rain storm or operations. Changing river conditions in the short term may cue fish to migrate, while long term variability may inhibit movement. We also calculated the cumulative average and variance, which described the average flow conditions experienced by a migrating shad while present at a location before moving. These variables were incorporated into the CoxPH models just like other time dependent covariates and provided new insight into reasoning behind shad movement in the Connecticut River.

FirstLight also developed metrics that incorporated the change in flow over a fish's presence. After enumerating bouts, FirstLight matched the start and end times of a presence with their nearest 15 min flow reading and calculated the change in flow over a presence (dQ), the absolute change in flow over a presence ($|dQ|$), and the rate of change in flow over a presence (dQ/dt). These flow variables, along with instantaneous gage readings, cumulative averages and variances over presences, and rolling averages and volatilities were used to assess the effect of flow and flow variability on the movement of American shad within the Connecticut River.

APPENDIX C – COX PROPORTIONAL HAZARD MODEL SUMMARIES

APPENDIX C:

COX PROPORTIONAL HAZARD MODEL SUMMARIES

APPENDIX C

Cox Proportional Hazard Model Summary tables

Table C1: Cox Proportional Hazard output for Project arrival to TFD Spillway (2015, 2018, 2019)

Model Number	Covariates	AIC	Robust LR Test	Hazard Ratio	SE	p	(+/-)	Proportional Hazard Assumption
1	Cabot to Bypass flow ratio	936.25	<0.001	0.764	0.1	**0.007**	(0.63/0.93)	0.06
	ATU (10 degrees)			0.516	0.14	**<0.001**	(0.39/0.68)	
	Bypass rolling variance (48 hr)			1.04	0.01	**0.003**	(1.01/1.07)	
	Q day 06:00 – 12:00			10.82	0.58	**<0.001**	(3.48/33.63)	
	Q day 12:00 – 18:00			16.47	0.59	**<0.001**	(5.18/52.42)	
	Q day 18:00 – 0:00			4.09	0.64	**0.03**	(1.16/14.40)	
2	Q day 06:00 – 12:00	1009.1	<0.001	9.0668	0.5311	<0.001	(3.31/24.86)	0.012
	Q day 12:00 – 18:00			14.9144	0.5192	<0.001	(5.4/41.26)	0.05
	Q day 18:00 – 0:00			3.3632	0.5809	0.04	(1.1/10.31)	0.09
3	Bypass rolling variance (48 hr)	1013.1	0.008	1.05	0.01	**<0.001**	(1.02/10.8)	0.04
4	ATU (10 degrees)	1044.9	<0.001	0.49	0.14	**<0.001**	(0.37/0.65)	0.28
5	Bypass rolling avg (48 hr)	1059	0.005	1.1	0.03	**0.002**	(1.04/1.17)	0.006
6	Bypass rolling avg (24 hr)	1059.9	0.006	1.09	0.03	**0.002**	(1.03/1.15)	0.01
7	Percent Change while present	1059.9	0.02	1.4	0.09	**<0.001**	(1.17/1.69)	0.13
8	Bypass rolling avg (1 hr)	1062.9	0.01	1.08	0.03	**<0.001**	(1.02/1.12)	0.02
9	Cumulative average bypass flow while present	1066.1	0.04	1.06	0.03	**0.03**	(1.0/1.12)	0.12
10	Cabot to Bypass flow ratio	1066.2	0.02	0.84	0.08	**0.03**	(0.71/0.99)	0.89
11	Bypass rolling variance (24 hr)	1067.3	0.09	1.04	0.02	**0.04**	(1.002/1.08)	0.01
12	Avg bypass flow change with time (dQ/dt)	1067.8	0.04	2.87	0.46	**0.02**	(1.17/7.07)	0.29
13	Bypass rolling variance (1 hr)	1069.2	0.08	0.7	0.44	**0.41**	(0.30/1.65)	0.28
14	Absolute change while present	1069.3	0.4	1.03	0.03	**0.37**	(0.96/1.10)	0.06
15	Cumulative Avg. Bypass Flow 2 – 4,000	1075.9	0.09	1.677	0.34	**0.12**	(0.87/3.23)	0.02
	Cumulative Avg. Bypass Flow 4 – 6,000			1.56	0.39	**0.26**	(0.72/3.93)	
	Cumulative Avg. Bypass Flow 6 – 8,000			2.617	0.47	**0.04**	(1.03/6.65)	
	Cumulative Avg. Bypass Flow 8 – 10,000			2.64	0.45	**0.03**	(1.07/6.48)	
	Cumulative Avg. Bypass Flow 10 – 12,000			2.561	0.43	**0.02**	(1.11/5.93)	
	Cumulative Avg. Bypass Flow 12 – 14,000			2.037	0.59	**0.22**	(0.64/6.48)	
	Cumulative Avg. Bypass Flow 14 – 16,000			0.00000127	0.51	**<0.001**	(<0.001/<0.001)	
	Cumulative Avg. Bypass Flow 16 – 18,000			1.281E-06	1	**<0.001**	(<0.001/<0.001)	

Cabot Tailrace movement:

Table C2: Cox Proportional Hazard output for Cabot tailrace to Cabot Ladder movement (2015, 2018, 2019)

Model Number	Covariates	AIC	Robust LR Test	Hazard Ratio	SE	p	(+/-)	Proportional Hazard Assumption
1	Ultrasound Array on	5197.1	<0.001	0.68	0.16	**0.02**	(0.49/0.94)	<0.001
	Duration (In the tailrace)			0.96	0.01	**<0.001**	(0.94/0.97)	<0.001
	Ultrasound Array on: Duration (In the tailrace/Ladder?)			1.02	0.01	**0.01**	(1.0/1.04)	0.01
2	Bypass Flow Rolling Average (2hr)	5238.1	0.1	1.03	0.02	0.08	(0.99/1.07)	<0.001
3	Accumulated Thermal Units	5261.9	<0.001	0.95	0.01	**<0.001**	(0.92/0.97)	<0.001
4	Tag Year 2018	5285.4	<0.001	2.29	0.26	**0.002**	(1.37/3.82)	<0.001
	Tag year 2019			2.35	0.27	**0.002**	(1.39/3.99)	<0.001
5	Cabot Discharge Rolling Variance (24hr)	5318.6	0.06	0.96	0.02	0.08	(0.92/1.0)	<0.001
6	Bypass Flow Rolling Variance (5hr)	5320.7	<0.001	0.71	0.13	**0.01**	(0.55/0.92)	0.17
7	Cabot discharge (kcfs)	5323.6	0.1	1.03	0.02	0.13	(1.0/1.07)	<0.001
8	Cabot Discharge Rolling Average (1hr)	5324.02	0.1	1.03	0.02	0.14	(0.99/1.06)	<0.001
9	Cabot Discharge Rolling Average (2hr)	5324.1	0.1	1.03	0.02	0.14	(0.99/1.06)	<0.001
10	Bypass Flow Rolling Variance (2hr)	5324.2	<0.001	0.6	0.25	**0.04**	(0.37/0.98)	0.11
11	Cabot Discharge Rolling Average (5hr)	5324.5	0.2	1.03	0.02	0.15	(0.99/1.07)	<0.001
12	Cumulative Average Cabot Discharge (kcfs)	5326.1	0.3	1.02	0.02	0.25	(0.98/1.06)	<0.001
13	Cabot Discharge Rolling Average (24hr)	5326.7	0.3	1.02	0.02	0.26	(0.98/1.06)	<0.001
14	Bypass Flow Rolling Average (24hr)	5327.2	0.1	1.04	0.02	0.06	(0.88/1.08)	<0.001
15	Bypass Flow Rolling Average (5hr)	5327.8	0.1	1.03	0.02	0.07	(0.99/1.07)	<0.001
16	Ultrasound Array on	5327.9	0.2	1.23	0.15	0.18	(0.91/1.66)	<0.001
17	Bypass Flow Rolling Average (1hr)	5328.2	0.1	1.03	0.02	0.08	(0.99/1.07)	<0.001
18	Cabot Discharge Rolling Variance (5hr)	5328.5	0.2	0.97	0.03	0.31	(0.92/1.03)	<0.001
19	Bypass Flow (kcfs)	5328.6	0.1	1.03	0.02	0.11	(0.99/1.07)	<0.001
20	Cumulative Average Bypass Flow (kcfs)	5329.02	0.2	1.03	0.02	0.18	(0.99/1.07)	<0.001
21	Bypass Flow Rolling Variance (1hr)	5329.1	0.008	0.74	0.2	0.11	(0.51/1.07)	0.28
22	Bypass Flow Rolling Variance (24hr)	5330.5	0.6	0.98	0.02	0.6	(0.94/1.04)	<0.001
23	Cabot Discharge Rolling Variance (1hr)	5330.6	0.2	0.95	0.06	0.39	(0.85/1.06)	0.26
24	Cabot Discharge Rolling Variance (2hr)	5330.8	0.4	0.98	0.04	0.5	(0.91/1.05)	0.001
25	Cabot Discharge slope	5330.9	0.5	1	<0.001	0.47	(1/1)	0.99
26	Bypass Flow slope	5330.9	0.4	0.99	<0.001	0.4	(0.99/1)	0.99
27	Cabot Discharge/Bypass Flow (kcfs)	5331.4	0.8	0.99	0.01	0.85	(0.98/1.03)	0.15

Table C3: Cox Proportional Hazard model outputs for Cabot tailrace to bypass reach movement (2015, 2018, 2019)

Model Number	Covariates	AIC	Robust LR Test	Hazard Ratio	SE	p	(+/-)	Proportional Hazard Assumption
1	Ultrasound Array Operational	2078.1	<0.001	3.82	0.21	**<0.001**	(2.54/5.75)	0.02
	Duration fish remains in tailace			0.98	0.01	**<0.001**	(0.97/0.99)	<0.001
	Array Operational:Duration			0.94	0.04	0.09	(0.87/1.01)	0.31
2	Ultrasound Array Operational	2208.6	<0.001	3.9	0.18	**<0.001**	(2.7/5.6)	<0.001
3	Cabot discharge (kcfs)	2237.3	<0.001	0.92	0.05	0.11	(0.83/1.02)	0.06
	ATU(10°C)			0.71	0.15	**0.03**	(0.53/0.96)	0.03
	Cabot discharge*ATU(10°C)			0.99	0.02	0.89	(0.97/1.03)	0.31
4	Cumulative average Cabot Discharge (kcfs)	2239.9	<0.001	0.9	0.02	**<0.001**	(0.87/0.93)	<0.001
5	Cabot Discharge Rolling Average (24hr)	2254.5	<0.001	0.9	0.02	**<0.001**	(0.87/0.93)	<0.001
6	Cabot Discharge Rolling Average (5hr)	2255.1	<0.001	0.91	0.02	**<0.001**	(0.88/0.94)	<0.001
7	Cabot Discharge Rolling Average (2hr)	2257.8	<0.001	0.91	0.02	**<0.001**	(0.88/0.94)	<0.001
8	Cabot Discharge Rolling Average (1hr)	2258.6	<0.001	0.91	0.02	**<0.001**	(0.88/0.94)	0.02
9	Cabot discharge (kcfs)	2259.3	<0.001	0.91	0.02	**<0.001**	(0.89/0.94)	0.02
10	Cabot Discharge/Bypass Flow	2261.6	<0.001	0.59	0.12	**<0.001**	(0.47/0.75)	0.002
	ATU (10°C)			0.64	0.1	**<0.001**	(0.53/0.79)	0.05
	Cabot Discharge/Bypass Flow*ATU(10°C)			1.07	0.02	**<0.001**	(1.04/1.1)	0.004
11	Bypass Flow (kcfs)	2272.9	<0.001	1.08	0.1	0.41	(0.9/1.3)	0.06
	ATU(10°C)			0.89	0.17	0.5	(0.64/1.24)	0.03
	Bypass Flow*ATU(10°C)			0.94	0.03	0.08	(0.88/1.01)	0.31
12	Cabot Discharge/Bypass Flow	2283.5	0.003	0.75	0.07	**<0.001**	(0.65/0.87)	0.002
13	Accumulated Thermal Units (ATU 10°C)	2286.2	<0.001	0.71	0.1	**<0.001**	(0.58/0.86)	0.17
14	Cumulative average Bypass flow (kcfs)	2302.6	0.02	0.91	0.04	**0.03**	(0.84/0.99)	<0.001
15	Bypass Flow (kcfs)	2304.4	0.02	0.93	0.03	**0.03**	(0.87/0.99)	0.02
16	Bypass Flow Rolling Average (1hr)	2304.5	0.02	0.93	0.03	**0.03**	(0.87/0.99)	0.004
17	Change in Cabot discharge (kcfs)	2304.7	0.02	1.07	0.03	**0.02**	(1.01/1.13)	0.8
18	Bypass Flow Rolling Average (2hr)	2305	0.03	0.93	0.03	**0.03**	(0.87/0.99)	0.003
19	Bypass Flow Rolling Average (5hr)	2305.4	0.03	0.93	0.03	**0.04**	(0.87/0.99)	0.001
20	Cabot Discharge Rolling Variance (5hr)	2306.6	0.06	1.04	0.01	**0.008**	(0.01/1.06)	0.44
21	Bypass Flow Rolling Average (24hr)	2307.1	0.08	0.94	0.04	0.09	(0.88/1.01)	<0.001
22	Bypass Flow Rolling Variance (24hr)	2309.4	0.1	0.96	0.03	0.2	(0.91/1.02)	0.02
23	Bypass Flow Rolling Variance (1hr)	2309.8	0.3	1.13	0.07	0.08	(0.98/1.29)	0.92
24	Cabot Discharge Rolling Variance (24hr)	2310	0.3	1.02	0.01	0.23	(0.99/1.04)	0.6
25	Cabot Discharge Rolling Variance (2hr)	2310.1	0.08	1.03	0.02	**0.05**	(0.97/1.06)	0.9
26	Bypass Flow Rolling Variance (2hr)	2310.5	0.4	1.1	0.09	0.26	(0.93/1.32)	0.82
27	Cabot Discharge Rolling Variance (1hr)	2311.3	0.3	1.02	0.02	0.26	(0.98/1.06)	0.93

Model Number	Covariates	AIC	Robust LR Test	Hazard Ratio	SE	p	(+/-)	Proportional Hazard Assumption
28	Bypass flow slope (kcfs)	2311.3	0.6	0.87	0.23	0.5	(0.55/1.37)	0.42
29	Change in Bypass flow (kcfs)	2311.6	0.8	0.99	0.03	0.8	(0.94/1.05)	0.36
30	Bypass Flow Rolling Variance (5hr)	2311.7	1	0.99	0.09	0.98	(0.83/1.19)	0.36

Bypass Reach movement:

Table C4: Cox Proportional Hazard model outputs for movement from Conte discharge to Spillway (2015, 2018, 2019)

Model Number	Covariates	AIC	Robust LR Test	Hazard Ratio	SE	p	(+/-)	Proportional Hazard Assumption
1	ATU	986.7	<0.001	0.55	0.15	**<0.001**	(0.41/0.73)	0.01
	Bypass Flow Rolling Average (24 hr)			1	0.03	0.95	(0.94/1.06)	0.74
	ATU:Bypass Flow Rolling Varaince (24 hr)			1.01	0.01	0.15	(0.99/1.03)	1.03
2	Accumulated Thermal Units (10°C) (Sqrt transformed)	993.8	<0.001	0.57	0.13	**<0.001**	(0.44/0.74)	0.002
3	ATU	993.8	<0.001	0.64	0.26	0.09	(0.39/1.08)	0.63
	Cumulative Average Bypass Flow (kcfs)			1.08	0.1	0.45	(0.88/1.32)	0.21
	ATU:Cumulative Average Bypass Flow (kcfs)			0.98	0.04	0.71	(0.91/1.07)	0.23
4	ATU	995.4	<0.001	0.59	0.2	**0.009**	(0.4/0.9)	0.07
	Bypass Flow (kcfs)			1.03	0.1	0.7	(0.91/1.16)	0.8
	ATU:Bypass Flow (kcfs)			1	0.02	0.9	(0.95/1.05)	0.74
5	Cumulative Avg. Bypass Flow (3,000 – 6,000)	1011.8	0.001	1.75	0.34	0.1	(0.91/3.4)	0.29
	Cumulative Avg. Bypass Flow (6,000 – 9,000)			0.69	0.43	0.39	(0.3/1.6)	0.15
	Cumulative Avg. Bypass Flow (9,000 – 12,000)			2.5	0.52	0.08	(0.89/6.9)	0.93
	Cumulative Avg. Bypass Flow (12,000 – 15,000)			3.2	0.44	**0.009**	(1.3/7.6)	0.36
	Cumulative Avg. Bypass Flow (15,000 – 18,000)			4.8	0.48	**<0.001**	(1.9/1.2)	0.54
	Cumulative Avg. Bypass Flow (18,000 – 21,000)			4.4	0.45	**<0.001**	(1.8/1.06)	0.86
	Cumulative Avg. Bypass Flow (21,000 – 24,000)			1.3	1.02	0.81	(0.17/9.5)	0.96
	Cumulative Avg. Bypass Flow (24,000 – 27,000)			<0.001	1.07	**<0.001**	(<0.001/<0.001)	0.85
	Cumulative Avg. Bypass Flow (27,000 – 30,000)			<0.001	1.24	**<0.001**	(<0.001/<0.001)	0.99
6	Bypass Flow Variance (24hr)	1013.5	0.004	1.05	0.01	**<0.001**	(1.02/1.07)	0.17
7	Cumulative Average Bypass Flow (kcfs)	1015.7	0.003	1.06	0.02	**<0.001**	(1.03/1.1)	0.11
8	Bypass Flow Rolling Average (5hr)	1016.4	0.01	1.05	0.02	**0.001**	(1.02/1.09)	0.4
9	Bypass Flow Rolling Average (24hr)	1016.5	0.01	1.06	0.02	**0.002**	(1.02/1.1)	0.27
10	Bypass Flow Rolling Average (2hr)	1016.6	0.01	1.05	0.02	**0.002**	(1.02/1.09)	0.43
11	Bypass Flow Rolling Average (1hr)	1016.7	0.01	1.05	0.02	**0.002**	(1.02/1.09)	0.47
12	Bypass Flow (kcfs)	1017.3	0.009	1.05	0.02	**0.001**	(1.02/1.09)	0.46
13	Absolute Delta Bypass Flow (kcfs)	1018.2	0.02	1.07	0.02	**0.002**	(1.03/1.12)	0.81
14	Station No.1 discharge/Bypass Flow	1020.9						
15	Tag Year – 2016	1021.7	0.1	0.88	0.45	0.77	(0.36, 2.12)	0.37
16	Tag Year – 2018	1021.7	0.1	1.32	0.35	0.43	(0.66, 2.63)	<0.001
17	Tag Year – 2019	1021.7	0.1	0.67	0.35	0.26	(0.34/1.33)	<0.001
18	Bypass Flow Variance (2hr)	1022.5	0.003	0.79	0.18	0.21	(0.55/1.14)	0.43
19	Bypass Flow Variance (5hr)	1023.3	0.02	0.92	0.05	0.08	(1.08/0.84)	0.6
20	Slope of Bypass discharge	1025.2	0.3	0.73	0.3	0.3	(0.41/1.31)	0.74

Table C5: Cox Proportional Hazard Model outputs for movement from the Conte discharge to Spillway (only flows <8,000 cfs included)

Model Number	Covariates	AIC	Robust LR Test	Hazard Ratio	SE	p	(+/-)	Proportional Hazard Assumption
1	ATU	713.9	0.002	1.26	0.21	0.27	(0.83/1.91)	0.85
	Cumulative Average Bypass Flow (kcfs)			1.91	0.18	**<0.001**	(1.35/2.7)	0.11
	ATU:Cumulative Average Bypass Flow (kcfs)			0.83	0.06	**<0.001**	(0.75/0.91)	0.11
2	ATU	717.5	<0.001	0.55	0.17	<0.001	(0.4/0.76)	0.006
	Bypass Flow Rolling Average (kcfs)			1.18	0.11	0.11	(0.96/1.45)	0.13
	ATU:Bypass Flow Rolling Variance (24 hr)			0.99	0.02	0.58	(0.95/1.03)	0.34
3	ATU	720.1	0.002	0.91	0.24	0.71	(0.57/1.47)	0.74
	Bypass Flow (kcfs)			1.42	0.22	0.1	(0.93/2.17)	0.23
	ATU:Bypass Flow (kcfs)			0.88	0.06	0.03	(0.79/0.99)	0.32
4	Accumulated Thermal Units (ATU)	720.3	0.001	0.57	0.16	**<0.001**	(0.42/0.78)	0.006
5	Tag Year – 2016	729.6	0.001	0.96	0.45	0.93	(0.4/2.3)	0.48
	Tag Year – 2018			1.38	0.35	0.35	(0.7/2.71)	0.001
	Tag Year – 2019			0.34	0.42	**0.01**	(0.15/0.77)	0.006
6	Bypass Flow Variance (2hr)	737.3	<0.001	0.003	3.88	0.13	(<0.001/5.8)	0.96
7	Bypass Flow Variance (24hr)	741.3	0.1	1.06	0.03	0.06	(0.99/1.14)	0.29
8	Absolute Delta Bypass Flow (kcfs)	741.6	0.2	1.11	0.06	0.08	(0.99/1.25)	0.75
9	Slope of Bypass discharge	741.8	0.03	0.3	0.49	**0.02**	(0.11/0.79)	0.45
10	Cumulative Average Bypass Flow (kcfs)	742.8	0.2	1.09	0.07	0.21	(0.95/1.24)	0.82
11	Bypass Flow Variance (5hr)	742.9	0.04	0.76	0.22	0.23	(0.49/1.19)	0.73
12	Bypass Flow Rolling Average (24hr)	743.8	0.6	0.97	0.06	0.62	(0.85/1.1)	0.92
13	Bypass Flow Rolling Average (1hr)	743.9	0.8	1.02	0.07	0.8	(0.89/1.16)	0.94
14	Bypass Flow Rolling Average (2hr)	743.9	0.8	1.01	0.07	0.83	(0.89/1.16)	0.88
15	Bypass Flow Rolling Average (5hr)	744	0.9	1	0.07	0.95	(0.88/1.15)	0.88
16	Bypass Flow (kcfs)	744.7	0.6	1.03	0.07	0.64	(0.9/1.18)	0.91

APPENDIX D – LIVE RECAPTURE DEAD RECOVERY (LRDR) MARK RECAPTURE MODEL

APPENDIX D:

LIVE RECAPTURE DEAD RECOVERY RESULTS

Appendix D: Live Recapture Dead Recovery - Cabot Canal release fish

Frequency Code	Route of Passage	R00 (Cabot Forebay)	R01 (Mobile tracking Tailrace)	R02 (Tailrace)	R03 (Mobile tracking to Montague)	R04 (Montague)	R05 (Mobile tracking to Nourse)	R06 (Nourse Farm)	R07 (Mobile tracking to Hatfield)
148.340 101	Powerhouse	1	0	1	0	0	0	0	0
148.340 102	Log Sluice	1	0	0	0	1	0	1	0
148.340 103	Powerhouse	1	0	0	0	1	0	1	0
148.340 104	Log Sluice	1	0	1	0	0	0	1	0
148.340 106	Powerhouse	1	0	1	0	0	0	1	0
148.340 107	Powerhouse	1	0	1	0	0	0	0	0
148.340 109	Log Sluice	1	0	1	0	0	0	1	0
148.340 110	Powerhouse	1	0	1	0	0	0	1	0
148.340 111	Log Sluice	1	0	0	0	1	1	0	0
148.340 112	Powerhouse	1	0	1	0	1	0	1	0
148.340 113	Powerhouse	1	0	1	0	0	0	1	0
148.340 115	Powerhouse	1	0	1	0	0	0	1	0
148.340 117	Log Sluice	1	0	1	0	0	0	1	0
148.340 121	Log Sluice	1	0	0	0	1	0	1	0
148.340 124	Log Sluice	1	0	1	0	0	0	0	0
148.340 126	Powerhouse	1	0	1	0	0	0	1	0
148.340 128	Powerhouse	1	0	1	1	0	0	0	0
148.340 132	Powerhouse	1	0	1	1	0	0	0	0
148.340 133	Log Sluice	1	0	0	0	0	0	1	0
148.340 134	Log Sluice	1	0	1	0	1	0	1	0
148.340 136	Powerhouse	1	0	1	0	1	0	1	0
148.340 137	Powerhouse	1	0	1	0	0	0	1	0
148.340 140	Log Sluice	1	0	1	0	1	0	1	0
148.340 141	Powerhouse	1	0	1	0	0	0	1	0
148.340 142	Powerhouse	1	0	1	1	0	0	0	0
148.340 144	Log Sluice	1	0	1	0	1	0	1	0

Frequency Code	**Route of Passage**	**R00** (Cabot Forebay)	**R01** (Mobile tracking Tailrace)	**R02** (Tailrace)	**R03** (Mobile tracking to Montague)	**R04** (Montague)	**R05** (Mobile tracking to Nourse)	**R06** (Nourse Farm)	**R07** (Mobile tracking to Hatfield)
148.340 148	Powerhouse	1	0	1	0	0	0	0	0
148.340 149	Log Sluice	1	0	0	0	1	0	1	0
148.340 150	Powerhouse	1	0	1	1	0	0	0	0
148.340 152	Powerhouse	1	0	1	0	0	0	0	0
148.380 100	Log Sluice	1	0	0	0	1	0	1	0
148.380 101	Log Sluice	1	0	1	0	0	0	1	0
148.380 103	Powerhouse	1	0	1	0	1	0	1	0
148.380 104	Powerhouse	1	0	1	0	0	0	1	0
148.380 105	Powerhouse	1	0	1	0	1	0	1	0
148.380 106	Powerhouse	1	0	0	0	0	0	0	0
148.380 108	Powerhouse	1	0	1	0	0	0	1	0
148.380 112	Log Sluice	1	0	1	0	1	0	1	0
148.380 113	Powerhouse	1	0	1	0	1	0	1	0
148.380 114	Powerhouse	1	0	1	0	0	0	0	0
148.380 116	Log Sluice	1	0	0	0	1	0	1	0
148.380 121	Powerhouse	1	0	1	0	0	0	0	0
148.380 123	Powerhouse	1	0	0	0	0	0	1	0
148.380 124	Log Sluice	1	0	0	0	0	0	1	0
148.380 125	Powerhouse	1	0	1	0	0	0	1	0
148.380 126	Powerhouse	1	0	1	0	1	0	1	0
148.380 129	Log Sluice	1	0	0	0	0	0	1	0
148.380 131	Powerhouse	1	0	1	0	1	0	1	0
148.380 132	Powerhouse	1	0	1	0	0	0	0	0
148.380 133	Powerhouse	1	0	1	0	0	0	0	0
148.380 136	Powerhouse	1	0	1	0	0	0	0	0
148.380 140	Powerhouse	1	0	1	0	0	0	1	0
148.380 142	Powerhouse	1	0	0	0	0	0	1	0

Frequency Code	Route of Passage	R00 (Cabot Forebay)	R01 (Mobile tracking Tailrace)	R02 (Tailrace)	R03 (Mobile tracking to Montague)	R04 (Montague)	R05 (Mobile tracking to Nourse)	R06 (Nourse Farm)	R07 (Mobile tracking to Hatfield)
148.380 144	Powerhouse	1	0	1	0	0	0	1	0
148.380 148	Log Sluice	1	0	0	0	0	0	1	0
148.380 150	Powerhouse	1	0	1	0	1	0	1	0
148.380 152	Log Sluice	1	0	1	0	0	0	1	0
148.380 153	Powerhouse	1	0	0	0	0	0	0	0
148.380 154	Log Sluice	1	0	1	0	0	0	0	0
148.380 155	Powerhouse	1	0	1	0	1	0	0	0
148.380 156	Powerhouse	1	0	1	0	0	0	1	0
148.380 157	Powerhouse	1	0	1	0	0	0	1	0
148.380 161	Log Sluice	1	0	1	0	0	0	1	0
148.380 162	Powerhouse	1	0	1	0	1	0	1	0
148.380 163	Log Sluice	1	0	0	0	1	0	1	0
148.380 167	Powerhouse	1	0	1	0	1	0	1	0
148.380 168	Log Sluice	1	0	1	0	1	0	1	0
148.380 169	Powerhouse	1	0	1	0	0	0	1	0
148.380 170	Powerhouse	1	0	1	0	0	0	1	0
148.380 171	Powerhouse	1	0	1	0	0	0	0	0
148.380 172	Log Sluice	1	0	0	0	0	0	1	0
148.480 100	Powerhouse	1	0	1	0	0	0	0	0
148.480 101	Log Sluice	1	0	1	0	1	0	1	0
148.480 102	Powerhouse	1	0	1	0	0	0	1	0
148.480 103	Powerhouse	1	0	1	0	0	0	1	0
148.480 106	Powerhouse	1	0	1	0	0	0	1	0
148.480 108	Powerhouse	1	0	1	0	1	0	1	0
148.480 109	Log Sluice	1	0	1	0	0	0	0	0
148.480 111	Log Sluice	1	0	0	0	0	0	1	0
148.480 112	Powerhouse	1	0	1	0	0	0	1	0

Frequency Code	**Route of Passage**	**R00** (Cabot Forebay)	**R01** (Mobile tracking Tailrace)	**R02** (Tailrace)	**R03** (Mobile tracking to Montague)	**R04** (Montague)	**R05** (Mobile tracking to Nourse)	**R06** (Nourse Farm)	**R07** (Mobile tracking to Hatfield)
148.480 113	Powerhouse	1	0	1	0	0	0	1	0
148.480 117	Log Sluice	1	0	1	0	0	0	1	0
148.480 118	Powerhouse	1	0	0	0	0	0	1	0
148.480 119	Powerhouse	1	0	1	0	0	0	0	0
148.480 121	Powerhouse	1	0	1	0	0	0	0	0
148.480 123	Log Sluice	1	0	1	0	1	0	1	0
148.480 124	Powerhouse	1	0	1	0	0	0	1	0
148.480 125	Powerhouse	1	0	1	0	0	0	1	0
148.480 127	Powerhouse	1	0	1	0	0	0	1	0
148.480 128	Powerhouse	1	0	1	0	0	0	0	0
148.480 132	Powerhouse	1	0	0	0	0	0	1	0
148.480 134	Powerhouse	1	0	1	0	0	0	0	0
148.480 135	Powerhouse	1	0	1	0	0	0	0	0
148.480 136	Powerhouse	1	0	1	0	0	0	0	0
148.480 139	Powerhouse	1	0	1	0	0	0	1	0
148.480 141	Powerhouse	1	0	1	0	0	0	1	0
148.480 142	Powerhouse	1	0	1	0	0	0	1	0
148.480 145	Log Sluice	1	0	0	0	0	0	1	0
148.480 147	Log Sluice	1	0	0	0	1	0	1	0
148.480 148	Log Sluice	1	0	1	0	0	0	1	0
148.480 150	Powerhouse	1	0	1	0	0	0	1	0
148.480 151	Powerhouse	1	0	1	0	0	1	0	0
148.480 152	Log Sluice	1	0	0	0	0	0	1	0
148.480 154	Log Sluice	1	0	0	0	0	0	1	0
148.480 155	Powerhouse	1	0	0	0	0	0	0	0
148.480 157	Log Sluice	1	0	1	0	0	0	1	0
148.480 162	Powerhouse	1	0	1	0	0	1	0	0

APPENDIX E - BYPASS FLOW DURATION CURVES

APPENDIX E:

BYPASS FLOW DURATION CURVES

Appendix E – Bypass flow exceedance curves

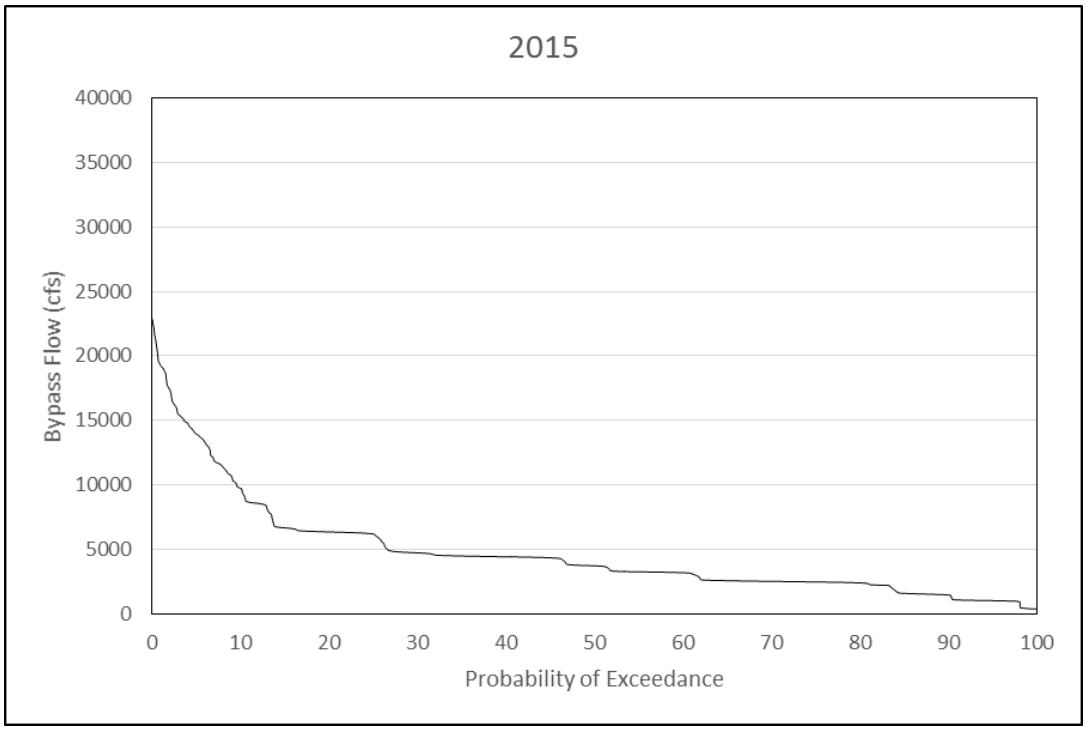

Figure E-1: Bypass flow exceedance curve for 2015 study period

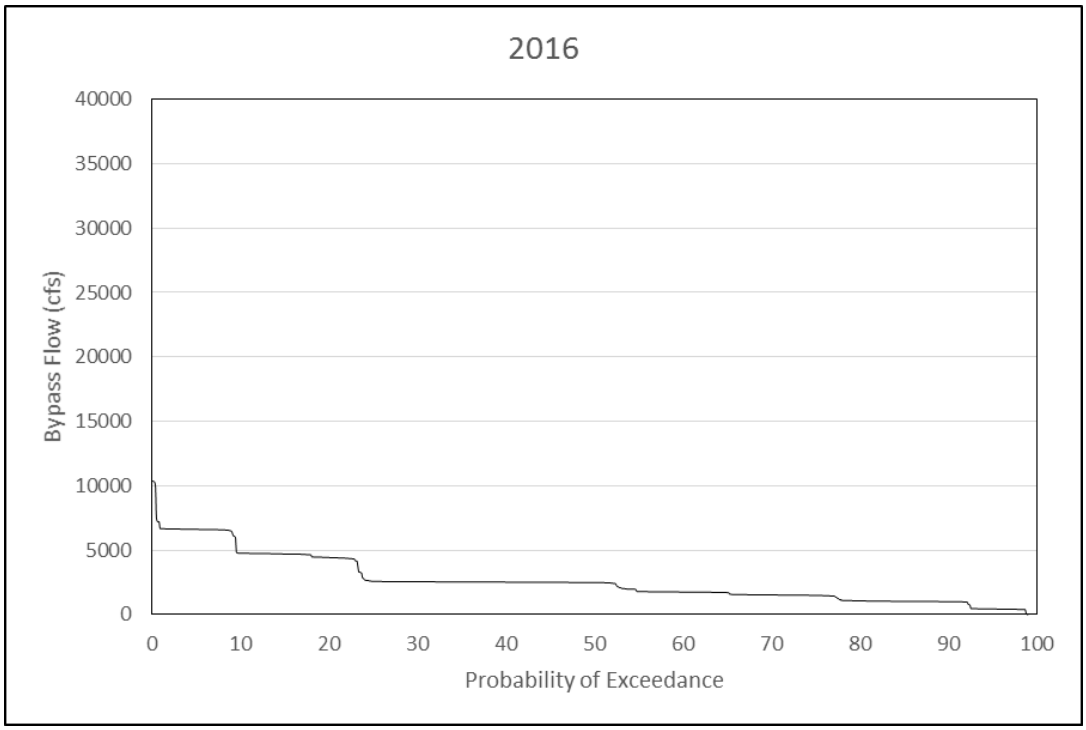

Figure E-2: Bypass flow exceedance curve for 2016 study period

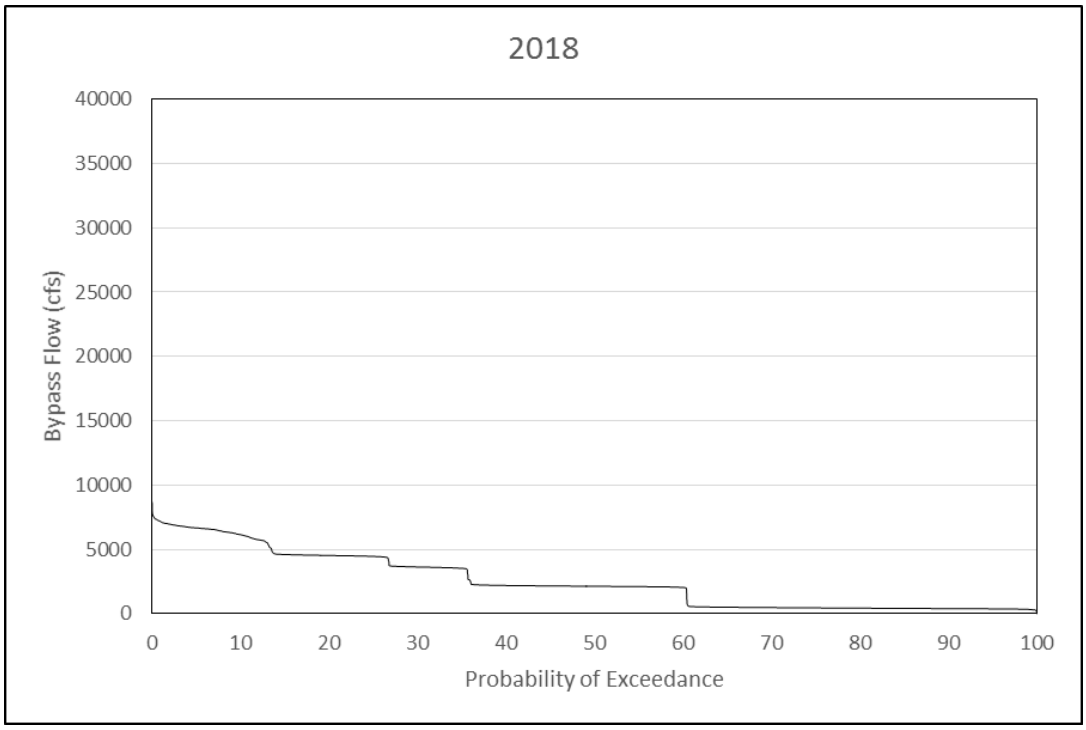

Figure E-3: Bypass flow exceedance curve for 2018 study period

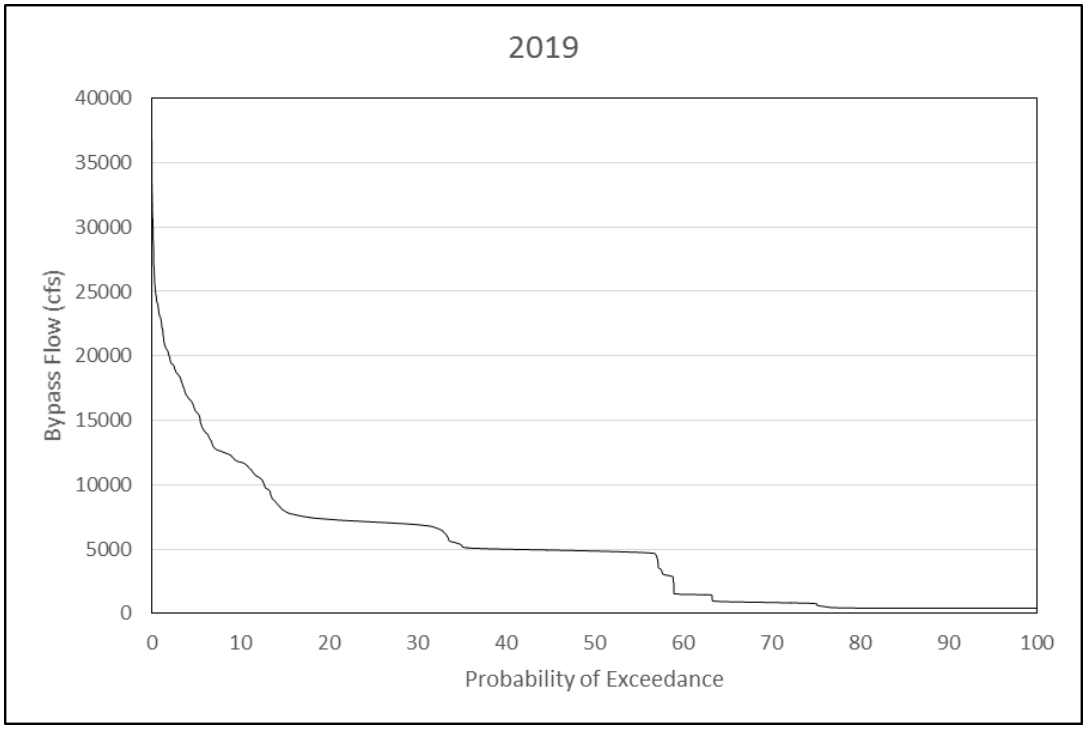

Figure E-4: Bypass flow exceedance curve for 2019 study period

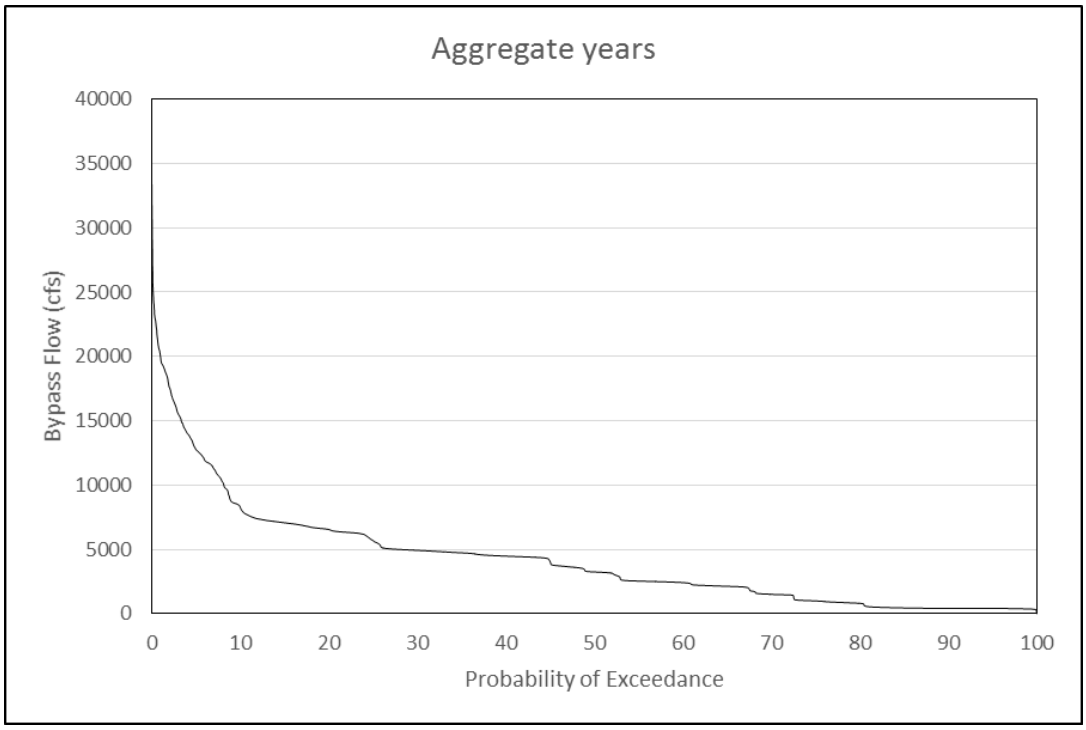

Figure E-5: Bypass flow exceedance curve for all years (2015, 2016, 2018, and 2019)